Investigation of the catalytic mechanism of RNase P: the role of divalent metal ions and functional groups important for catalysis

Dissertation

zur

Erlangung des Doktorgrades

der Naturwissenschaften

(Dr. rer. nat.)

dem Fachbereich

Pharmazeutische Chemie

der Philipps-Universität Marburg

vorgelegt von

Simona Cuzic - Feltens

aus Corlateni-Botosani/Rumänien

Marburg/Lahn 2006

Vom Fachbereich Pharmazeutische Chemie

der Philipps-Universität Marburg als Dissertation am:.............................angenommen

Erstgutachter: **Prof. Dr. rer. nat. Roland K. Hartmann**

Zweitgutachter: **Prof. Dr. rer. nat. Albrecht Bindereif**

Tag der mündlichen Prüfung am: **15.02.2006**

Content

1 *Introduction*

1.1 Ribozyme

In 1982-1983, Cech and Altman reported that RNA is able to catalyse chemical reactions, a discovery that opened a new field of biological research. For two independent RNA molecules, it was found that the RNA performed phosphodiester bond cleavage reactions that were site-specific, had rates that were enhanced many orders of magnitude over background rates, and were biologically required (Kruger et al., 1982; Guerrier-Takada et al., 1983). Naturally existing catalytic RNAs include small ribozymes like the hammerhead, hairpin, hepatitis delta virus and Varkud satellite ribozymes (Symons, 1992; Carola & Eckstein, 1999) and large ribozymes like Group I and II introns (Kruger et al., 1982) and the RNA subunit of RNase P (P RNA; Guerrier-Takada et al., 1983). In addition to that, RNA-catalysed chemistry has also been proposed for two major ribonucleoprotein machines, the ribosome (Nissen et al., 2000; Muth et al., 2000, Steitz & Moore, 2003) and the spliceosome (Collins & Guthrie, 2000; Valadkhan & Manley, 2001).

In general, ribozymes catalyse the endonucleolytic transesterification of a phosphodiester bond. All known ribozymes have an absolute requirement for at least one divalent cation, which is generally Mg^{2+}. Some ribozymes (mostly large catalytic RNAs) require divalent cations for proper assembly of the tertiary structure as well. On this basis, catalytic RNAs are considered to be metalloenzymes, and a general two-metal-ion reaction mechanism has been proposed for the large catalytic RNAs, based on analogy to the properties of protein metalloenzymes (Steitz & Steitz, 1993). The role of divalent cations for the small catalytic RNAs is less clear, but they are generally considered to be essential for efficient catalysis (Walter & Burke, 1998).

Although the cleavage mechanism is different, there are certain features common to all of the RNA-catalysed reactions. Specifically, the RNA is required to: (1) activate the nucleophile, (2) stabilise a negatively charged transition state, and (3) stabilise the leaving group. There are three ribozymes, namely Group I and II introns and P RNA, which accept external nucleophiles (e.g. the 2'-OH group of an internal adenosine in the case of group II intron). By contrast, small ribozymes use an internal nucleophile, namely the 2'-oxygen of the ribose moiety at the cleavage site, with resultant formation of 3'-terminal 2', 3'-cyclic phosphate and 5'-hydroxyl groups.

With one exception, all ribozymes catalyse reactions by which they modify themselves. Hence, they cannot be considered true enzymes or catalysts. The exception is P RNA, which processes the 5' end of tRNA precursors (ptRNA) and is the only known

example of a naturally occurring, *trans*-acting RNA-based enzyme. However, all these ribozyme molecules can be converted, with some clever engineering, into true RNA enzymes that cleave RNAs in *trans* (Uhlenbeck, 1987; Haseloff & Gerlach, 1988; Hampel & Tritz, 1989). Also, RNase P RNA can be attached to an <u>e</u>xternal <u>g</u>uide <u>s</u>equence (EGS) designed in such a way that it anneals to the target RNA and forms a mimic of a natural RNase P substrate (Forster & Altman, 1990; Altman, 1995). All these possibilities opened up the perspective to use ribozymes in gene therapy, in most cases based on the enzymatic cleavage of messenger RNAs, thereby blocking gene expression in living cells.

Furthermore, new ribozymes identified by *in vitro* selection (Beaudry & Joyce, 1992; Bartel & Szostak, 1993) extended the repertoire of reactions catalysed by RNA enzymes: the formation of ester- and amide-bonds, formation of C-C-bonds and insertion of metal ions into porphyrine rings. Successful selection of allosteric ribozymes that can be regulated by binding of small molecules or metal ions was reported as well (Koizumi et al., 1999; Komatsu et al., 2002).

1.2 RNase P

RNase P is a ribonucleoprotein enzyme responsible for generating the mature 5' end of tRNAs by a single endonucleolytic cleavage of their precursors. It is an essential, ubiquitous enzyme present in all cells and cellular compartments that synthesise tRNA: bacterial cells, eukaryotic nuclei, mitochondria and chloroplasts. The essential function of RNase P *in vivo* has been demonstrated so far in several organisms and organelles like bacteria (Schedl & Primakoff, 1973), yeast nuclei (Lee et al., 1991) human (Jarrous & Altman, 2001) and mitochondria (Morales et al., 1992; 1989). All known RNase P enzymes are ribonucleoproteins and contain an RNA subunit essential for catalysis, with the possible exception of RNase P in some plant chloroplasts and from trypanosome mitochondria (Wang et al., 1988; Salavati et al., 2001; Thomas et al., 1995). The chemical mechanism of RNase P involves essential divalent metal ion cofactors (Altman & Kirsebom, 1999) and is thought to be an in-line SN_2 displacement reaction (Altman et al., 1993). The endonucleolytic cleavage generates terminal 5' phosphate and 3' hydroxyl groups.

1.2.1 The RNA subunit of RNase P (P RNA)

The RNA component of RNase P (P RNA) from bacteria is encoded by the *rnpB* gene and varies in length between 350 and 450 nucleotides (Brown & Pace, 1992). *In vitro*, it is enzymatically active in the absence of the protein subunit at high ionic strength (Guerrier-Takada et al., 1983). There is little sequence similarity among the 300 bacterial P RNA sequences analysed so far except for a few short segments. Phylogenetic covariation

analysis of the large data set has allowed the precise definition of the secondary structure and the identification of several tertiary interactions. The RNA subunit of bacterial RNase P can be divided into two distinct structural classes: type A (Fig. 1.1 A), represented by *E. coli*, which is the ancestral type found in most bacteria (the RNA subunit of the enzyme from *E. coli* is called M1 RNA), and type B (Fig. 1.1 B), represented by *B. subtilis*, which is found in the low GC content gram-positive bacteria (Haas et al., 1996). An intermediate structure (type C) is found in green non-sulfur bacteria (Haas & Brown, 1998).
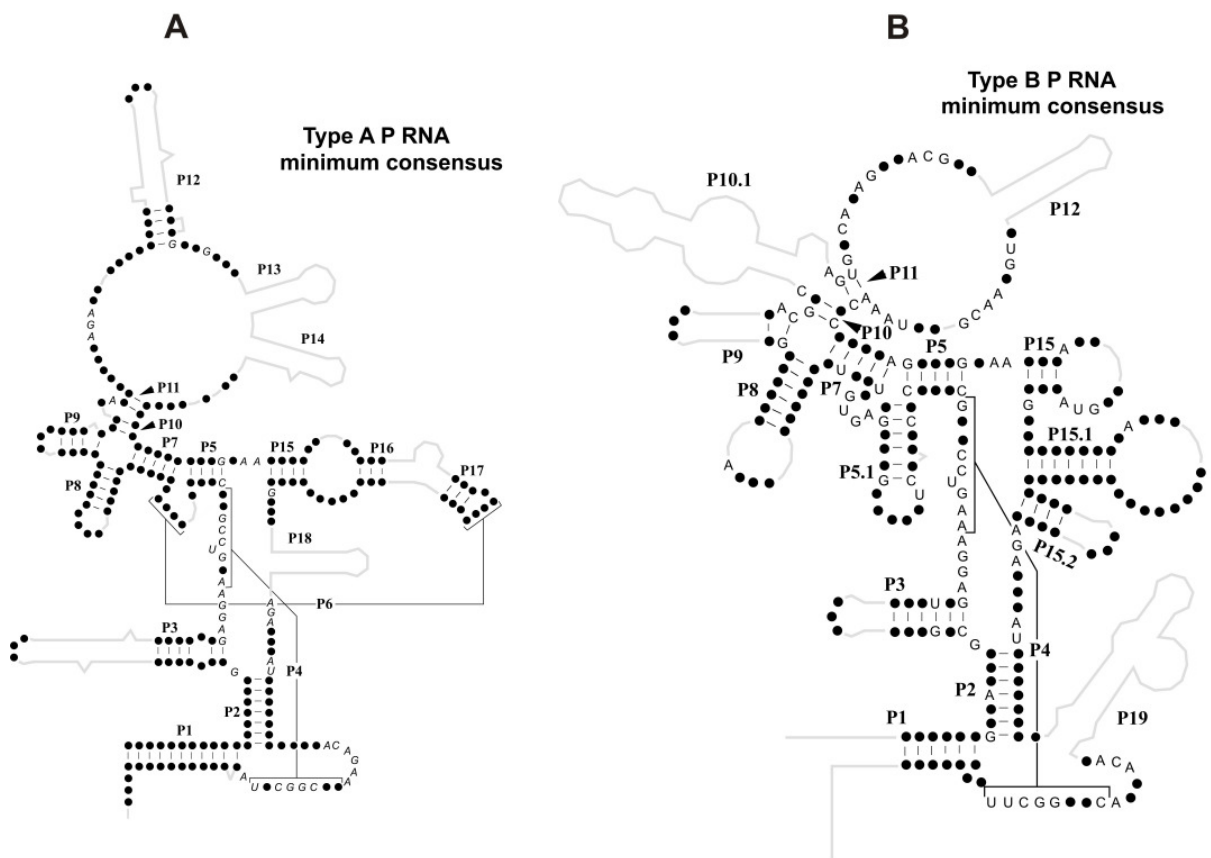
Fig. 1.1: Consensus secondary structure of type A and B P RNAs. (A) the type A consensus RNA and (B) the type B consensus RNA. Only nucleotide positions that are present in all instances of each type of RNA are shown, as letters (A, G, C or U) if invariant or dots (•) if variable in identity. Grey lines indicate elements of the *E. coli* (type A) or *B. subtilis* (type B) RNAs that are absent in some of the RNAs of each type and are therefore absent in the consensus. P stands for helical regions. Helices P4 and P6 are indicated by black lines.

Despite differences in the secondary structure organization of type A and type B, both RNAs can be modelled into a similar three-dimensional structure (Chen et al., 1998; Massire et al., 1998; Tsai et al., 2003) with the evolutionarily conserved nucleotides placed in nearly

identical positions (Haas et al., 1996; legend to Fig. 1.1). These computer-aided modelling efforts illustrate a common phenomenon in RNA architecture, wherein different, non-homologous modules are used for long-range structural interactions that result in functionally equivalent structures.

Recently the tertiary structure of RNase P RNA from *Thermotoga maritima* (type A; Torres–Larios et al., 2005) and *Bacillus stearothermophilus* (type B; Kazantsev et al., 2005) was solved by *X-ray* crystallography. The crystal structures reveal all the interactions between domains predicted by a variety of biochemical approaches and agrees well with earlier models and with secondary structure predictions (Harris et al., 1994; Chen et al., 1998; Massire et al., 1998; Tsai et al., 2003). For more details see 1.2.3.

RNase P RNA from Archaea can also be divided into two structural classes, type A, the most common and similar to the ancestral bacterial type A structure, and type M, a derived structure found only in two species so far (Harris et al., 2001).

Similarly, the eukaryal RNase P sequences can also be fit to a minimal consensus secondary structure reminiscent of the bacterial RNase P RNA structure (Frank et al., 2000). Despite the low sequence conservation, it has been possible to identify several conserved regions and helical elements present in all these RNAs (Frank et al., 2000; Harris et al. 2001). Two of the conserved sequence elements correspond to helix P4 and adjacent sequences, which is an essential part of the catalytic centre of the bacterial enzyme (Christian et al., 2000; 2002; Crary et al., 2002). Another case of RNase P RNA variation is found in yeast mitochondria, where there are large differences in length (between 227 and 490 nt) between different yeast species (Wise & Martin, 1991), although they can be drawn into a two-dimensional structure similar to the other RNase P RNAs.

1.2.2 The active center of RNase P

The RNA subunit of bacterial RNase P is composed of two domains (separated by the broken line; Fig. 1.2) that can fold independently (Pan, 1995; Loria & Pan, 1996). The S-, or specificity, domain (above the broken line; Fig. 1.2) is composed of helices P7–P14 and a region of this domain (highlighted grey) contacts the T-arm of the ptRNA substrate (Fig. 1.6), as demonstrated by kinetic experiments (Pan et al., 1995; Loria & Pan, 1998) and photocrosslinking studies (Nolan et al., 1993; Chen et al., 1998). The C-, or catalytic, domain (below the broken line, Fig. 1.2) is composed of helices P1–6 and P15–18, and contains the majority of nucleotide positions that are conserved among all known RNase P RNAs (Chen & Pace, 1997). One of the most important aspects of the function of the C-domain is its interaction with the divalent metal ion cofactors that are essential for folding, substrate binding and catalysis. Based on what is known about protein phosphodiesterases as well as
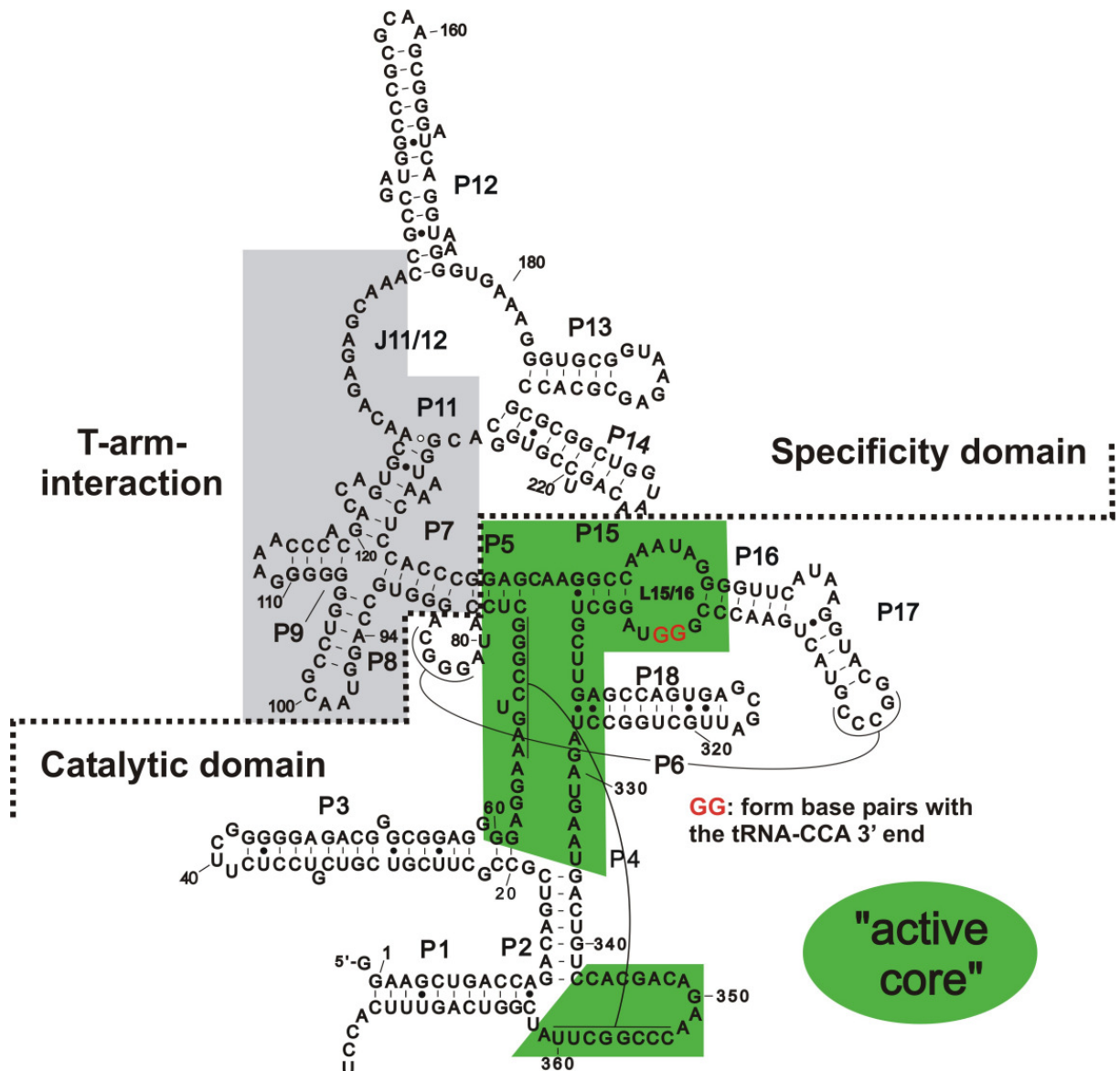
Fig. 1.2: The secondary structure of *E. coli* RNase P RNA (M1 RNA). The broken line shows the boundary between the specificity (S-) and the catalytic (C-) domain. The grey background highlights the region of the S-domain that interacts with the T-arm of ptRNA. The active core consisting of helix P4 and loop L15 / 16 in the C-domain is highlighted green. The two positions (GG) that form base pairs with the 3' –CCA of tRNA are shown in red.

other large ribozymes, it is anticipated that the RNase P active site will contain a network of several metal ions. Brannvall and Kirsebom (Brannvall & Kirsebom, 2001), in examining this concept, demonstrated that different mixtures of divalent metal ions can have profoundly different effects on cleavage specificity and catalytic rate, leading to the conclusion that catalysis involves the cooperation of metal ions bound at different sites. The binding site for the substrate 3'–CCA sequence is located in a single stranded region (L15 / 16; the two guanosine residues shown in red; Fig. 1.2) within the C-domain (Kirsebom & Svard, 1994). Evidence that one or more classes of metal ions important for catalysis are coordinated or

recoordinated via the 3'–CCA –L15 / 16 interaction comes from the observation that mutations in L15 / 16 result in different sensitivities to metal ion identity. Several lines of evidence indicate that a second, crucial site of metal ion binding within the C-domain occurs in the highly conserved region characteristic of all RNase P RNAs (helix P4; Christian et al., 2000). Photocrosslinking studies have identified sites of contact between regions in the C-domain of RNase P RNA and nucleotides proximal to the cleavage site in the ptRNA (Burgin & Pace, 1990; Kufel & Kirsebom, 1996; Christian & Harris, 1999). Taken together, these results demonstrate that the C-domain contains the active site (highlighted green; Fig.1.2) of the ribozyme.

Based on the crystal structure of *T. maritima* P RNA, it was proposed that the region around A 213 (A 248 in *E. coli*), highly conserved in bacteria located at the J5 / 15 junction and implicated in direct contacts with the substrate (Zahler et al., 2003; 2005), together with the vicinity of the universally conserved nucleotides A 49 (A 66 in *E. coli*), and A 314 (A 352 in *E. coli*) may correspond to the general location of the active site (Torres-Larios et al., 2005).

Helix P4 (highlighted green; Fig. 1.2), located in the C-domain of the ribozyme, has been suggested to contain functional groups and sites of metal ion coordination central to ribozyme activity. This suggestion is based in part on phylogenetic comparative analysis of RNase P RNA sequences that demonstrated that nucleotides in helix P4, and adjoining single-stranded regions, are universally conserved in bacterial, archaeal, and eukaryal RNase P RNAs (Chen & Pace, 1997). In addition, nucleotide analogue interference experiments identified functional groups in P4 that are important for both substrate binding and catalysis (Hardt et al., 1995, 1996; Harris & Pace, 1995; Kazantsev & Pace, 1998; Heide et al., 1999; Siew et al., 1999). Site-specific functional group modification experiments identified non-bridging phosphate oxygens in helix P4 that, when substituted with sulfur, dramatically inhibit ribozyme activity. Rescue of the phosphorothioate interference effects by Mn^{2+} and Cd^{2+} strongly argues that one role of helix P4 is to position divalent metal ions that are important for catalytic function (Christian et al., 2000). This hypothesis is supported by the observation that single point mutations in helix P4 can alter the ribozyme specificity for divalent metal ions. A single nucleotide exchange, namely a cytosine-to-uracil mutation at position 70 that converts a naturally invariant C-G base pair within helix P4 to a U-G pairing, leads to stimulation of Ca^{2+}-dependent activity while diminishing Mg^{2+}-dependent activity. (Frank & Pace, 1998). These experiments, however, do not distinguish between effects on ribozyme structure, substrate positioning or direct effects on active site function. Moreover, it is not known how many metal ions interact with the P4 metal binding site, or what other structural elements contribute to the affinity of metal ions in the C-domain. An Os(III)

hexamine substitute, which mimics a fully hydrated octahedrally coordinated Mg^{2+} ion and is expected to bind RNA only by outer-sphere coordination, was recently used in *X-ray* crystallography to analyse the metal ion binding sites of *B. stearothermophilus* P RNA (Kazantsev et al., 2005). Three Os(III) hexamine binding sites were found in the major groove of helix P4. One of them, which is formed by consecutive base pairs U 56-A392 and G 57-C391, overlaps with a Pb(II) binding site, which suggests low cation specificity for this site. Two more sites were found in the cleft formed by nucleotides A 256, A 332-G 335, A 390, C 391 and G 275-A277, suggested to be the site of catalysis. Although the latter metal-binding sites are candidates for direct involvement in cleavage chemistry, the sites in the major groove of P4 are remote from the proposed active site and therefore most probably serve a different function. Docking of tRNA onto the RNase P RNA structure positions the backbone of the acceptor stem of tRNA directly in the major groove of helix P4. Therefore, it was proposed that the primary role of the metal-binding sites in helix P4 is to screen electronegative repulsion between the negatively charged substrate and ribozyme RNAs.

1.2.3   The tertiary structure of the RNA component of RNase P

Knowledge of the structure of RNase P RNA is essential for understanding its function. Phylogenetic comparative analyses of RNase P RNA sequences have established the secondary and some tertiary structure of the RNA in a broad diversity of organisms (Brown et al., 1996; Massire et al., 1997; Harris et al., 2001). Photochemical crosslinking studies provided structural information to orient the helical elements and identified nucleotides associated with the active site of the RNA (Burgin & Pace, 1990; Chen et al., 1998). There are two major structural types of bacterial RNase P RNA, A (ancestral) and B (*Bacillus*), which differ in a number of structural elements attached to a homologous conserved structure. About two-thirds of any bacterial RNase P RNA is shown by sequence covariations to be involved in Watson-Crick base-pairing interactions, but the interactions that form the global structure have been speculative.

Recently, the crystal structure of the ancestral A-type (*T. maritima*; Torres-Larios et al., 2005) as well as the B-type (*B. stearothermophilus*; Kazantsev et al., 2005) RNA component of RNase P has been solved. Both structures reveal an remarkable flat architecture formed by helical subdomains connected by a variety of long range interactions.
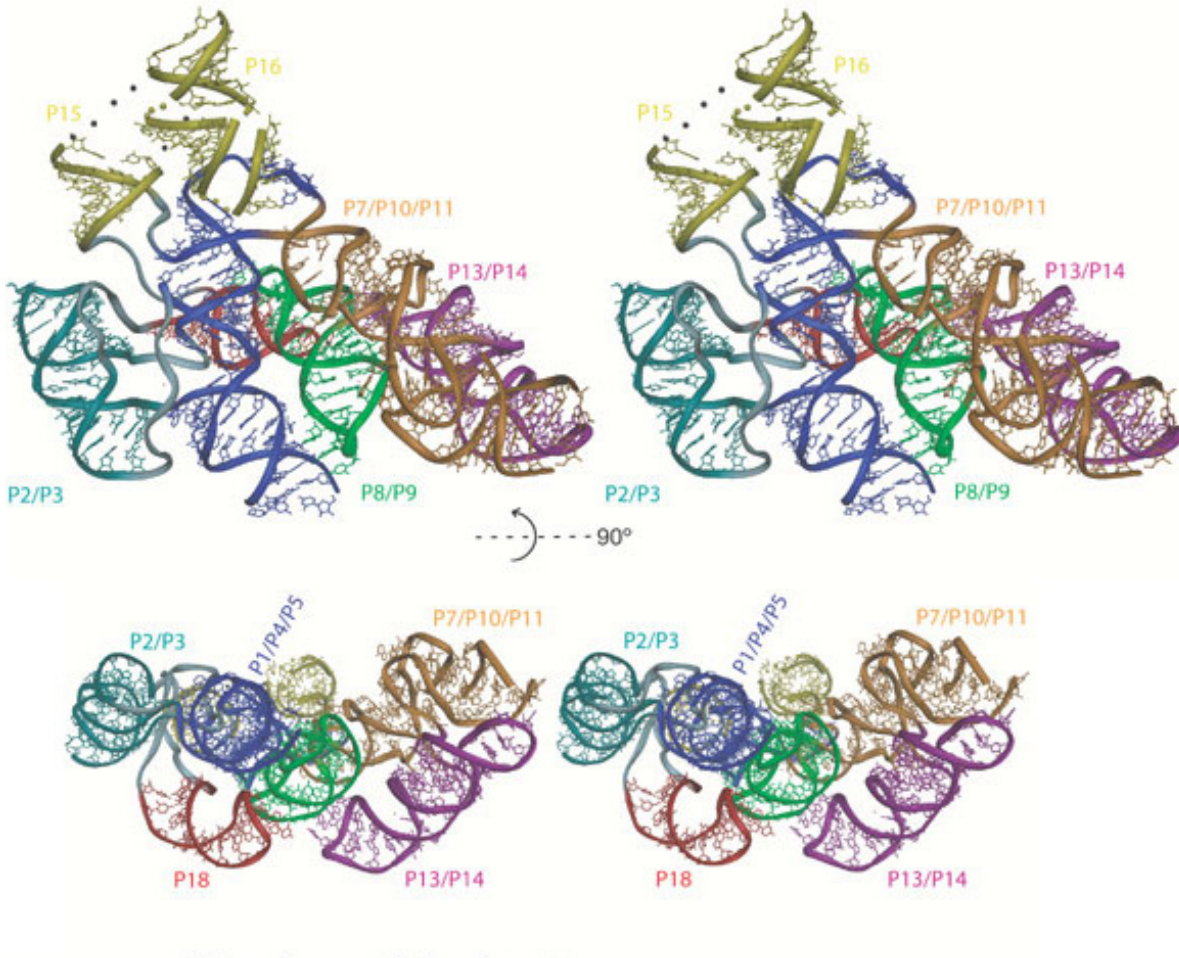
Fig. 1.3: Crystal structure of the RNA component of *T. maritima* RNase P (Torres-Larios et al., 2005). A stereo ribbon diagram of two orthogonal views of the structure is shown.

The RNase P RNA of *T. maritima* (Torres-Larios et al., 2005) is made up of two layers, each one-helix thick. The larger layer is composed of paired P1–P12 and P15–P17, and including the junctions J5 / 15, J11 / 12–J12 / 11 and loop L15 regions (Fig. 1.3 top). The second layer comprises helical stems P13, P14 and P18 (Fig. 1.3 bottom). The two layers interact extensively with each other through P8 and P9 in the specificity domain (S-domain; 1.2.2; Fig. 1.2) and P1, P4 and P18 in the catalytic-domain (C-domain; 1.2.2; Fig. 1.2). The larger layer of the structure contains most of the universally conserved regions, the areas expected to contact the ptRNA substrate (see 1.2.6) and the putative active site. The S- and C-domains represent independent structural units that form extensive inter-domain interactions. The central organiser of the domains is the P8 / P9 stack. Tetraloop–tetraloop receptor interactions occur between P8 and L14, P8 and L18 and L9 and P1 (Massire et al., 1997). All these interactions ensure that the two domains are positioned correctly and oriented in the manner appropriate for tRNA binding. On the tertiary structure level, interactions between hairpin loops and helices dominate.

The role of P4 has been extensively analysed due to its sequence conservation, proximity to the catalytic site and its potential to bind metal ions involved in catalysis. Nevertheless, the crystal structure suggests that its function might merely structural and its sequence conservation could be due to constraints imposed by its proximity to and interaction with the connectors in the C-domain.

The molecule was crystallised as dimer via formation of an intermolecular version of the pseudoknot P6. The functional significance of this dimer could not be assessed. However, it is not clear whether this intermolecular pseudoknot is preferred over the intramolecular one *in vivo*.

The *X-ray* structure of P RNA from *Bacillus stearothermophilus* (type B RNA) was solved (Kazantsev et al., 2005; not shown). This RNA enzyme is constructed from a number of coaxially stacked helical domains joined together by local and long-range interactions. These helical domains are arranged to form a remarkably flat surface, which is implicated by a wealth of biochemical data in the binding and cleavage of pRNA substrate. The *X-ray* structure agrees with the structure predicted on phylogenetic grounds. Patterns of coaxial stacking of the helices and their overall spatial arrangement agree remarkably well between the crystal (Kazantsev et al., 2005) and phylogenetic-crosslinking structure models (Haas et al., 1996; Massire el al., 1998). Comparative and modeling studies with RNase P also indicated some tertiary structural elements, although these generally proved, in the light of the crystal structure, to be more complex than predicted. Phylogenetic comparisons perceive only base interactions and so cannot detect the wealth of backbone and other contacts that are revealed by the crystal structure.

Both crystal structures (Kazantsev et al., 2005; Torres-Larios et al., 2005) agree with the existing biochemical data, but still cannot explain the details of the cleavage mechanism of RNase P. A fuller understanding of the ptRNA recognition and RNase P catalysis requires further structural work at atomic resolution.

1.2.4 The protein subunit(s) of RNase P

In bacteria, RNase P contains a single protein subunit of about 120 amino acid residues (Fig. 1.4 A). The sequences of this protein are poorly conserved (Kirsebom & Vioque, 1995). There is, however, a short conserved basic sequence motif essentially shared by all of them. This conserved sequence is called the RNR motif and can be defined as K-X4-5-A-X2-R-N-X2-(K/R)-R-X2-(R/K). Other conserved residues include a few aromatic amino acids close to the amino terminus of the protein. Despite the low conservation in primary sequence, the three-dimensional structures of *Bacillus sublilis, Thermotoga maritima* and *Staphylococcus aureus* RNase P proteins determined by *X-ray* crystallography or NMR are very similar (Stams et al., 1998; Kazantsev et al., 2003; Spitzfaden et al.,2000).

Moreover, complementation studies showed that several RNase P protein subunits are functionally interchangeable, and heterologous reconstitution of RNase P using an RNA of one source and protein from a different source is generally feasible (Guerrier-Takada et al.; 1983; Morse & Schmidt, 1992; Pascual & Vioque, 1996), suggesting that bacterial RNase P proteins adopt very similar structures.
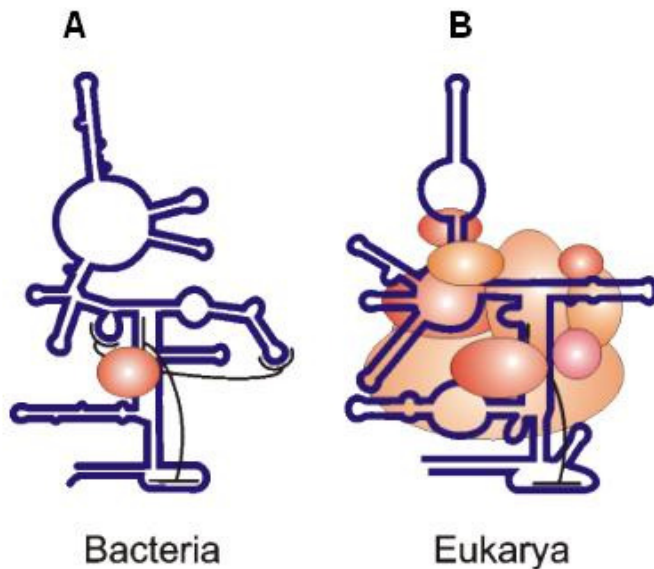
Fig. 1.4: The RNase P holoenzyme. A. Bacterial RNase P holoenzyme with one RNA subunit drawn in blue and a single protein subunit (rose). B. RNase P from eukaryotic cells consists of one RNA subunit, as in bacteria, but many protein subunits

The protein composition of eukaryotic RNase P has been mainly studied in yeast and humans. Compared with the simplicity of the bacterial RNase P protein component, there is a significant increase in complexity in the nuclear enzyme (Fig. 1.4 B). Nine proteins have been identified as subunits of yeast nuclear RNase P, ranging in size from 16 to 100 kDa (Xiao et al., 2001). For the human nuclear enzyme, ten proteins have been identified ranging in size from 14 to 115 kDa (van Eenennaam et al., 2000; 2001). At least four of the human proteins are homologues of proteins from yeast RNase P, but none shows clear homology to the bacterial protein subunit. Most of the nuclear RNase P protein subunits are shared with the related endonuclease MRP, which also contains an RNA subunit.

Despite the presence of a bacterial-like RNA, archaeal RNase P possesses a eukaryotic RNase P -like protein set. Four RNase P protein subunits were identified in *Methanothermobacter thermoautotrophicus* (Hall & Brown, 2002). These protein subunits are similar to specific nuclear yeast and human RNase P proteins and have homologues in other archaeal species (Koonin et al., 2001; Tatusov et al., 2001).

1.2.5 The catalytic mechanism

In the reaction catalysed by the RNA subunit of bacterial RNase P, there is a requirement for both divalent and monovalent cations (Chen et al., 1997). Monovalent cations appear to be involved in the stabilisation of the structure during the cleavage reaction. By contrast, divalent metal cations are required for the chemical cleavage itself, not only for the structural stabilisation. During cleavage, a hydroxide ion activated by metal ions is thought to act as a nucleophile (Guerrier-Takada et al., 1986; Smith & Pace, 1993; Warnecke et al., 1996; Chen et al., 1997; Fig. 1.5). Though the details of the reaction mechanism are not fully understood, it has been proposed that three Mg^{2+} ions participate in the transition state (Fig. 1.5), because the slope of the Hill plot for the cleavage rate versus the concentration of Mg^{2+} ions was 3.2. Moreover, at least one Mg^{2+} ion coordinates directly to the *pro*-Rp oxygen at the scissile phosphate. The cleavage rate of the substrate
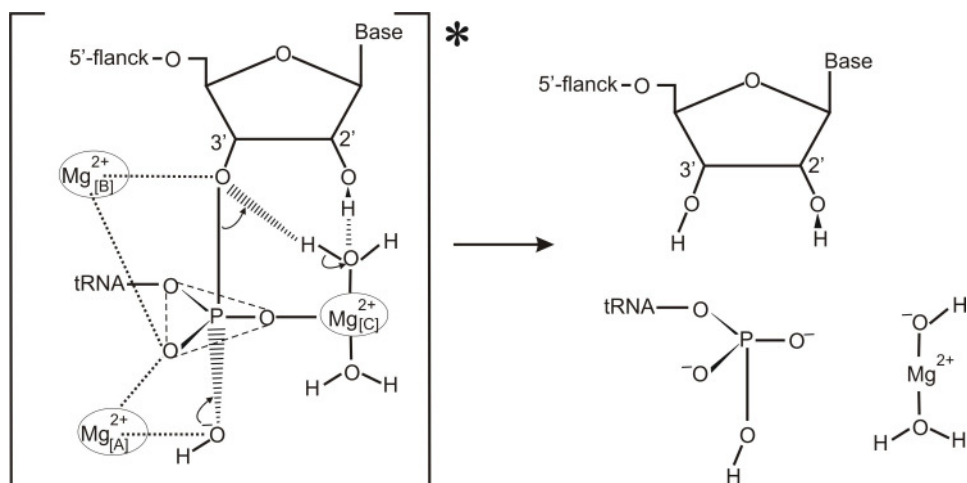
Fig. 1.5: A proposed catalytic mechanism of RNase P. Metal ions [A] and [B] are positioned similar to those involved in self-splicing of the group I ribozyme (Steitz & Steitz, 1993). The metal at site [C] is positioned in the vicinity of the 2'-hydroxyl group of nucleotide −1 of ptRNA to explain the dramatic effects on cleavage of substrates carrying 2'-substitutions at nucleotide −1 (Smith & Pace, 1993). The same metal directly coordinates the *pro*-Rp oxygen explaining the effects caused by replacing this oxygen with sulphur.

carrying a sulphur substitution of the *pro*-Rp oxygen in the presence of Mg^{2+} ions was at least 1000 fold lower than the cleavage rate of the natural substrate. This effect was rescued by thiophilic metal ions like Cd^{2+} or Mn^{2+} ions, suggesting direct coordination of one or two metal ions to the *pro*-Rp oxygen (Warnecke et al., 1996; 1999; Chen et al., 1997).

2' deoxy substitution at the cleavage site reduced the apparent number of bound Mg^{2+} ions and decreased the apparent affinity for Mg^{2+} ions, suggesting that this 2' -hydroxyl might contribute to one of the Mg^{2+}-binding sites. Furthermore, a 2' -methoxy

substitution at the cleavage site decreased the cleavage rate dramatically, suggesting that the 2'-OH might be involved in stabilising the 3' -leaving oxygen via donation of a hydrogen bond (Smith & Pace, 1993).

1.2.6 Substrate recognition by RNase P
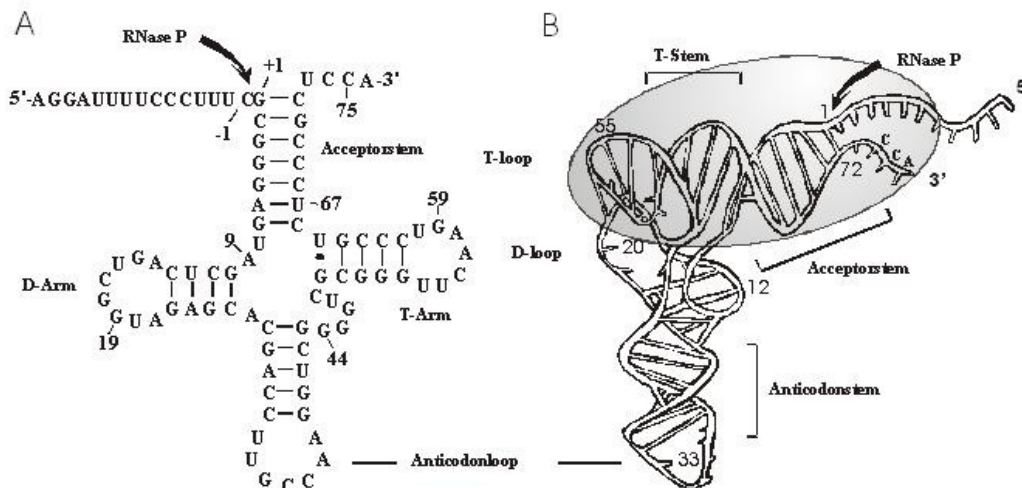
Fig. 1.6: Secondary structure of ptRNA^{Gly} (A) and tertiary structure of ptRNA^{Asp} (B) from *Thermus thermophilus*. The recognition region is marked by the grey oval (B; according to Thurlow et al., 1991).

The well understood secondary and tertiary structure of tRNA has been applied to understanding the substrate recognition and cleavage site selection requirements of RNase P. The interaction of RNase P with the substrate depends on the highly conserved features of the mature tRNA domain rather than on aspects of the highly variable precursor segment (Carrara et al., 1995). Substrate interaction experiments have identified the acceptor stem and the T stem-loop (Fig. 1.6) as the critical recognition elements (Holm & Krupp, 1992; Kahle et al., 1990). The acceptor stem of most ptRNAs contains a 7 –bp helix that appears critical for correct cleavage site selection (Kirsebom & Svard, 1992; Svard & Kirsebom, 1992; 1993). *E. coli* RNase P (RNA-subunit as well as holoenzyme) has been shown to require specific nucleotides to be present near the cleavage site of the ptRNA (Svard & Kirsebom, 1992). A 3' -CCA tail, present in all tRNAs, was not found to be essential for RNase P processing *in vitro* but does substantially influence rate and cleavage site positioning (Guerrier-Takada et al., 1984; Kirsebom & Svard, 1994; Krupp et al., 1991; Oh &

Pace, 1994).

There are two specific Watson-Crick base pairs formed between the enzyme and substrate RNAs. The GG sequence on the 3' side of the P15 / 16 loop of *E. coli* P RNA (Fig. 1.2) forms base pairs with the CC sequence in the 3' -CCA-tail of the substrate. Thus, a function of *E. coli* P RNA is to anchor the substrate through this base pairing, thereby exposing the cleavage site in a way that cleavage is accomplished at the correct position (Kirsebom & Svard, 1994). The end of the acceptor stem of tRNA is thought to be a Mg^{2+} binding site and important for RNase P cleavage activity (Smith & Pace 1993; Zuleeg et al., 2001).

The tRNA was modelled into the recently solved crystal structure of *T. maritima* (Fig. 1.7; Torres-Larios et al., 2005). In this model, the T (TΨC) stem loop lies in the S-domain opening and the 5' end of the tRNA lies near the P4 / P5 region. The acceptor stem of the tRNA sits on the shallow groove created by the concave C-domain. The tRNA stem runs almost parallel to P1 / P4 / P5 and passes near the conserved nucleotides in this region. The cleavage site sits near the universally conserved residues A 49 (A 66 in *E.coli*; Fig. 1.4) in P4 and A 314 (A 352 in *E. coli*; Fig. 1.4) in J2 / 4. The cleavage site is also near J5 / 15, although some changes would be required to form interactions between this region and the tRNA. J5 / 15 contains A 213, which is highly conserved in all bacteria and implicated in specific interactions with tRNA (Zahler et al., 2003). A 213 is found between the region involved in base pairing with the CCA at the 3' end (Kirsebom & Svard, 1994) and the conserved regions around P4. Conserved U 52 (U 69 in *E. coli*; Fig. 1.4) in P4 is an unstacked base that could not be seen in the electron density map. In this model the phosphate of U 52 is found near the tRNA, but on the other side of the stem from where the conserved nucleotides are located. Thus, it seems that A 49, A 213 and A 314 mark the general location of the active site. Finally, in the tRNA / RNase P model, the unpaired CCA at the 3' end of tRNA is close to the L15 region. The L15 loop would have to move in order to interact with the ptRNA substrate. The fact that the P15 / L15 / P16 region seems to be quite dynamic indicates that this may be a region where conformational changes occur to accommodate the substrate. The model, although built independently, has an overall similarity to an RNA / holoenzyme model previously proposed (Tsai et al., 2003), suggesting that the holoenzyme model captures the general location of the protein correctly.
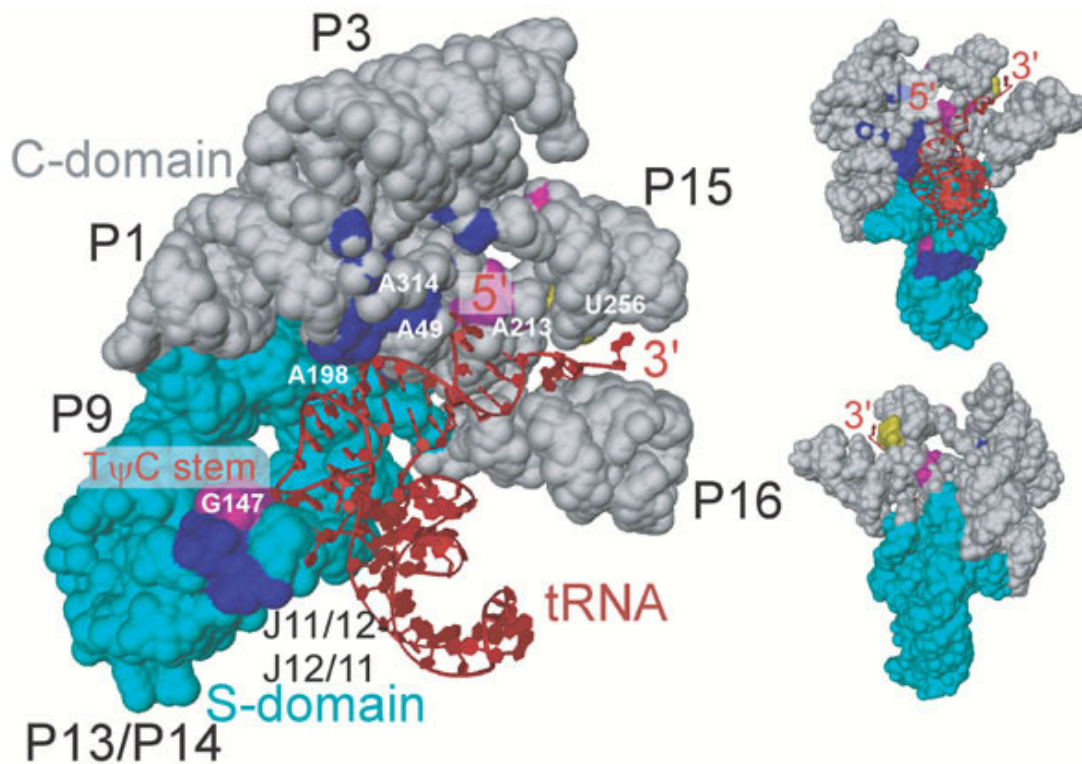
Fig. 1.7: Model of RNase P - tRNA interaction (Torres-Larios et al., 2005). The diagram shows the accessible surface area of P RNA and a diagram of tRNA[Phe]. The model was built using the higher resolution structure of the *T. thermophilus* S-domain as a guide, as the interactions between the S-domain nucleotides and the tRNA T (TΨC) stem are well characterised (Loria & Pan, 1997). Colour coding is as follows: dark blue, nucleotides in the universally conserved regions; pink, highly conserved nucleotides in bacteria; and yellow, the L15 region that interacts with the ptRNA CCA 3' end. The views are as follows: the concave side of RNase P (left); down the anti-codon arm of tRNA (top right); and backside of the molecule (bottom right). The general active site location is marked by the 5' end of the tRNA molecule, in the vicinity of universally conserved nucleotides A49, A314 and the highly conserved bacterial nucleotide A213. The model conveys the general arrangement of the two molecules and the excellent fit between the tRNA and the two major regions of interaction with P RNA.

The full-length ptRNAs are not the only substrates recognised by RNase P RNAs and holoenzymes. The 4.5S RNA is a natural non-ptRNA substrate for RNase P that mimic the structure of the tRNA acceptor stem (Kirsebom & Vioque, 1995). The 10 SA RNA and certain plant viral RNAs have tRNA structural mimics near the end of RNA sequences that are processed by RNase P (Guerrier-Takada et al., 1988; Komine et al., 1994; Mans et al., 1990). Also, the 5' maturation of C4 RNA of phages P1 and P7 depends on the RNase P (Hartmann et al., 1995). Studies of small model substrates have demonstrated that an RNA mini-helix consisting solely of T and acceptor stem (and including a 5' leader) is cleaved by RNase P, albeit with an approx. 100-fold increased K_m (McClain et al., 1987; Hardt et al., 1993; Schlegl et al., 1994; Hansen et al., 2001). The loss of binding energy for the

interaction of RNase P with the mini-helix could be either due to the loss of recognition elements in the D and anticodon arms or to a loosening of the T-loop structure, which is normally fixed in space by interactions with the D loop.

2   *The goal of the project*

The ribonucleoprotein enzyme ribonuclease (RNase) P is an endonuclease that generates the mature 5' -ends of tRNA. Bacterial RNase P enzymes are composed of a catalytic RNA subunit of about ~400 nucleotides (nt) in length, and a single small protein of typically 120 amino acids. Under physiological conditions, both subunits are essential for catalysis. However, it was shown *in vitro* that the catalytic function resides in the RNA subunit (P RNA) and can be activated in the absence of the protein by elevated metal ion concentrations. Although much progress has been made, there are still many questions that have not been answered. The enzyme-substrate and RNA-protein subunit interactions as well as the chemical details of the hydrolysis reaction are not fully understood. The focus of this study was to investigate the role played by divalent cations as well as functional groups in P RNA catalysis. Specific aspects of substrate binding and cleavage were analysed and discussed separately in three different parts.

The role of divalent cations in E. coli P RNA catalysis: studies with Zn^{2+} as catalytic cofactor

The reaction catalysed by *E. coli* P RNA requires mono- and divalent cations. Monovalents cations are required for the stabilisation of the RNA structure in a functionally active conformation. Divalent cations are predominantly involved in the cleavage reaction itself. In order to obtain new information into how metal ions modulate this ribozyme system, different effects of Zn^{2+} and Sr^{2+} on processing by *E. coli* P RNA were investigated: catalysis and its inhibition by Sr^{2+} in particular, changes in enzyme-substrate affinity and alterations in the fraction of substrate able to bind to the enzyme.

Chemical modification studies: the role of 2'-hydroxyl groups at the cleavage site and neighbouring positions

2'-hydroxyls within the ptRNA may serve as H-bond donors or acceptors for specific residues of RNase P RNA and, furthermore, may be involved in binding of metal ions. Moreover, the 2'-substituent of ribose is the primary determinant of the ribo-conformation. In order to analyse separately different functional aspects of the 2'-hydroxyl groups (e.g. H-bond donor or acceptor function, stabilisation of the ribo-conformation) that may contribute to P RNA catalysis, the effects of different chemical modifications (deoxy, fluoro, methoxy and LNA) introduced into the ptRNA substrate (analysed positions: –2, –1 and +1) were investigated.

Modification interference studies: an approach to identify functional groups that interfere with the cleavage reaction

Nucleotide analogue interference mapping (NAIM) is a biochemical approach that allows to identify important functional groups within catalytically active RNA molecules. This method has been previously applied to detect positions within P RNA that interfere with substrate binding (Heide et al., 1999). In that study, the gel retardation method was applied in order to separate active molecules (P RNA - tRNA complexes) from those with impaired function (unbound fraction). The focus of the work described here was to develop a new approach suitable for the detection of functional groups important for the cleavage reaction itself. These groups may contact the substrate or coordinate catalytic metal ions, and their substitution is expected to interfere with processing. Therefore, a *cis*-cleaving RNA conjugate consisting of P RNA tethered to a tRNA 5' -half was constructed. By annealing of this conjugate to a tRNA 3' -half construct, a functional substrate was reconstituted. Using the *cis*-cleavage assay, active molecules (i.e. RNA cleavage products containing the RNase P sequence) could be separated from those less active or inactive (uncleaved RNA conjugates). An optimisation of the cleavage reaction and characterisation of the RNA conjugate by kinetic experiments was necessary in order to establish conditions under which *trans*-cleavage is excluded. Additionally, other parameters to be used in the modification interference experiments, like pH, salt concentrations temperature and time course of the reaction had to be defined first. Finally, the principle of the method was proved with an application example, in which IMPαS interference patterns obtained via the *cis*-cleavage assay (the new method) were compared with those obtained by the gel retardation approach (Heide et al., 1999).

3   *Materials & Methods*

3.1 Methods of bacterial cell culture

3.1.1 Sterilisation

All media and buffers were sterilised for 20 minutes at 121 °C and 1 bar. Solutions that are unstable or sensitive to heat were filtered using nonpyrogenic 0.2 µm filtration units.

3.1.2 Cell culture in liquid medium

LB- (Luria Bertani-) medium:

10 g / l Pepton 140

5 g / l Yeast extract

10 g / l NaCl

the pH was adjusted with NaOH to 7.5

E. coli cells from either an agar plate, overnight culture or glycerol stock were inoculated in sterile LB medium and incubated overnight at 37 °C while shaking. In order to select *E. coli* cells that contain a certain plasmid, the appropriate antibiotic was added to the medium (e.g. 100 µg / ml ampicillin if the plasmid harbours the ampicillin resistance cassette). To prepare glycerol stocks, 500 µl cell culture were thoroughly mixed with 500 µl 99.8 % sterile glycerol, frozen in nitrogen and stored at -70 °C.

3.1.3 Cell growth on agar plates

For preparing agar plates, 12 g agar were added to 1 l LB medium (3.1.2) and sterilised (3.1.1). After sterilisation, the agar solution was homogenised by stirring and then cooled down. When the temperature reached approximately 50 °C, the appropriate antibiotic was added. Aliquots (~ 20 ml) were poured into sterile Petri dishes. After the agar medium became solid, the plates were transferred to 4 °C and stored upside down until use. In order to grow *E. coli* cells on agar plates, the cell suspension (150 to 200 µl of a transformation) was streaked out on a plate using a sterile glass pipette. When the surface of the agar plates became dry, they were turned upside down and incubated overnight at 37 °C.

3.1.4 Competent cells

In order to take up exogenous DNA, cells must first be made permeable. This state is referred to as competency. Incubating with $CaCl_2$ and cold treatment affects the structure and permeability of the cell wall. This causes bacterial cells (*E. coli*) to become competent

and take up plasmid DNA during transformation.

To prepare competent cells, an *E. coli* strain was streaked directly from a frozen stock onto an LB medium agar plate and incubated overnight at 37°C. A single colony was selected, transferred to 3 ml LB medium and incubated overnight at 37°C with vigorous shaking. 500 ml LB medium were inoculated with 1 ml from the overnight culture in a 1 l flask and incubated with vigorous shaking at 37°C until an optical density (OD_{600}) of 0.6-0.8 (~ 3 h; cell growth in the logarithmic phase) was obtained. The OD_{600} was measured every 20-30 minutes. The cell culture was transferred into a sterile 500 ml centrifuge basket, cooled on ice for 10 minutes and cells were harvested by centrifugation at 3200 x g and 4°C for 10 min. After centrifugation, the medium was carefully decanted and the bacterial pellet resuspended in 100 ml of ice-cold 100 mM $CaCl_2$. The volume was divided into two 50 ml tubes and the cells were recovered by a second centrifugation at 10000 x g and 4°C for 10 minutes. After resuspending each pellet in 7.5 ml ice-cold 75 mM $CaCl_2$ / 25 % glycerol, ~ 200 µl aliquots were withdrawn, transferred to sterile microfuge tubes and stored at -70°C.

3.1.5 Transformation of *E. coli* cells

The uptake of exogenous DNA by cells that alters the phenotype or genetic trait of a cell is called transformation. The number of cells transformed per 1 µg of DNA is called the transformation efficiency. Too little DNA can result in low transformation efficiencies, but too much DNA also inhibits the transformation process.

E. coli cells are normally killed by the antibiotic ampicillin. Ampicillin damages the bacterial cell wall by inhibiting the crosslinking of polysaccharide chains during cell wall synthesis. The resulting, structurally weak cells are prone to spontaneous lysis in the hypotonic media in which they are grown. For *E. coli* to survive in the presence of ampicillin, the organism needs a resistance-conferring gene (β-lactamase encoding gene). During transformation, this gene is introduced with the plasmid. Therefore, by adding ampicillin to the culture medium, only bacteria that contain the plasmid will survive.

Sterile SOC medium:	2 % (w / v) Pepton 140
	0.5 % (w / v) Yeast extract
	2.5 mM KCl
	10 mM NaCl
	10 mM $MgCl_2$
	10 mM $MgSO_4$
	20 mM Glucose
	the pH was adjusted with NaOH to 7.5

E. coli competent cells were thawed on ice; 50 µl of the cell suspension were mixed with 20 ng plasmid DNA, 5 µl of a DNA ligation (3.3.8) reaction mix or 2 µl of a PCR mutagenesis (3.3.5) reaction product in an microfuge tube and incubated on ice for 30 minutes. Then the cells were exposed to a short heat shock (60 s at 42°C). After 2 minutes cooling on ice, 800 µl SOC medium were added and the cells incubated for 1 h at 37°C in a thermo-mixer with gentle agitation. After a short centrifugation in a bench top centrifuge, 700 µl of the supernatant were removed and the cell pellet was resuspended in the remaining supernatant (about 150 µl). Finally, the cell suspension was streaked out on LB agar plates (3.1.3) containing the appropriate antibiotic. For further details see 3.1.3.

3.2 General nucleic acid techniques

3.2.1 Nucleic acid gel electrophoresis

When molecules are placed in an electric field, they will migrate to the respective electrode with a velocity (electrophoretic mobility) proportional to the field strength and the net charge of the molecule. Polynucleotide chains of DNA or RNA are polyanions and migrate to the positive electrode (anode) when placed in an electric field. Since nucleic acid molecules migrate to the anode through the pores of a matrix of polyacrylamide or agarose, their velocity is significantly influenced by the size of both the molecule and the pores. Therefore, in a gel, larger molecules show a decreased electrophoretic mobility compared to smaller molecules with the same charge density. Generally, optimal electrophoresis conditions are often determined empirically for each situation, taking into consideration fragment length, required resolution and available time.

Agarose gel electrophoresis

TBE-buffer (5 x concentrated):

445 mM Tris-HCl

445 mM Boric acid

10 mM EDTA

the pH was adjusted to 8.0 with HCl

DNA sample buffer (5 x concentrated):

0.25 % (w / v) Bromophenol blue

0.25 % (w / v) Xylene cyanol blue

25 % (w / v) Glycerol

in 5 x TBE buffer; pH 8.0

Ethidium bromide-dye solution:

10 mg / ml in 1 x TBE buffer

Crystal violet solution:

10 mg / ml in 1 x TBE buffer

Agarose (a linear polysaccharide of galactose and a galactose derivative) is crosslinked by hydrogen bonds. Adjusting the agarose concentration can vary the pore size in the gel matrix. The pores in agarose gels are larger than in polyacrylamide gels, and these gels are used to resolve large double-stranded DNA fragments (table 3.1).

Table 3.1: Range of separation in gels containing different amounts of agarose

% agarose (w / v)	DNA fragment size (kbp)
0.5	1.0 – 30
0.7	0.8 – 12
1	0.5 – 7.0
1.2	0.4 – 6.0
1.5	0.2 – 3.0
2.0	0.1 – 2.0

The agarose is dissolved in 1 x TBE buffer by heating up to the boiling point in a microwave oven. For analytic gels, 2 µl of 10 mg / ml ethidium bromide solution were added to 50 ml agarose solution and thoroughly mixed. The solution was cooled down under stirring to avoid solidifying of agarose on the walls of the glass bottle. When it reached 50 – 60°C, the solution was poured into the electrophoresis tray.

Since ethidium bromide is a powerful mutagen and DNA fragments stained with ethidium bromide dye are visible only under UV-light, for preparative gels, crystal violet at a final concentration of 10 µg / ml (in the agarose solution as well as in the running buffer) was used preferentially.

Before loading onto the gel, the samples were mixed with 1 / 4 volume of native (non-denaturing) DNA sample buffer (5 x). To determine the size of the separated DNA fragments, a commercially available DNA size marker was resolved in a parallel lane. The electrophoresis was performed at 60 or 120 mA, depending on the width of the gel. After electrophoresis, the DNA fragments were detected under UV-light (ethidium bromide agarose gels, orange fluorescent bands) or visible light (crystal violet agarose gels, dark blue bands).

Polyacrylamide Gel Electrophoresis (PAGE)

Polyacrylamide gels are generated by crosslinking polymers of acrylamide with the

co-monomer bis-acrylamide. The covalent crosslinking reaction is catalysed by TEMED, a tertiary amide, and initiated by ammonium persulfate (APS). Varying the concentration of acrylamide and bis-acrylamide can generate a wide range of pore sizes.

Denaturing PAGE

Denaturing sample buffer (2 x concentrated):

> 0.02 % (w / v) Bromphenol blue (BPB)
>
> 0.02 % (w / v) Xylene cyanol blue (XCB)
>
> 2.6 M urea
>
> 66 % (v / v) Formamide
>
> in 2 x TBE buffer; pH 8.0

For separation and purification of single-stranded DNA or RNA it is necessary that the gel is polymerised in the presence of a denaturing agent (7-8 M urea, or less frequently, 98% formamide) that suppresses base paring in nucleic acids.

In table 3.2, the sizes of DNA / RNA fragments (in nucleotides) are given that co-migrate with the two dyes of the sample buffer in denaturing polyacrylamide gels.

Table 3.2: Single-stranded fragments (in nucleotides) that migrate with dyes in denaturing polyacrylamide gels

% polyacrylamide	BPB	XCB
5	35	130
6	26	106
8	19	70-80
10	12	55
20	8	28

The gel solution contains: 8 M urea

> 1 x TBE buffer pH 8.0
>
> acrylamid / bis-acrylamide
>
> (the appropriate concentration)

After the urea was completely dissolved the final volume was adjusted with water and the solution was filtered through a filter paper to remove potential impurities. The glass plates were cleaned with 70 % ethanol and eventually treated with silicon solution (blue slick) that prevents the gel from sticking tightly to the glass plates and reduces the possibility that the gel will tear when it is removed from the plates after electrophoresis is completed. When the glass plates were assembled, APS (1 / 100, v / v) and TEMED (1 / 1000, v / v) were added to the gel solution and thoroughly mixed. The solution was poured immediately

between the glass plates to avoid premature polymerisation. A comb was introduced into the upper end of the mold to create pockets for loading the samples. After polymerisation (about 1 h after pouring the gel solution), the comb was carefully removed and the resulting pockets were immediately rinsed using a syringe with 1 x TBE buffer to remove unpolymerised acrylamide. Shortly before loading the samples, the pockets were rinsed again with 1 x TBE buffer to remove urea that diffuses from the gel matrix and tends to accumulate in the pockets. After all samples were loaded, a current of 8 to 30 mA (depending on the concentration of acrylamide / bis-acrylamide and the size of the gel) was applied.

Native PAGE

Native polyacrylamide gels are non-denaturing. They do not contain denaturing agents and are used for separation and purification of double-stranded DNA / RNA. The electrophoretic mobility of DNA / RNA fragments through native polyacrylamide gels is affected by their structure, so that DNA fragments of exactly the same size can differ in mobility by up to 10 %. This is why native polyacrylamide gels can only be used to determine the size of double-stranded DNAs accurately. In table 3.3, the approximate sizes of DNA fragments (in base pairs) that co-migrate with the two dyes of the sample buffer in non-denaturing polyacrylamide gels of different concentration are given.

Table 3.3: Double-stranded DNA fragments (in base pairs) that migrate with dyes in non-denaturing polyacrylamide gels

% polyacrylamide	BPB	XCB
3.5	100	460
5	65	260
8	45	160
12	20	70
20	12	45

The composition of native polyacrylamide gels is similar to that of denaturing gels except for the absence of a denaturing agent:

<div align="center">

1 x TBE buffer pH 8.0

The appropriate concentration of

Acrylamid / Bis-acrylamide

</div>

The procedure was exactly the same as described for denaturing PAGE.

Choice of gel system

For most instances, the size range of the samples determined the choice of gel system for both analytical and preparative work. Double-stranded DNA fragments shorter than 100 bp were resolved on native polyacrylamide gels, while agarose gels were used for fragments between 100 bp and 10 kbp,

To resolve single-stranded DNA / RNA, denaturing polyacrylamide gels were used. Typical polyacrylamide gels of 1 mm thickness and a wide size range of pockets (0.5 to 6 cm) were used for analytical reasons as well as purification of large amounts of RNA. For purification of small amounts of RNA, thinner gels of 0.5 mm were preferred because elution by diffusion was more efficient and a better resolution was obtained.

The 0.5 mm thin gels were also preferred in those cases where high resolution was required (e.g. to separate a multitude of products generated by iodine cleavage as well as alkaline or enzymatic hydrolysis of RNA or partially modified RNA pools). A long separation distance was also prefered in these cases (the length of the gel was about 40 cm) to completely resolve the RNA fragments of interest.

3.2.2 Ethanol precipitation of nucleic acids

Ethanol precipitation is the most straightforward method to concentrate nucleic acids from aqueous solutions. In 70 % ethanol the nucleic acids become insoluble and precipitate, while most salts will remain predominantly in solution and can thus be removed. Therefore, ethanol precipitation is also very useful when changes in salt conditions are required. When short RNA / DNA molecules (< 20 nucleotides in length) or very small amounts of RNA / DNA had to be precipitated, a better recovery was obtained if glycogen (20 to 40 μg) was used as carrier during the precipitation.

For precipitation, to 1 volume of RNA / DNA solution either $^1/_{10}$ volume of 3 M NaOAc pH 5 for precipitating unmodified RNA / DNA or $^1/_5$ volume of 2 M NH_4OAc pH 7 for NMPαS modified RNA (to avoid RNA degradation due to low pH) were added. After addition of 2.2 or 2.7 volumes of absolute ethanol, respectively, the sample was thoroughly mixed. If necessary, 20 to 40 μg glycogen or carrier RNA was added. The sample was stored at –20°C for at least 1 h and then centrifuged at 15 000 x g and 4°C for 1 h. The supernatant was removed with a sterile tip and the pellet eventually washed with 70 % ethanol, if a high salt concentration was present in the initial RNA / DNA solution, and centrifuged for another 15 minutes at 15 000 x g and 4°C. Finally, the supernatant was removed completely and the pellet dried at room temperature. The required time for drying the pellet depended on pellet size. When drying was complete (pellet became transparent), the pellet was resuspended in the desired volume of sterile double distilled water or appropriate buffer.

3.2.3 Phenol / Chloroform extraction

This method was applied to remove proteins from aqueous nucleic acids solutions. The DNA / RNA solution was thoroughly mixed (for about 2 min) with an equal volume of phenol (saturated with 10 mM Tris-HCl, 1 mM EDTA, pH 7.5-8.0) on a shaker and centrifuged for 2 min at 15 000 x g and room temperature. During extraction with phenol, the proteins accumulate in the organic phase and the interphase while the nucleic acids remain in the aqueous phase (the upper phase). Because phenol is a strong inhibitor for many enzymes, it is necessary to remove it completely in order to avoid problems in downstream applications. This was accomplished by two sequential extractions with an equal volume of chloroform applying the same procedure as in the case of phenol extraction. The phenol / chloroform extraction was usually followed by NAP / NICK gel filtration for desalting (3.2.7) and / or ethanol precipitation (3.2.2).

3.2.4 Detection of nucleic acids

Ethidium bromide staining

Ethidium bromide staining solution:

300 ng / ml in 1 x TBE buffer; pH 8.0

Non-radioactive RNA / DNA was most frequently visualised in polyacrylamide gels by staining with the intercalating dye ethidium bromide. When electrophoresis was complete, the current was turned off and the glass plates were carefully removed from the gel. Analytic gels were incubated for 10 minutes at room temperature in ethidium bromide staining solution with gentle agitation. After incubation, the gel was transferred onto the glass plate of an UV-transilluminator (366 nm) and the RNA / DNA fragments were visualised and documented using a dedicated digital camera system. For double stranded DNA the limit of detection was 40 ng / 1 cm wide band. In the case of single stranded DNA and RNA; the interaction between nucleic acid and the dye is considerably weaker and the colour intensity may be 5 to 10 fold lower using the same amount of nucleic acid. Depending on the specific sequence, some oligonucleotides do not stain at all with the ethidium dye.

Ethidium bromide was used also to detect DNA in agarose gels. In this case the ethidium bromide dye was incorporated in the agarose gel before electrophoresis (0.4 µg / ml; see agarose gel electrophporesis 3.2.1) and not by staining in dye solution.

UV-shadowing

In the case of polyacrylamide preparative gels, DNA / RNA fragments were visualised by UV-shadowing (256 nm) without staining. After electrophoresis, the glass plates were carefully removed; the gel was wrapped in transparent foil and placed on a fluorescent

chromatography plate covered in plastic wrap. A short wave hand-held UV lamp was used to locate the band of DNA or RNA, which, when absorbing the UV light, appears as a dark shadow against the bright green plate. The limit of detection is about 1 µg / 1 cm wide band. Exposure time was minimised to avoid accumulation of UV-induced damage.

Autoradiography

^{32}P radiolabelled RNA / DNA was detected with the help of a phosphorimaging analyser. The gel was wrapped with plastic foil and an image plate was exposed to it. The exposition time depended on the amount of radioactivity loaded on the gel (e.g. 1 min for a labelling reaction; overnight to resolve kinetic experiments). Then the image plate was scanned with the help of a phosphoimager using the BasReader software. The obtained image was analysed and quantified using the program AIDA.

Double-stranded DNA detection using crystal violet

Crystal violet is a dye that binds to DNA via electrostatic interactions. These interactions are strong in the presence and weak in the absence of an electric field. Therefore the DNA band of interest should be excised immediately after the electric field is switched off; the limit of detection (80 ng / cm band) using crystal violet is higher than that for ethidium bromide (40 ng / cm band).

For preparing and electrophoresis of agarose gels with crystal violet see paragraph describing the agarose gel electrophoresis (3.2.1). Immediately after electrophoresis, the agarose gel was placed on a clean glass plate. The glass plate was placed on a white surface (white paper) for a better detection of DNA bands of interest. The bands were excised under visible light using a sterile scalpel.

3.2.5 Gel elution of nucleic acids

The elution method adopted depended on the gel matrix, the molecular weight and the type of the nucleic acid.

Elution by diffusion

Elution by diffusion was applied to elute RNA molecules or DNA oligonucleotides from denaturing polyacrylamide gels. The DNA / RNA band of interest, detected by UV-shadowing or using a phosphoimager (radiolabelled RNA / DNA), was excised and incubated overnight in 5-8 volumes of elution buffer at 4°C while shaking. The eluate was precipitated with ethanol (see 3.2.2) and the RNA / DNA pellet dissolved in sterile RNase / DNase free water.

Different elution buffers were used depending on the application:

RNA elution buffer 1:

200 mM Tris / HCl, pH 7.0; 1 mM EDTA; 0.1% SDS; (SDS was also omitted when the eluted RNA was to be used in a downstream application that could be inhibited by the presence of small amounts of residual detergent). This buffer was efficient for elution of P RNA and P RNA –tRNA tandem constructs.

RNA elution buffer 2:

1 M NH$_4$OAc; pH 7.0. This buffer was preferentially used for elution of RNAs randomly modified with nucleotide analogues.

RNA elution buffer 3:

1 M NaOAc; pH 5.0. This buffer was preferentially used for elution of radiolabelled ptRNA substrates. This buffer limits RNase induced degradation due to the low pH.

Spin column elution

Spin column elution was applied for extraction of (double stranded) DNA fragments from agarose gels. The method involves mechanical destruction of the gel matrix and extraction of DNA-containing buffer by centrifugation. The band containing the DNA fragment of interest was excised from an ethidium bromide- or crystal violet-stained agarose gel and cut into smaller pieces. These were loaded onto special spin columns with filters that retain the agarose. The spin columns, placed on top of microfuge tubes, were centrifuged for 1 min at high speed and the DNA in the flowthrough was precipitated with ethanol (3.2.2).

Different commercially available spin columns were used as well as homemade ones. The self-prepared ones were constructed using a 1.5 ml microfuge tube (without lid) with a piece of Whatmann paper inside, serving as filter and a small hole at the bottom. The agarose gel slice was placed on top of the whatmann paper and the tube on top of another tube. After 1 min centrifugation, the DNA solution could be collected from the lower tube and precipitated (3.2.2).

3.2.6 **Concentration determination of nucleic acids**

By determining the absorbance at 260 nm (A$_{260}$), the concentration of nucleic acids can be calculated according to the Lambert-Beer law:

$$E = \varepsilon \text{ x c x d}$$

where ε = molar extinction coefficient [1 / (M x cm)]; d = the path length of the cuvette [cm]; c = molar concentration of DNA / RNA [M].

1 µl of stock DNA / RNA solution was diluted in 299 µl water and the absorbance at 260 nm (A_{260}) measured relative to water using a UV-spectrophotometer. The concentration was calculated using the known values $c(1\ A_{260})$ that represents the concentration corresponding to one absorbance unit at 260 nm ($1\ A_{260}$):

1 A_{260} double-stranded DNA corresponds to a $c(1\ A_{260})$ of ~ 50 µg / ml

1 A_{260} single-stranded DNA corresponds to a $c(1\ A_{260})$ of ~ 33 µg / ml

1 A_{260} RNA corresponds to a $c(1\ A_{260})$ of ~ 37 µg / ml

The general formula for calculation of RNA / DNA concentration was:

$$c\,[\mu g / \mu l] = \frac{A_{260} \times c(1 A_{260}) \times D_f}{1000} \qquad (3.2.1)$$

c = concentration in µg / µl; D_f = dilution factor that was applied to the stock solution (= 300).

To determine concentrations with high precision (e.g. for enzyme kinetic experiments), a more laborious procedure was applied. 1 µl RNA was diluted in 299 µl of 50 mM NH_4OAc solution, pH 7.0 and the A_{260} of the RNA dilution ($A_{260}^{\text{intact RNA}}$) was measured relative to the NH_4OAc reference solution. Then a mixture of RNases (0.5 µg RNase A, 0.01 U RNase T1, 0.01 U RNase T2) was added to this dilution and incubated for at least 3 hours at room temperature or 37°C to ensure that the RNA was quantitatively degraded to single nucleotides. Then the A_{260} for the solution of hydrolysed RNA ($A_{260}^{\text{hydrolysed RNA}}$) was measured. The RNA concentration that corresponds to 1 A_{260} was calculated as follows:

- The molar extinction coefficient for the whole RNA molecule was calculated as the sum of extinction coefficients of the individual nucleotides:

$$\varepsilon_{\text{RNA}} = \sum_{1}^{n_A} \varepsilon_A + \sum_{1}^{n_C} \varepsilon_C + \sum_{1}^{n_G} \varepsilon_G + \sum_{1}^{n_U} \varepsilon_U \qquad (3.2.2)$$

where $\varepsilon_A, \varepsilon_C, \varepsilon_G, \varepsilon_U$ are the extinction coefficients for the individual ribonucleotides after hydrolysis; n_A, n_C, n_G and n_U are the numbers of each nucleotide contained in the RNA sequence.

- A new extinction coefficient was calculated:

$$\varepsilon'_{RNA} = \frac{A_{260}^{intact\ RNA}}{A_{260}^{hydrolysed\ RNA}} \times \varepsilon_{RNA}$$

(3.2.3)

- Using the new extinction coefficient, the concentration that corresponds to 1 A_{260} was calculated:

$$c(1\ A_{260})\ [\mu g\ /\ \mu l] = \frac{1}{\varepsilon'_{RNA} \times d} \times M_r$$

(3.2.4)

where M_r is the molecular weight of the analysed RNA. The concentration of the RNA stock solution was then calculated using equations (3.2.1) and c(1 A_{260}) calculated with equation (3.2.4).

3.2.7 NAP / NICK gel filtration

NAP / NICK columns sold by Pharmacia are filled with Sephadex G 25 or G 50, a gel filtration matrix. They are used to remove salts and mononucleotides from nucleic acid solutions. By this method up to 97 % RNA / DNA can be recovered while more than 90 % of the low molecular weight impurities are removed. In this work NAP 5 and NAP 10 columns were used.

The columns were equilibrated with RNase free water. An exact volume (as defined by the supplier) of the nucleic acid solution was loaded onto the column and entered the gel matrix by gravity flow. Elution of the nucleic acids was accomplished by adding another precisely defined volume of RNase free water. For details, refer to the respective instruction manuals.

3.3 DNA techniques

3.3.1 Plasmid DNA isolation from *E.coli* cells

Plasmid purification protocols are based on a modified alkaline lyses procedure (Birnboim & Doly, 1979; Birnboim, 1983), followed by binding of plasmid DNA to an anion exchange resin (preparative plasmid preparation) or a silica membrane (analytical preparation) under appropriate low salt and specific pH conditions. RNA, proteins, dyes, and low-molecular-weight impurities are removed by a wash at intermediate ionic strength.

Plasmid DNA is eluted in high salt buffer and then concentrated and desalted by isopropanol precipitation. Two different brands of commercially available plasmid purification kits (Macherey-Nagel, Qiagen) were used.

Analytical plasmid preparation

For analytical porposes, small-scale plasmid preparation was applied using the miniprep kits from Macherey-Nagel or Qiagen. The cells from 2 ml of an overnight *E. coli* LB culture were harvested by centrifugation for 2 minutes in a bench top centrifuge. After discarding the supernatant, the cell pellet was resuspended in 250 μl of cell resuspension buffer. Then 250 μl lysis buffer were added and mixed gently by inverting the tube 6-8 times. The lysate was incubated at room temperature for a maximum of 5 min, then 300 μl of neutralisation buffer were added and mixed gently by inverting the tube 6-8 times. The supernatant was clarified by centrifugation for 5-10 min in a bench top centrifuge and loaded onto a DNA binding column equipped with a silica membrane. The column was placed on top of a microfuge tube and centrifuged for 1 min in a bench top centrifuge. After discarding the flowthrough, ethanol-containing wash buffer was added to the column which was centrifuged again for 1 min at 11000 x g. After discarding the flowthrough, the DNA was eluted with 80 μl elution buffer in the same manner, this time using a clean tube to collect the eluate. A small aliquot of this solution was checked by restriction digest or sequencing.

Preparative plasmid preparation

Cell resuspension buffer: 50 mM Tris / HCl, pH 8.0; 10 mM EDTA; 100 μg / ml RNase A;
Lysis buffer: 200 mM NaOH; 1 % SDS;
Neutralisation buffer: 3 M KOAc, pH 5.5;
Column equilibration buffer: 750 mM NaCl; 50 mM MOPS, pH 7.0; 15 % isopropanol; 0.15 % Triton X-100;
Wash buffer: 1 M NaCl; 50 mM MOPS, pH 7.0; 15 % isopropanol;
Elution buffer: 1.25 M NaCl; 50 mM Tris / HCl, pH 8.5; 15 % isopropanol;

Preparative plasmid preparation was applied to purify large amounts of DNA (~ 500 μg from a maxiprep and ~ 200 μg from a midiprep).

- A single colony, picked from an agar plate incubated overnight, was used to inoculate a starter culture of 3 ml LB medium containing the appropriate selective antibiotic and incubated overnight at 37°C with vigorous shaking.
- 2 ml of the starter culture were added to 150 ml (midiprep) or 500 ml (maxiprep) selective LB medium and incubated at 37°C for 12 − 20 h (until OD_{600} ~ 1) with

vigorous shaking. An Erlenmeyer flask of 250 ml (midiprep) or 1500 ml (maxiprep) volume was used.

- The bacterial cells were harvested by centrifugation at 10000 (midiprep) or 3200 (maxiprep) x g for 15 min at 4°C and the supernatant was removed.

- The bacterial pellet was homogenously resuspended in 4 ml (midiprep) or 10 ml (maxiprep) of cell resuspension buffer by vortexing.

- 4 ml (midiprep) or 10 ml (maxiprep) lysis buffer were added, mixed gently by inverting 4 – 6 times, and incubated at room temperature for 5 min.

- 4 ml (midiprep) or 10 ml (maxiprep) of neutralisation buffer were added, mixed immediately but gently by inverting the tube 4 – 6 times and incubated on ice for 15 min. Precipitation of cell debris and inclusion bodies is enhanced by using neutralisation buffer and incubating on ice.

- The suspension was then centrifuged at 10000 x g for 15 min at 4°C, the plasmid - containing supernatant was loaded onto the anion exchange column previously equilibrated 3 times with 4 ml (midiprep) or 10 ml (maxiprep) equilibration buffer.

- After the supernatant had entered the column by gravity flow, two washing steps with 10 ml (midiprep) or 30 ml (maxiprep) wash buffer were applied. When the column stopped flowing, the DNA was eluted with 5 ml (midiprep) or 15 ml (maxiprep) elution buffer and precipitated with 0.7 volumes of isopropanol, followed by centrifugation at 4°C and 10000 x g for 1 h.

- The supernatant was removed, the DNA pellet washed with 2 ml of 70 % ethanol to remove residual salt and centrifuged for another 10 min. The ethanol was completely removed, the pellet dried at room temperature and resuspended in an appropriate volume of sterile water using a shaker. When the pellet was completely dissolved, the DNA yield was determined (see 3.2.6).

3.3.2 Digesting DNA with restriction endonucleases

Type II endonucleases recognise sequences (generally palindromes) in double-stranded DNA with a length of 4 to 8 base pairs. They catalyse the hydrolysis at a very well defined location (generally on both strands of the double helix) within this recognition site and, depending on the enzyme, generate 5' or 3' overhangs ('sticky' ends) or blunt ends with 3'-hydroxyl and 5'-phosphate termini.

For the cleavage reaction with restriction enzymes, the 10 x buffer supplied with the respective enzyme was used.

Restriction digest, 20 µl:		final concentration
DNA 1 µg / µl	16 µl	0.1 µg / µl
10 x restriction buffer	2 µl	1 x
10 U / µl restriction enzyme	2 µl	0.01 U / µl

The reaction mix was incubated for 3 h at the appropriate temperature (specified by the supplier). After digestion, the enzyme was removed by phenol / chloroform extraction (3.2.3) or deactivated by heating. The digested DNA was precipitated with ethanol (3.2.2) and dissolved in water. Depending on the size of the DNA fragments obtained after digestion, the restriction reaction was checked either by native PAGE for fragments shorter than 100 bp or agarose gel electrophoresis for DNA fragments longer than 100 bp (3.2.1).

In some cases (e.g. when digested DNA was further subjected to a ligation reaction), it was necessary to separate and purify the DNA fragments by agarose gel electrophoresis (3.2.1) followed by gel elution (3.2.5).

Simultaneous DNA digestion with two restriction enzymes (usually supplied in 50 % glycerol) was performed if the buffer conditions were suitable for both endonucleases. In this case, only half the amount of each enzyme (1 µl instead of 2 µl) was added (in order to keep the glycerol concentration ≤ 5 %).

3.3.3 Removing the 5'-terminal phosphate group from nucleic acids

<u>C</u>alf <u>I</u>ntestinal <u>P</u>hosphatase (CIP) catalyses the hydrolysis of terminal 5´-phosphate groups from DNA, RNA, as well as ribonucleoside and deoxyribonucleoside triphosphates. This enzyme was mostly used to prevent religation or catenation of vector DNA (i.e. plasmids) by removing phosphate groups from both 5´-termini.

5' dephosphorylation reaction, 20 µl:		final concentration
DNA (x µg / µl)	x µl	0.1 µg / µl
10 x dephosphorylation buffer	2 µl	1 x
calf intestinal phosphatase (CIP) 0.1 U / µl	2 µl	0.01 U / µl
RNase / DNase free water	to 20 µl	

The reaction components listed above were mixed and incubated for 1 h at 37°C.

Then 190 µl RNase-free water were added, CIP was removed by phenol-chloroform extraction (3.2.3) and the RNA / DNA from the aqueous phase precipitated with ethanol (3.2.2) and dissolved in water or in an appropriate buffer.

3.3.4 Polymerase Chain Reaction (PCR)

Polymerase chain reaction (PCR; Saiki et al., 1985) is a powerful method to amplify very small amounts of DNA. The components required for PCR are listed below:

- a thermostable DNA polymerase that catalyses template-dependent synthesis of DNA. In this work, a DNA polymerase with proofreading activity from *Pyroccocus furiosus* (Pfu polymerase; Promega) was generally used to avoid mutations in the amplification product.

- a DNA template that contains the target sequence. It can be added to the PCR in single- or double-stranded form.

- a forward and a reverse DNA primer. Careful design of primers is required to obtain the desired product in high yield, to avoid amplification of unwanted sequences, and to facilitate subsequent manipulation of the amplified product

- a buffer containing magnesium ions. Divalent cations are required for the activity of the enzyme. Because deoxynucleoside triphosphates (dNTPs) bind magnesium ions, the molar concentration of divalent cations should exceed the concentration of phosphate groups contributed by dNTPs and primers.

- the four deoxynucleoside triphosphates (dNTPs). They are the substrates for the DNA polymerase and are generally added in equimolar amounts to the PCR mix.

There are three major steps in a PCR, which are repeated for 25 to 30 cycles. These are performed on an automated cycler that can heat and cool the tubes with the reaction mixture very fast.

Denaturation at 94°C: During the denaturing step, the double strand is melted to yield single-stranded DNA, while polymerase activity is stopped.

Annealing at 55°C to 65°C depending on the primer sequences.

Extension at 72°C: This is the ideal working temperature for the DNA polymerase. Primers that have bound to the template at a position that is not entirely complementary to their sequence dissociate at this temperature. Nucleotides are incorporated sequentially at the 3' side of the primer, complementary to the sequence of the template. The time for the extension reaction depends on the length of the amplified fragment.

A standard protocol for PCR is described below:

PCR, 100 µl:		final concentration
DNase-free water	84.5 µl	
DNA template (plasmid) 0.1 µg / µl	0.5 µl	0.5 ng / µl
10 x PCR buffer	10 µl	1 x
dNTP mix 10 mM	2 µl	0.2 mM
Forward primer 100 µM	1 µl	1 µM
Reverse primer 100 µM	1 µl	1 µM
Pfu polymerase 3 U / µl	1 µl	0.03 U / µl

All components listed above except for the Pfu polymerase were added to a 0.2 ml PCR tube. The tube was placed in a thermocycler and the following PCR program was started:

denaturation	3 min	95℃	
denaturation	1 min	95℃	
annealing	1 min	55℃ to 65℃	25 to 30 cycles
extension	1 to 2 min	72℃	
extension	5 min	72℃	

When the temperature in the tube reached 90℃, the DNA polymerase was added (hot start). The above program was run for 2.5 to 3 h. An aliquot (5 to 10 µl) of the reaction product was checked on an agarose gel (3.2.1). When the PCR product had to be ligated into a vector, it was first purified on a preparative agarose gel (3.2.1).

3.3.5 PCR mutagenesis

In vitro site-directed mutagenesis was performed according to the protocol offerd by Stratagene. The mutagenic oligonucleotide primers were designed individually according to the desired mutation (single or multiple base excange; deletions or insertions). Several aspects were considered for designing the mutagenic primers:

- Both primers must contain the desired mutation and anneal to the corresponding sequence on opposite strands of the plasmid.

- The primers should have a higher melting temperature (~ 65℃) than those normally used in a standard PCR.

- The desired mutation(s) should be positioned in the middle of the primer.

- The concentration of the template was optimised by varying template concentration and keeping the primer concentration constant (1 µM). In this work, 50 ng template (plasmid DNA) per 50 µl reaction volume was found to be optimal.

- The template has to be a circular vector; extension stops when the polymerase has completely moved around the circular template and hits the 'roadblock', the 5' -end of the primer that started elongation (there is no strand displacement activity). The resulting product is a double-stranded plasmid with two nicks flanking the region defined by the primers, on opposite strands.

The procedure is identical to that described for the standard PCR (3.3.4) only that the time for extension should be longer due to the long amplification product (entire plasmid DNA). Normally, the extension time is ~2 min per kilobase for Pfu polymerase.

After the reaction was completed, a digestion with the endonuclease DpnI (catalyses the hydrolysis of methylated DNA; the recognition site GATC is generally found several

times in a plasmid DNA; DNA methylation occurs in bacterial cells; in *E. coli* the adenosine in GATC is methylated) was performed to destroy the original, methylated template plasmid which otherwise would compete with the mutagenesis product during transformation. 1 µl DpnI was added to the reaction mix and incubated for 10 to 30 min at 37 °C. 5 µl of the mix were then used for transformation (3.1.5). Several single colonies were selected and the extracted plasmids were analysed by restriction digest and sequencing.

3.3.6 Primer elongation

DNA polymerase can elongate primers having an overlapping region of complementary sequence (fill-up reaction). The melting temperature of the overlapping region should be between 55 °C and 65 °C as for a standard PCR.

Primer elongation, 100 µl:		final concentration
DNase-free water	85 µl	
10 x PCR buffer	10 µl	1 x
dNTP mix 10 mM	2 µl	0.2 mM
primer A 100 µM	1 µl	1 µM
primer B 100 µM	1 µl	1 µM
Pfu polymerase 3 U / µl	1 µl	0.03 U / µl

All components listed above except for the Pfu-polymerase were added to a 0.2 ml PCR tube. The tube was placed in the thermocycler and the following PCR program was started:

denaturation	3 min	95 °C	
denaturation	1 min	95 °C	
annealing	1 min	55 °C to 65 °C	20 cycles
extension	1 to 2 min	72 °C	
extension	5 min	72 °C	

When the tube temperature reached 90 °C, the DNA polymerase was added (hot start). The above program was run for 2.5 to 3 h. An aliquot (5 µl) was analysed by native PAGE (3.2.1), using the original primers as controls. The elongation product was concentrated by ethanol precipitation (3.2.2).

3.3.7 Fill-up reaction of DNA helices

When two double-stranded DNA fragments share a region with identical sequences at their ends and they are denatured, at least some of the strands of the first DNA fragment will anneal to strands of the second DNA fragment when the solution is cooled down. Those two strands that have hybridised via their 3' -ends will be elongated by the DNA polymerase,

thereby generating a 'full-length' duplex in quite the same fashion as in the primer elongation reaction (3.3.6). To generate the maximum amount of full-length product, it is necessary to repeat the denaturation, annealing and elongation steps several times to repeatedly provide hybrid duplexes, since the equilibrium lies on the side of reanneald original duplexes.

Fill-up reaction, 100 µl:		final concentration
10 x PCR buffer	10 µl	1 x
dNTP mix 10 mM	2 µl	0.2 mM
1st DNA fragment x µM	x µl	0.33 µM
2nd DNA fragment x µM	x µl	0.33 µM
Pfu polymerase 3 U / µl	1 µl	0.03 U / µl
RNase / DNase-free water	to 100 µl	-

For this type of fill-up reaction, the same program was used as described for the primer elongation (3.3.6). An aliquot (5 µl) was checked on an agarose gel (3.2.1), using the original DNA fragments as controls. If the reaction was successful, the product was precipitated (3.2.2) and purified by agarose gel electrophoresis (3.2.1).

3.3.8 Ligation of DNA fragments

DNA ligation is used in order to link DNA fragments end to end using either complementary overhangs ('sticky' ends) or blunt ends. In this work the method was used to insert DNA fragments into a vector (plasmid). The enzyme used to catalyse the ligation reaction was T4 DNA ligase from *E coli* phage T4. This enzyme covalently links the DNA strands by generating a phosphodiester bond between 3'-hydroxy and 5'-phosphate groups.

The vector (dephosphorylated at the 5' end; 3.3.3) and the DNA fragment to be inserted (with 5' –phosphate termini) into the vector were purified by agarose gel electrophoresis (3.2.1), eluted (3.2.5) and their concentration determined as described (3.2.6). The components of the reaction (see below) were added to a 0.2 ml PCR tube and incubated for 3 h at 20 °C.

DNA ligation reaction, 20 µl:		final concentration
Vector DNA 0.5 µg / µl or 0.6 µM	1 µl	0.03 µM
Insert DNA 0.4 µg / µl or 1.1 µM	1.8 to 6 µl	0.1 to 0.33 µM
10 x T4 ligase buffer	2 µl	1 x
T4 DNA ligase 1 U / µl	1 µl	0.05 U / µl
RNase-free water	to 20 µl	

Parallel reactions were performed varying the molar concentration of the insert (3 to 10 fold over the vector concentration; see above). A reaction containing water instead of insert DNA was prepared as a negative control: here, only re-circularised plasmids (after

incomplete dephosphorylation) or plasmids that were not linearised at all and could not be separated from the linearised plasmids by agarose gel electrophoresis are able to successfully transform cells. After incubation, 2 µl of each reaction mix, 2 µl of the negative control and 0.001 µg of the original circular vector as positive control were used for transformation (3.1.5). Plasmids obtained from different clones (miniprep; 3.3.1) were analysed by restriction digest (3.3.2). The size of the DNA fragments obtained by the digest was inspected using an agarose or a native polyacrylamide gel (3.2.1). Finally, the DNA plasmids were sequenced (MWG-Biotech) and glycerol stocks (3.1.2) from those plasmids containing the desired sequence were prepared.

3.4 RNA techniques

3.4.1 *In vitro* transcription

DNA-dependent phage RNA polymerases can transcribe double-stranded as well as single-stranded DNA (Milligan & Uhlenbeck, 1989). T7 RNA polymerase recognises the 17-nt double-stranded promoter sequence (5'-TAATACGACTCACTATA-3'; sense strand) and starts polymerisation immediately downstream. The potential of standard *in vitro* transcription reactions can be dramatically expanded if nucleotide analogues are used as building blocks in combination with standard nucleotides 5' triphosphates (NTPs). Guanosine or short oligonucleotides that terminate in guanosine effectively compete with guanosine 5' triphosphate (GTP) as starter building blocks and are incorporated at the 5' -end of transcripts (provided that the template codes for a G at this position). This is very useful if the transcribed RNA is further subjected to 5' -end labelling with γ^{32}P-ATP where 5'-OH termini are required. In this case, the starter can be guanosine or the dinucleotide ApG. To generate 5'-monophosphate termini, the transcription can be started with guanosine 5' monophosphate (GMP). In this work, the RNAs were synthesised by so called run-off transcription (i.e., the polymerisation is terminated when the polymerase reaches the DNA template's end). This was accomplished by using DNA plasmids as templates that were linearised with restriction enzymes (3.3.2).

T7 transcription of unmodified RNA

For analytical purposes, small-scale transcription (50 µl final volume) was performed.

transcription reaction, 50 µl:		final concentration
RNase-free water	24.45 µl	
HEPES pH 8.0, 1 M	4 µl	80 mM
DTT 100 mM	7.5 µl	15 mM
MgCl$_2$ 3 M	0.55 µl	33 mM
spermidine 100 mM	0.5 µl	1 mM
NTP mix (25 mM each)	7.5 µl	3.75 mM (each)
template (linearised plasmid) 1 µg / µl	4 µl	40 µg / ml
pyrophosphatase 200 U / ml	0.5 µl	2 U / ml
T7 RNA Pol. 200 U / µl	1 µl	4000 U / ml

All components (see above) were added to a 1.5 ml tube and the reaction mix was incubated at 37 °C for 2 h. An aliquot of 2 to 10 µl was checked by denaturing PAGE (3.2.1). If nothing was known about the transcription efficiency of the respective template, several volumes were analysed on the gel in parallel (e.g. 2, 5 and 10 µl). If the small-scale transcription was successful, a large-scale transcription reaction (preparative) was performed as described below.

transcription reaction, 1000 µl:		final concentration
RNase-free water	499 µl	
HEPES pH 8.0, 1 M	80 µl	80 mM
DTT 100 mM	150 µl	15 mM
MgCl$_2$ 3 M	11 µl	33 mM
spermidine 100 mM	10 µl	1 mM
NTP mix (25 mM each)	150 µl	3.75 mM (each)
template (linearised plasmid) 1 µg / µl	80 µl	40 µg / ml
pyrophosphatase 200 U / ml	10 µl	2 U / ml
T7 RNA Pol. 200 U / µl	20 µl	4000 U / ml

The reaction mix was prepared by adding the components – except for the T7 RNA polymerase – at room temperature in the order in which they are listed above. The mixture was aliquoted into 5 microfuge tubes of 1.5 ml, each containing a volume of 198 µl, and the reaction started by addition of 2 µl enzyme into each tube.

The reaction mix was incubated for 2 h at 37 °C; then a second aliquot (2 µl) of T7 RNA polymerase was added (400 U / 200 ml reaction mix), followed by another 2 h of incubation at 37 °C. A small aliquot (2 to 10 µl) was analysed by denaturing PAGE (3.2.1). If the large scale transcription was successful, the RNA transcript was purified as follows:

- phenol / chloroform extraction (3.2.3) to remove the enzyme
- NAP 5 or NAP 10 gel filtration for desalting and removing the mononucleotides (3.2.7)

- ethanol precipitation in the presence of NaOAc (3.2.2)
- denaturing PAGE purification (3.2.1); Some aspects had to be considered before starting the PAGE purification: (1) the size of the pocket had to be chosen depending on the amount of RNA loaded. Generally, for the product of a 1 ml transcription reaction to be separated on a 1 mm thick gel, a pocket width of 5 cm was sufficient. (2) the electrophoresis running time should be long enough to fully separate the desired RNA band from shorter secondary fragments obtained during transcription (sometimes long gels of ~ 40 cm are required for separation)
- elution by diffusion in buffer 1 or 3 (3.2.5)
- ethanol precipitation in the presence of NaOAc (3.2.2)
- resuspesion in water
- concentration determination (3.2.6)

Finally, the quality of the purified RNA transcript (ca. 200 ng) was analysed by denaturing PAGE (3.2.1). To verify the correct size of the purified RNA, a sample from an older lot or an RNA of similar length was used as control.

Note: the same protocol was used for RNA preparation by T7 transcription using guanosine as starter nucleotide. For 1 ml transcription reaction, 300 µl of 30 mM guanosine were used. The amount of water was adjusted accordingly (199 µl instead of 499 µl). Working with guanosine is described in the next paragraph.

T7 transcription of RNA carrying randomly distributed phosphorothioate analogues

T7 RNA polymerase incorporates Sp-NTPαS analogues, yielding Rp-phosphorothioate-modified RNAs due to inversion of configuration at the phosphorus atom during polymerization. Many nucleotide analogues (such as those with modifications at the 2'-position of the ribose moiety) that are poor substrates for the wild-type T7 RNA polymerase are better accepted by the Y639F mutant T7 RNA polymerase which shows a greater tolerance towards changes of functional groups in the minor groove. There were two aspects that had to be taken into consideration regarding the extent of the analogue modification:

- the amount of modified nucleotides should be optimised such that each RNA molecule carries about one modification.
- analogues are not incorporated with the same efficiency at all transcript positions, the incorporation pattern being largely specific for the analogue and the individual RNA investigated. One observation is the lack or reduction of analogue incorporation at homodi- or homooligo-nucleotide stretches

The reaction was started with guanosine because the 5'-OH termini were required for 5'-end labelling. Before preparing the reaction mix, the guanosine stock solution was incubated at 75°C in a thermoshaker until the guanosine was completely dissolved. Then, shaking was stopped and the solution left at 75°C to maximise solubility.

The reaction mix was prepared by adding the components – except for guanosine and T7 RNA polymerase – at room temperature in the order they are listed below, and afterwards the mixture was prewarmed to 37°C before adding guanosine. An appropriate amount of the pre-heated guanosine solution was quickly added to the reaction mix, which was vortexed immediately to avoid guanosine precipitation. The reaction was started by addition of enzyme (T7 RNA polymerase).

transcription reaction, 500 µl:		final concentration
RNase-free water	83.5 µl	
HEPES pH 8.0, 1 M	40 µl	80 mM
DTT 100 mM	75 µl	15 mM
MgCl$_2$ 3 M	5.5 µl	33 mM
spermidine 100 mM	5 µl	1 mM
NTP mix (25 mM each)	75 µl	3.75 mM (each)
ITPαS 4.33 mM	11 µl	0.095 mM
template (linearised plasmid) 0.5 µg / µl	40 µl	40 µg / ml
pyrophosphatase 200 U / ml	5 µl	2 U / ml
guanosine (30 mM, kept at 75 C)	150 µl	9 mM
T7 RNA Pol. 200 U / µl	10 µl	4000 U / ml

The reaction mixture was incubated for 4 h at 37°C. The RNA transcript was purified as described for unmodified RNA with the following exceptions:

- all precipitation steps were performed in the presence of NH$_4$OAc, pH 7.0 (3.2.2), to avoid degradation (hydrolysis) of RNA randomly modified with phosphorothioate analogues (acid-sensitive).

- for elution, the buffer 2 was chosen (3.2.5).

T7 transcription of internally labelled RNA

For efficient incorporation of radiolabelled nucleotides into RNA molecules, the concentration ratio between the non-radioactive (GTP) and radioactive (α^{32}P-GTP) nucleotide should not be higher than 1000. The reaction components were:

transcription reaction, 25 μl:		final concentration
HEPES pH 8.0, 1 M	2 μl	80 mM
DTT 100 mM	3.75 μl	15 mM
MgCl$_2$ 0.3 M	2.75 μl	33 mM
spermidine 50 mM	0.5 μl	1 mM
NTP mix (A, U, C, 25 mM each)	3.75 μl	3.75 mM (each)
GTP 10 mM	2.5	1 mM
α^{32}P GTP (3000 Ci/mmol, 10 μCi/μl, 3.3 μM)	7.5 μl	1 μM
template (linearised plasmid) 1 μg / μl	2 μl	80 μg / ml
pyrophosphatase 200 U / ml	0.25 μl	2 U / ml
T7 RNA pol. 200 U / μl	1 μl	8000 U / ml

The reaction mix was incubated at 37°C for 2 h and purified as described for the unmodified RNA, but omitting the phenol / chloroform extraction and NAP 5 or NAP 10 gel filtration steps. The final volume (resuspension of RNA pellet after purification and precipitation) for internally labelled RNA was 10 μl. 1 μl of this solution was checked for incorporation of radiolabelled nucleotide using a scintillation counter.

Generating homogenous ends during T7 transcription

Uniform 5' ends; an elegant way to produce transcripts with uniform 5' ends is to use a construct consisting of a self-cleaving hammerhead sequence attached immediately upstream of the RNA sequence of interest. The hammerhead ribozyme is a small structural element, originally identified in pathogenic plant viroids and virusoids, which catalyses phosphodiester bond hydrolysis at a single defined position. Since this ribozyme sequence is able to fold into the catalytically active form immediately after synthesis, cleavage occurs already during transcription – provided that magnesium ions are present at sufficiently high concentrations, as is the case under standard transcription conditions (see above). Beside creating homogenous ends, such hammerhead ribozymes have two additional advantages: (1) optimal transcription start sequences can be used upstream of the ribozyme cassette in favor of high transcription yields and (2) hammerhead *cis*-cleavage generates products with 2', 3' cyclic phosphate at the 3' ends (ribozyme part) and 5'-hydroxyls. This is very useful when the RNA of interest has to be labelled at the 5' end for further analysis.

Homogenous 3' ends; for the production of RNAs with homogeneous 3' ends, again hammerhead cassettes can be tethered to the RNA of interest. As in the case of hammerheads at the 5' end of the RNA of interest the cleavage occurs during transcription. The disadvantages of this method are: (1) the RNA of interest has to end with the sequence GUC (required for efficient hammerhead cleavage) and (2) after cleavage the RNA of interest ends with a 2', 3' cyclic phosphate at the 3' end. This has to be removed if the RNA of interest is further subjected to 3' -end labelling or to a ligation (e.g. of another RNA) to the

RNA's 3' -end.

3.4.2 Phosphorylation of nucleic acids at the 5' -end

The T4 polynucleotide kinase (T4 PNK) from *E. coli* phage T4 was used to either transfer the radioactive terminal phosphate group of γ^{32}P-ATP or the nonradioactive γ–phosphate of ATP to the free 5'-OH group of nucleic acids.

5' phosphorylation requires a 5'- hydroxyl group, either produced by hammerhead cis-cleavage during RNA transcription, by transcription of RNA with guanosine or ApG as starter nucleotides (3.4.1) or by dephosphorylation at the 5' -end (3.3.3).

5' -end labelling of RNA with γ- ^{32}P ATP

The reaction mix was prepared by adding the components in the order they are listed below and incubated at 37°C for 1 to 2 h.

Labelling reaction, 15 µl:		Final concentration
10 x T4 PNK buffer (forward reaction)	1.5 µl	1 x
25 mM DTT	1.5 µl	2.5 mM
RNase-free water	6 to 7 µl	
RNA purified by denaturing PAGE	1 to 2 µl (10-100 pmol)	0.66 to 1.33 µM
γ-^{32}P ATP (3000 Ci/mmol, 10 µCi/µl, 3.3 µM)	3.0 µl	0.66 µM
10 U / µl T4 PNK	1 µl	0.66 U / µl

After incubation, 35 µl of water were added and the labelled RNA was precipitated with ethanol, (3.2.2), purified by denaturing PAGE (3.2.1), eluted by diffusion (3.2.5) and concentrated by ethanol precipitation (3.2.2). The pellet was dissolved in 10 µl of RNase-free water and the overall yield of labelled RNA determined by measuring 1 µl using a scintillation counter.

5' -end phosphorylation of RNA using trace amounts of γ- ^{32}P ATP

To phosphorylate RNA with at a low specific activity, the following recipe was used:

Phosphorylation reaction, 55 µl:		Final concentration
10 x T4 PNK buffer (forward reaction)	5 µl	1 x
100 mM ATP	2.5 µl	5 mM
RNase-free water	to 55 µl	
RNA purified by denaturing PAGE	x µl (2000-3000 pmol)	35 to 55 µM
γ-^{32}P ATP (3000 Ci/mmol, 10 µCi/µl, 3.3 µM)	3.0 µl	0.2 µM
10 U / µl T4 PNK	2.5 µl	0.5 U / µl

The mixture was incubated for 2 h at 37°C, and then the following components were added:

100 mM ATP	2.5 µl	9 mM
10 U / µl T4 PNK	2.5 µl	0.9 U / µl

The reaction mix was incubated for another 1 h at 37°C

The labelled RNA was ethanol precipitated (3.2.2), purified by denaturing PAGE (3.2.1), eluted (3.2.5) and concentrated by ethanol precipitation (3.2.2). The pellet was dissolved in 20 µl of RNase-free water and the RNA concentration was determined (3.2.6).

3.4.3 3' -end labelling of RNA

Labelling of RNA molecules at the 3' -end was achieved by ligation of 5'-^{32}P cytidine-3',5'-bisphosphate (pCp) to the 3'-terminal hydroxyl group (England & Uhlenbeck, 1978). The ligation reaction was catalysed by the T4 RNA ligase that can covalently link the 5'-phosphate group of one RNA to the 3'-OH group of another RNA molecule, using ATP as cofactor. The smallest 3'-substrates recognised by this enzyme are nucleoside-3',5'-bisphosphates (such as pCp). If the RNA to be labelled carries a cyclic phosphate (generated by hammerhead *cis*-cleavage) at its 3' -end, it has to be removed first (Cameron & Uhlenbeck, 1997; see 3.4.4).

3' -end labelling reaction, 6 µl:		Final concentration
10 x T4 RNA ligase buffer	0.6 µl	1 x
1.5 mM ATP	0.33 µl	82.5 µM
RNA purified by denaturing PAGE	x µl (5 to 10 pmol)	0.83 to 1.66 µM
[5'-^{32}P] pCp (3000 Ci/mmol, 10 µCi/µl)	4 µl	2.2 µM
10 U / µl T4 RNA ligase	1 µl	1.67 U / µl

The reaction mix was prepared by adding the components in the order given above and incubated at 8°C overnight. After incubation, 10 µl gel loading buffer were added and the radiolabelled RNA was purified by denaturing PAGE (3.2.1), eluted by diffusion (3.2.5) and concentrated by ethanol precipitation (3.2.2). The RNA pellet was dissolved in 10 to 20 µl RNase-free water and the overall yield of labelled RNA determined. This was achieved by measuring the amount of incorporated radioactivity contained in 1 µl of RNA solution using a scintillation counter.

3.4.4 Removing the 2',3' cyclic phosphate at the 3' -end of RNA

Removing the 2',3' cyclic phosphate (e.g. generated by *cis*-cleavage of a hammerhead ribozyme) from the 3' -end of RNA molecules is required if the RNA is further subjected to 3' -end labelling with pCp by T4 RNA ligase (3.4.3). The enzyme that catalyses the removal of a 2',3' cyclic phosphate is the T4 polynucleotide kinase (T4 PNK)

which,besides its 5' kinase activity used for 5' -end phosphorylation of RNA molecules (3.4.2), also has a 3' phosphatase activity.

Removal of 2',3' cyclic phosphates, 100 µl:		Final concentration
1 M Imidazole-HCl pH 6.0	10 µl	0.1 M
10 mM ATP	1 µl	0.1 mM
RNA solution (24.5 µM)	12.5 µl (300 pmol)	3 µM
2 M MgCl$_2$	0.5 µl	10 mM
10 % β-mercaptoethanol	0.7 µl	0.07 %
2 mg / ml BSA	1 µl	0.02 µg / µl
RNase-free water	72.3 µl	
10 U / µl T4 PNK	2 µl	0.2 U / µl

The reaction mix was incubated for 6 h at 37°C. Then 200 µl RNase-free water were added and the solution was subjected to phenol / chloroform extraction (3.2.3) followed by ethanol precipitation (3.2.2). The pellet was resuspended in 20 µl of RNase-free water and the concentration was determined (3.2.6).

3.4.5 RNA ligation

T4 RNA ligase catalyses the ATP-dependent intra- and intermolecular formation of phosphodiester bonds between 5'-phosphate and 3'-hydroxyl termini of poly- and oligonucleotides, single-stranded RNA and DNA. The minimal donor substrates are nucleoside-3',5'-bisphosphates (e.g. pCp, see 3.4.3) for intermolecular reactions or oligonucleotides of 8 bases for intramolecular reactions.

Ligation reaction, 15 µl:		Final concentration
124 pmol / µl weakly labelled RNA with 5' phosphate termini (see 3.4.2)	1.7 µl	14 pmol / µl
45 pmol / µl RNA with 3' OH termini (e.g. a synthetic oligonucleotide)	6.7 µl	20 pmol / µl
1 M HEPES pH 7.5	1.5 µl	100 mM
100 mM DTT	1.5 µl	10 mM

The mixture, consisting of the components above, was heated for 3 min at 90°C and 10 minutes at 65°C. It was then cooled down slowly (0.02°C / sec) to 16°C in a thermocycler. When reaching 16°C, the following components were added:

250 mM MgCl$_2$	0.9 µl	15 mM
10 mM ATP	0.75 µl	0.5 mM
100 % DMSO	0.75 µl	5 %
15 U / µl T4 RNA ligase	1.5 µl	1.5 U / µl

The reaction mix was incubated overnight (~ 16 hours) at 16°C, then the RNA was precipitated (3.2.2), purified by denaturing PAGE (3.2.1), eluted by diffusion (3.2.5); concentrated by ethanol precipitation (3.2.2) and if necessary subjected to 5' -end labelling (3.4.2).

3.4.6 Partial alkaline hydrolysis of RNA

The RNA phosphodiester bond between two ribonucleotides can be broken by alkaline hydrolysis. Here, the nucleophilic attack of an activated 2'-hydroxyl group results in the generation of a 2',3' cyclic phosphate and a 5'-hydroxyl as the leaving group. The cyclic phosphate is not stable under alkaline conditions and further hydrolysed to either a 2' or 3' monophosphate.

The partial alkaline hydrolysis was performed in NaOH solution (pH ~12.5) as described below.

Alkaline hydrolysis 20 μl:		Final concentration
10^5 cpm / μl 5' -end labelled RNA	0.5 μl (5 x 10^4 cpm)	2500 cpm / μl
50 mM NaOH	19.5	48.8 mM

The mixture was incubated for 10 min at 100°C in a heating block. To avoid condensation, a hot (> 100°C) metal block was placed on top of the reaction tube. After incubation, the reaction tube was placed on ice, the RNA precipitated (3.2.2) and analysed by denaturing PAGE (3.2.1).

3.4.7 Partial hydrolysis by nuclease P1

P1 nuclease from *Penicillium citrinum* is a zinc-dependent enzyme consisting of 270 amino acid residues. Nuclease P1 (nuclease 5'-nucleotidehydrolase, 3'-phosphohydrolase) hydrolyses both 3'-5'-phosphodiester bonds in RNA and heat-denatured DNA (single-stranded) and 3'-phosphomonoester bonds in mono- and oligonucleotides without base specificity.

Like RNase P, nuclease P1 generates 5'-phosphate and 3'-hydroxyl termini. Therefore, RNA fragments generated by this method were used as size markers for analysis of the cleavage products generated by RNase P.

Nuclease P1 hydrolysis 10 µl:		Final concentration
10^5 cpm / µl 5' -endlabelled RNA	0.5 µl (5 x 10^4 cpm)	2500 cpm / µl
carrier RNA (unlabelled RNA; 0.75 µg / µl)	1.5 µl	
10 x nuclease P1 buffer	1 µl	1 x
RNase free water	6 µl	
The RNA mix was pre-incubated for 1 min at 70°C, then the nuclease P1 enzyme was added:		
0.1 ng / µl nuclease P1	1 µl	0.01 ng / µl

The whole mixture was incubated for 20 sec at 70°C in a heating block. To avoid condensation, a hot metal block was placed on top of the reaction tube. After incubation, the reaction tube was placed on ice, the RNA precipitated (3.2.2) and analysed by denaturing PAGE (3.2.1).

3.4.8 Iodine induced hydrolysis of phosphorothioate analogue-modified RNA

All nucleotide analogues incorporated into RNA during transcription carried phosphorothioate modification (one non-bridging phosphate oxygen replaced with sulfur), which permits to specifically cleave the nucleic acid chain with iodine at the sites of analogue incorporation. Iodine treatment thus results in A-, C-, G- or U-specific sequence ladders on denaturing polyacrylamide gels.

1 mg / ml I_2 solution was freshly prepared before use by mixing the components listed below:

I_2 solution, 50 µl:		Final concentration
10 mg / ml I_2 in ethanol	5 µl	1 mg / ml
ethanol abs.	5 µl	20 %
RNase-free water	40 µl	

The iodine hydrolysis reaction mix was prepared as follows:

Iodine-induced hydrolysis reaction, 50 µl:		Final concentration
5'- or 3' -endlabelled RNA	1 to 10 µl (5 x 10^4 cpm)	1000 cpm / µl
100 mM HEPES pH 7.5	5 µl	10 mM
1 mg / ml I_2 solution	5 µl	0.1 mg / ml
RNase-free water	30 to 39 µl	

The reaction mix was incubated for 10 to 20 min at 37°C in a thermoshaker. 150 µl RNase-free water was added to the mixture and the RNA precipitated with ethanol (3.2.2) in the presence of NH_4OAc and glycogen. The pellet was resuspended in 5 µl of water and 5 µl of denaturing gel loading buffer and analysed by denaturing PAGE (3.2.1) to resolve the

iodine-induced cleavage pattern.

3.5 Methods for the analysis of RNase P activity

3.5.1 Kinetic and thermodynamic analysis of RNase P

Kinetic experiments can be performed in order to analyse in detail the influence of buffer conditions (pH, monovalent cations, divalent cations, anions), chemical modifications, deletions and mutations on substrate processing by RNase P. Using appropriate reaction conditions, individual steps in RNase P-induced catalysis can be explored.

Using an excess of substrate relative to enzyme (Michaelis-Menten conditions), the measured reaction velocity is dependend on the slowest reaction step. Each enzyme molecule runs through the reaction cycle many times (*multiple turnover*). In the case of tRNA precursor (ptRNA) processing by *E. coli* P RNA, the rate determining step under conditions of 0.1 M $MgCl_2$ and 0.1 M NH_4OAC is the dissociation of mature tRNA (tRNA) from the enzyme complex (Hardt et al., 1995).

The reaction scheme is:

$$E + S \underset{k_{-1}}{\overset{k_1}{\rightleftharpoons}} ES \overset{k_2}{\longrightarrow} EP \underset{k_{-3}}{\overset{k_3}{\rightleftharpoons}} E + P$$
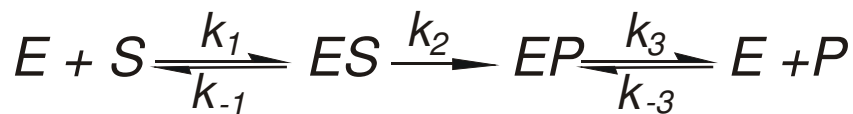
where E = P RNA; S = ptRNA; P = tRNA

If the enzyme is in excess relative to substrate, each enzyme molecule can maximally process one substrate molecule. Thus, it goes through the reaction cycle only once (*single turnover*). In this case, product release does not contribute to the speed of substrate conversion. Consequently, the reaction velocity depends on substrate binding (k_1, k_{-1}) or on the rate of the chemical step (k_2).

3.5.2 *Single turnover* kinetic experiments

In the case of *single turnover* experiments, the enzyme concentration is much higher than the concentration of substrate ([E]>>[S]). Performing *single turnover* kinetic experiments, three different constants could be determined:

- K_M = the enzyme concentration at the half-maximal cleavage rate;
- k_{obs} = the rate constant observed in the *single turnover* reaction at a certain enzyme concentration;
- k_{react} = the rate constant corresponding to the highest possible reaction velocity in a *single turnover* reaction. This condition is met when enzyme concentration becomes

saturating.

In this work almost all kinetic experiments were performed under *single turnover* conditions and at enzyme concentrations in the saturating range where $k_{react} = k_{obs}$. Standard protocols for performing *single turnover* kinetic experiments are described below.

P RNA alone reaction

5 x S&P buffer, pH 5.0 to 8.2:

5 M NH_4OAc; 250 mM buffering substance (PIPES, MES or HEPES); pH as indicated (5.0 to 8.2);

Before starting the reaction, enzyme and substrate were preincubated separately in the same buffer. The enzyme (*E. coli* P RNA) was preincubated for 1 h at 37 °C and the substrate for 5 min at 55 °C and 25 minutes at 37 °C.

P RNA preincubation, 16 µl		Final concentration
x µM P RNA	x µl (100 pmol)*	6.25 µM *
5 x S&P buffer	3.2 µl	1 x
x mM Me^{2+} **	x µl	x mM
RNase-free water	to 16 µl	

Substrate preincubation, 5.5 µl		Final concentration
5′ -endlabelled substrate	x µl (20000 cpm)	< 1 nM
5 x reaction buffer	1.1 µl	1 x
x mM Me^{2+} **	x µl	x mM
RNase-free water	to 5.5 µl	

* in some kinetic reactions where the influence of enzyme concentration was analysed, the actual value was lower.

** in this work, acetate or chloride salts of the different divalent cations (Me^{2+}) like Mg^{2+}, Mn^{2+}, Zn^{2+}, Sr^{2+} etc. were used. The concentration of divalent cations varied and it is specified for each set of experiments in the Results and Discussion section (4).

After preincubation, 4 µl of the substrate solution were mixed with the P RNA solution (both solutions were pre-warmed at 37 °C). This was considered the reaction start point. The P RNA-substrate mix was further incubated at 37 °C and aliquots were withdrawn at different timepoints. The remaining substrate solution (1.5 µl) was considered the zero control and was incubated at 37 °C until the last aliquot of the P RNA-substrate mix was withdrawn. The RNA of each aliquot including the zero control was precipitated (3.2.2) and analysed by denaturing PAGE (3.2.1). For data evaluation, see (3.5.5)

RNase P holoenzyme reaction

Single turnover kinetic experiments to analyse the reaction catalysed by RNase P holoenzymes were carried out similarly with those described for the P RNA alone reaction.

Exceptions were the reaction conditions and the enzyme concentration. An additional step for reconstitution of the holoenzyme (see below) was performed.

5 x F buffer:

500 mM KCl; 250 mM MES; pH 6; 10 or 50 mM $MgCl_2$

Enzyme preincubation and holoenzyme reconstitution, 16 µl		Final concentration
x µM P RNA	x µl (2 pmol)	100 nM
5 x F buffer *	3.2 µl	1 x *
RNase-free water **	up to 16 µl**	
	incubate 5 min. at 55°C and 50 min.at 37°C	
x µM P protein ***	x µl (8 or 20 pmol)	400 or 1000 nM
	incubate 2 min. at 37°C	

Substrate pre-incubation, 5.5 µl		Final concentration
5' end labelled substrate	x µl (20000 cpm)	< 1 nM
5 x F buffer *	1.1 µl	1 x *
RNase-free water	up to 5.5 µl	
	incubate 5 min. at 55°C and 25 min.at 37°C	

* the concentration of $MgCl_2$ in the 5 x buffer was 10 or 50 mM; the final concentration of $MgCl_2$ in the reaction mix was 2 or 10 mM.

** 16 µl represents the total volume including the volume of P protein.

*** the P protein was stored at –80°C in small aliquots and thawed shortly before use. For reconstitution of the holoenzyme 4 fold excess of *B. subtilis* and 10 fold of *E. coli* P protein over the molar concentration of P RNA were used.

The further procedure is identical with that described for the P RNA alone reaction.

3.5.3 Binding experiments using the gel filtration method

Binding of ptRNA to E. coli P RNA

Binding buffer 1:

1 M NH_4OAc; 50 mM MES / NaOH, pH 6.0; 0.1 % SDS; 0.05 % Nonidet P40; 5 to 80 mM Me^{2+} ion salt;

5 x S&P buffer pH 6:

5 M NH_4OAc; 250 mM MES; pH 6;

Binding experiments were performed using self-prepared spin columns (Microspin [TM] columns; Amersham Pharmacia) filled with Sephadex G75. To avoid substrate processing by P RNA during gel filtration experiments, divalent cations like Ca^{2+} and Sr^{2+} were used

that allow substrate binding but do support catalysis inefficiently or not at all.

2.5 g of Sephadex G75 were suspended in 50 ml binding buffer 1 and left overnight at room temperature for swelling. The columns were filled with 800 µl of this suspension, placed in a microfuge tube and centrifuged for 1 min at 2000 x g. The tube with the flowthrough was removed and the columns with the Sephadex matrix were placed in new microfuge tubes. At this stage they were ready to use.

P RNA preincubation, 10 µl		Final concentration
x µM P RNA	x µl (0 to 50 pmol)	x µM
5 x S&P buffer	2 µl	1 x
x mM Me^{2+} *	x µl	as specified
1 % SDS	1 µl	0.1 %
0.5 % Nonidet P40	1 µl	0.05 %
RNase-free water	to 10 µl	

Substrate preincubation, 10 µl		Final concentration
x µM 5' -endlabelled ptRNA	x µl (4000 cpm)	< 1nM
5 x S&P buffer	2 µl	1 x
x mM Me^{2+} *	x µl	x mM
1 % SDS	1 µl	0.1 %
0.5 % Nonidet P40	1 µl	0.05 %
RNase-free water	to 10 µl	

* for binding experiments, 5 or 80 mM $SrCl_2$ or 2 to 150 mM $CaCl_2$ were used.

As in the kinetic experiments, enzyme (P RNA) and substrate (ptRNA) were pre-incubated separately under the same buffer conditions. The enzyme (P RNA) concentration was varied between 0 and 2.5 µM and trace amounts of radiolabelled substrate were used. P RNA was preincubated for 1 h at 37°C and the substrate 30 minutes at 37°C.

After preincubation, ptRNA was mixed with P RNA and incubated at 37°C for 2 min. The entire P RNA-ptRNA mix was transferred onto the Sephadex G75 column, which was placed in a microfuge tube and centrifuged for 1 min at 2000 x g. After centrifugation, the fraction of ptRNA molecules not bound to P RNA remained in the column matrix, while the flow-through contained the fraction of substrate molecules bound to P RNA. With the help of a scintillation counter, the yields of radiolabelled RNA within the Sephadex column and in the flow-through were determined. This procedure was repeated for all concentrations of P RNA (from 0 to 2500 nM).

Binding of ptRNA to B. subtilis RNase P holoenzyme

Binding buffer 3:

200 mM NH_4OAc; 50 mM Tris / CH_3COOH, pH 7.1; 0.05 % Nonidet P40;

15 mM $Ca(OAc)_2$;

5 x B3 buffer:

1 M NH_4OAc; 250 mM Tris / CH_3COOH, pH 7.1;

The procedure applied for preparing the Sephadex matrix was as that described for ptRNA binding to P RNA, only that instead of binding buffer 1, the binding buffer 3 was used.

The reconstitution of the holoenzyme was performed as described below. Parallel a control RNA alone mixture and a dilution buffer were prepared.

Reconstitution of the holoenzyme				
	holoenzyme (10 µl)	RNA alone (10 µl)	Dilution buffer (1000 µl)	Final concentration
x µM *B. subtilis* P RNA	x µl (10 pmol)	x µl (10 pmol)		1 µM
5 x B3 buffer	2 µl	2 µl	200	1 x
100 mM $Ca(OAc)_2$	1.66 µl	1.66 µl	150	15 mM
1 % Nonidet P40	0.5 µl	0.5 µl	50	0.05 %
RNase-free water *	to 10 µl *	to 10 µl	600	
Incubate for 1 h at 37℃				
x µM *B. subtilis* P protein	x µl (50 pmol)			5 µM
Incubate for 15 min. at 37℃				

* 10 µl represents the total volume including the volume of P protein.

The reconstituted holoenzyme and the RNA alone mixtures were diluted with the dilution buffer (prewarmed at 37℃) as follows:

Dilution of reconstituted holoenzyme mix		Dilution of RNA alone mix		Final enzyme concentration
Holoenzyme mix	Dilution buffer	RNA alone mix	Dilution buffer	
0 µl	50 µl	0 µl	50 µl	0 nM
0.5 µl	500 µl	0.5 µl	500 µl	1 nM
0.5 µl	250 µl	0.5 µl	250 µl	2 nM
0.5 µl	125 µl	0.5 µl	125 µl	4 nM
0.5 µl	50 µl	0.5 µl	50 µl	10 nM
0.5 µl	25 µl	0.5 µl	25 µl	20 nM
1 µl	25 µl	1 µl	25 µl	40 nM
2.5 µl	25 µl	2.5 µl	25 µl	100 nM

All dilutions were incubated at 37 °C for 5 min.

Substrate preincubation, 200 µl		Final concentration
x µM 5' -endlabelled ptRNA	x µl (80000 cpm)	< 1nM
5 x B3 buffer	40 µl	1 x
100 mM $Ca(OAc)_2$	30 µl	15 mM
1 % Nonidet P40	10 µl	0.05 %
RNase-free water	up to 200 µl	
	Incubate for 30 minutes at 37 °C	

10 µl of substrate mix were mixed with 10 µl of each enzyme (holoenzyme and RNA alone) dilution (both prewarmed at 37 °C) and incubated for 5 min at 37 °C. The further procedure is identical with that described for the P RNA alone.

Data evaluation of ptRNA binding experiments

The fraction of bound substrate was calculated as described below:

$$\text{cpm}_{\text{total}} = \text{cpm}_{\text{free substrate}} + \text{cpm}_{\text{complex}} \tag{3.5.1}$$

where $\text{cpm}_{\text{total}}$ is the amount of radiolabelled RNA loaded onto the Sephadex column; $\text{cpm}_{\text{free substrate}}$ is the amount of radiolabelled RNA that remained on the matrix; $\text{cpm}_{\text{complex}}$ is the amount of radiolabelled RNA in the flowthrough.

In the absence of enzyme, the fraction of cpm retained in the matrix was determined as:

$$f_{zero} = cpm_{matrix} / cpm_{total} \qquad (3.5.2)$$

normally determined f_{zero} was ~ 0.05 to 0.1

Then, the fraction of substrate in complex with the enzyme was calculated:

$$f_{complex} = (cpm_{complex} / cpm_{total}) - f_{zero} \qquad (3.5.3)$$

$f_{complex}$ was represented as a function of the concentration of free (i.e. unbound) enzyme in solution [enzyme]$_{free}$, considered equal with the total enzyme concentration under conditions of E>>S, and the data were fitted (Grafit 3.0, Erithacus Software) to the equation:

$$f_{complex} = f_{substrate} \times [enzyme]_{free} / (K_d + [enzyme]_{free}) \qquad (3.5.4)$$

where $f_{substrate}$ is the fraction of substrate that is able to bind to the enzyme at saturating concentration ([enzyme]$_{free}$ → ∞) and K_d is the binding constant, representing the concentration of P RNA at which 50 % of the fraction of substrate able to bind ($f_{substrate}$) is in complex with the enzyme. Using this curve fitting algorithm K_d and $f_{substrate}$ values are obtained. From the K_d value, the free binding energy of the P RNA-ptRNA complex can be calculated according to the equation:

$$\Delta G = R \times T \times \ln (1 / K_d) \qquad (3.5.5)$$

with R being the gas constant (0.00198 kcal mol^{-1} K^{-1}) and T the absolute temperature in Kelvin.

3.5.4 *Cis*-cleavage experiments of P RNA – tRNA tandem constructs

In this work, two types of tandem constructs were used: *E. coli* P RNA covalently linked to the 5' -half of tRNA (P RNA - tRNA 5' -half) and *E. coli* P RNA conjugated to a full-length tRNA (P RNA - tRNA). In both cases, the enzyme was connected to the (partial) substrate by a string of ribonucleotides, the RNA linker, to provide the freedom of movement necessary for correct intramolecular alignment of enzyme and substrate.

4 x annealing buffer:

400 mM MES-NaOH or Tris-HCl, pH 5.9 to 7.5; 400 mM NH$_4$Cl

Both tandem constructs were preincubated for annealing and folding, followed by dilution and concomitant addition of Mg^{2+} to start the *cis*-cleavage reaction. The P RNA -

tRNA 5' -half was used in combination with the 3' -half of the tRNA in order to reconstitute a full-length substrate.

A general protocol is described below. Please note that there are variations between different sets of experiments and deviations from the standard protocol. The respective reaction conditions are specified for individual experimental settings in the Results and Discussion section (4.3).

The annealing mix consisted of:

Annealing mix 1, 16.5 µl: (for P RNA - tRNA 5' -half)		Final concentration
4 x annealing buffer	4.125 µl	1 x
30 mM CaCl$_2$	2.75 µl	5 mM
5' -endlabelled P RNA - tRNA 5' -half	x µl (2 x 10^4 cpm)	~ 0.3 nM
x µM unlabelled P RNA - tRNA 5' -half	x µl (0 to 2.52 pmol)	0 to 0.153 µM
x µM tRNA 3' -half	x µl (0.495 to 2525 pmol)	0.03 to 153 µM
RNase-free water	to 16.5 µl	

or

Annealing mix 2, 16.5 µl: (for P RNA - tRNA)		Final concentration
4 x annealing buffer	4.125 µl	1 x
30 mM CaCl$_2$	2.75 µl	5 mM
5' -endlabelled P RNA - tRNA	x µl (2 x 10^4 cpm)	~ 0.3 nM
RNase-free water	to 16.5 µl	

The annealing mix was incubated for 1 h at 50 °C. Then the components listed below were added, mixed thoroughly and incubated for 2 min at 50 °C.

Self-cleavage reaction, 63.25 µl:		Final concentration
annealing mix (1 or 2)	16.5 µl	0.26 x annealing mix / buffer
30 mM CaCl$_2$	7.8 µl	5 mM
4 x annealing buffer	11.69 µl	0.74 x annealing buffer
5 M urea	1.27 µl	100 mM
RNase-free water	to 63.25 µl	

The *cis*-cleavage reaction was started by adding 0.76 µl 3 M MgCl$_2$ (final concentration 36 mM). Aliqouts were withdrawn at different timepoints, the RNA of each aliquot was precipitated (3.2.2) and analysed by denaturing PAGE (3.2.1.). For data evaluation, see (3.5.5).

3.5.5 Data evaluation of RNase P cleavage experiments

The reaction products from the kinetic experiments were resolved by denaturing PAGE (4.2.1), an image plate was exposed to the polyacrylamide gel for at least 3 h,

scanned and digitised using a Fuji FLA 3000 phosphorimage analyser and the software BasReader. Images were imported into the program AIDA and quantification boxes were positioned around bands representing substrate or uncleaved complex and product or cleaved complex. The data report, containing the values corresponding to the intensity of marked bands, was imported into the curve fitting software (Grafit 3.0) and the fraction of product corresponding to each time point was calculated:

$$f_{product} = I_{product} / (I_{product} + I_{substrate}) \tag{3.5.6}$$

where $I_{product}$ is the band intensity corresponding to product or cleaved complex and $I_{substrate}$ is the band intensity corresponding to substrate or uncleaved complex. The fraction of product ($f_{product}$) was corrected by subtracting the fraction of product calculated for the zero control (f_{zero}):

$$f_{zero} = f_{product} \text{ when } t = 0$$

The corrected $f_{product}$ was represented as a function of time and the data were fitted to the equation:

$$f_{product} = f_{endpoint} \times (1 - e^{-k_{obs} \times t}) \tag{3.5.7}$$

where $f_{endpoint}$ represents the maximal fraction of substrate that can be cleaved, t is time and k_{obs} is the observed reaction velocity rate constant.

4   *Results and discussion*

4.1 The role of divalent cations in RNase P RNA catalysis: studies with Zn^{2+} as catalytic cofactor

Studies with P RNA from *Escherichia coli* (structural P RNA subtype A) and *Bacillus subtilis* (subtype B) have implied a specific role for two or more metal ions in substrate binding and cleavage chemistry (Smith and Pace, 1993; Warnecke et al., 1996; 1999; Kurz & Fierke, 2002). Mg^{2+} and Mn^{2+} efficiently support the precursor tRNA (ptRNA) processing reaction catalysed by bacterial P RNAs (Smith et al., 1992), which generates 3'-OH and 5'-phosphate termini. For *E. coli* P RNA (called also M1 RNA), processing under standard assay conditions was reported to be essentially abolished when Mg^{2+} (earth alkaline metal) or Mn^{2+} (transition metal) was replaced with other earth alkaline metals such as Sr^{2+} or other transition metal ions such as Zn^{2+}, Co^{2+} or Ni^{2+}, or Co(NH$_3$)$_6$$^{3+}$ as a potential mimic of hexaaquo Mg^{2+} (Guerrier-Takada et al., 1986; Brannvall & Kirsebom, 2001). Ca^{2+}, as an exception, supported the reaction, although inefficiently (Smith et al., 1992; Brannvall & Kirsebom, 2001). While the ribozyme failed to cleave the substrate in the presence of Ba^{2+}, Sr^{2+}, Zn^{2+} or Co(NH$_3$)$_6$$^{3+}$ alone, some cleavage activity was restored with the combinations Zn^{2+}/Sr^{2+}, Zn^{2+}/Ba^{2+} or Zn^{2+}/Co(NH$_3$)$_6$$^{3+}$ (Brannvall & Kirsebom, 2001). Catalysis by *E. coli* P RNA with Sr^{2+} or Ba^{2+} alone has only been observed with low efficiency under very specialised conditions (at pH >> 7 and in the presence of ethanol; Kazakov & Altman, 1991). From Pb^{2+}-induced hydrolysis patterns of *E. coli* P RNA generated in the presence of different divalent metal ions and Co(NH$_3$)$_6$$^{3+}$ (Brannvall et al., 2001), it was concluded that *E. coli* P RNA conformation is very similar in the presence of earth alkaline metal ions (Mg^{2+}, Ca^{2+}, Sr^{2+} and Ba^{2+}), Mn^{2+} and apparently also Co(NH$_3$)$_6$$^{3+}$, whereas other transition metals, such as Zn^{2+} and particularly Cd^{2+}, Co^{2+}, Cu^{2+} and Ni^{2+} induce changes of the native *E. coli* P RNA conformation.

To obtain a deeper insight into how different metal ions modulate this ribozyme system, the effects of Zn^{2+} and Sr^{2+} on different aspects of processing by *E. coli* P RNA were investigated in this study, namely catalysis and its inhibition by Sr^{2+} in particular, enzyme-substrate affinity and changes in the fraction of substrate able to bind to the enzyme. The well-characterised bacterial ptRNA^{Gly}, used as the substrate for processing by *E. coli* P RNA, is illustrated in Fig. 4.1.1, including the variants carrying single-site 2'-ribose

modifications at nt −1. These were obtained by ligation of a synthetic oligonucleotide (24-mer oligonucleotide with 3'-OH termini, representing the first 24 bases from the 5' end; Fig. 4.1.1) to the 3' portion of a tRNA starting with position +18 in the ptRNA (tRNA$_{18-79}$, obtained by *in vitro* transcription) and carrying a 5' phosphate terminus. Catalysis was analysed under single turnover conditions (E>>S), and all assays included a relatively high monovalent salt concentration (1 M NH$_4$OAc) to focus on roles of metal ions which cannot be replaced by monovalent cations. The pH of 6.65 was chosen to combine substantial substrate turnover with conditions under which the rate of cleavage is determined mainly by the cleavage chemistry (Warnecke et al., 1996).
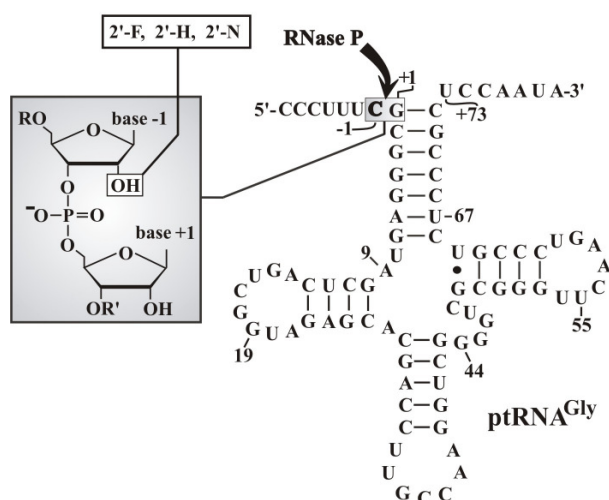

Fig. 4.1.1: Secondary structure of the ptRNA^{Gly} substrate. 2'-ribose modifications introduced at the canonical RNase P cleavage site (nt -1) are illustrated in the grey-shaded box on the left. The arrow marks the canonical RNase P cleavage site between nt -1 and +1. For further details, see Persson et al., 2003.

4.1.1   *E. coli* P RNA catalysis with Zn^{2+} as the sole divalent metal ion and Zn^{2+}/ Sr^{2+} combinations

In this study it is shown that *E. coli* P RNA catalysis occurs in the presence of Zn^{2+} as the only divalent metal ion present in the cleavage assay (termed Zn^{2+} alone conditions in the following; Fig. 4.1.2), an observation that contrasts with findings from previous studies (Guerrier-Takada et al., 1986; Brannvall & Kirsebom, 2001). This discrepancy can be explained by the fact that here experiments were performed under single turnover conditions (E>>S) and in the presence of high concentrations of NH$_4$OAc. The catalysis with Zn^{2+} was supported only in the presence of ammonium salts (Fig. 4.1.2 A). The nature of the counter anion (chloride or acetate) was not critical (Fig. 4.1.2 A), although some RNA degradation was observed with chloride salts. With potassium or sodium instead of ammonium salts, *E. coli* P RNA-catalysed cleavage under Zn^{2+}-alone conditions was not detected (Fig. 4.1.2 A). One explanation for this could be that some of the water ligands surrounding the Zn^{2+} ions are replaced with ammonia (Cotton & Wilkinson, 1988) as a requirement to be able to sustain

catalysis by *E. coli* P RNA.

Although proficient in catalysis (see Fig. 4.1.2), Zn^{2+} was unable to support thermodynamically stable E•S complex formation (4.1.2 and Fig. 4.1.5), in contrast to other divalent metal ions, such as Mg^{2+} and Mn^{2+}, which support both E•S complex formation and cleavage. Yet selection of the canonical cleavage site (between nt −1 and +1) was not changed in the presence of Zn^{2+} alone (relative to Mg^{2+} alone; data not shown), despite the very low substrate affinity under Zn^{2+} alone conditions. This shows that low affinity substrate ground state binding not necessarily favours aberrant cleavage (between nt −2 and −1) relative to cleavage at the canonical site. One interpretation is that the large activation barrier difference for aberrant cleavage (at −2/−1) relative to canonical cleavage (−1/+1) is maintained under these conditions. In conclusion, P RNA catalysis with Zn^{2+} as the metal
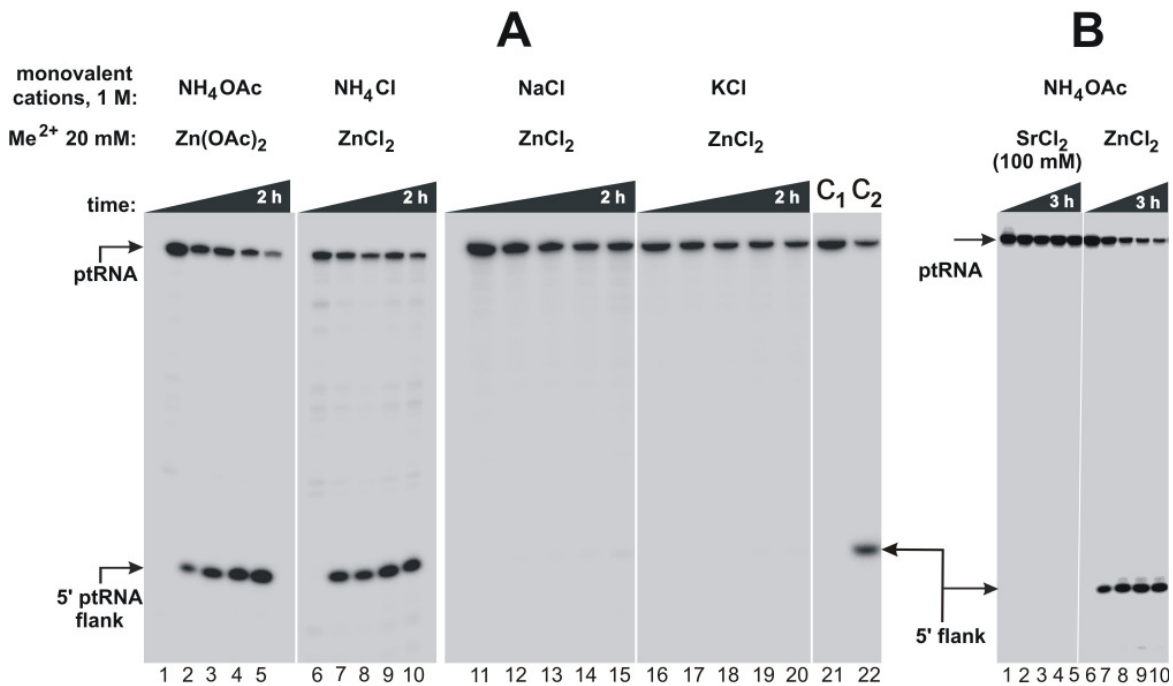

Fig. 4.1.2: Processing of all-ribose ptRNA^{Gly} by *E. coli* P RNA under single turnover conditions at 37 °C in the presence of 20 mM Zn^{2+}. (A) dependence on the type of monovalent cation; processing occurred in the presence of ammonium, but not sodium or potassium salts; reaction conditions: 5 µM P RNA, < 1 nM ptRNA, 50 mM PIPES, pH 6.65, 1 M monovalent salt as indicated, 20 mM $ZnCl_2$ or $Zn(OAc)_2$; control lanes 1, 6, 11, 16, 21: incubation for 2 h in the absence of P RNA; time points were 5 min (lanes 2, 7, 12, 17, 22), 20 min (lanes 3, 8, 13, 18), 1 h (lanes 4, 9, 14, 19) and 2 h (lanes 5, 10, 15, 20); lanes 21 and 22 (C_1, C_2) are equal to lanes 1 and 2. (B) assay documenting that no processing occurs in the presence of Sr^{2+} as the sole metal ion; reaction conditions: 5 µM P RNA, < 1 nM ptRNA, 50 mM PIPES, pH 6.65, 1 M NH_4OAc and 100 mM $SrCl_2$ (left) or 20 mM $ZnCl_2$ (right). Control lanes 1 and 6: incubation for 3 h in the absence of P RNA; time points were 5 min (lane 7), 20 min (lanes 2, 8), 40 min (lane 3), 1 h (lanes 4, 9) and 3 h (lanes 5, 10).

cofactor represents a ribozyme case where the specific transition state is achieved despite a dramatic destabilisation of substrate ground state binding.

In contrast to Zn^{2+}, Sr^{2+} alone did not support *E. coli* P RNA catalysis (Fig. 4.1.2 B) but mediated ground state binding (4.1.2 and Fig. 4.1.5). In the combination with Zn^{2+}, Sr^{2+} stimulated the cleavage reaction at low concentrations by increasing E•S complex formation but inhibited catalysis at higher concentrations (Fig. 4.1.3 A). The failure of Sr^{2+} to support catalysis as well as the inhibition by Sr^{2+} under standard assay conditions can be attributed to a coordination geometry different from the canonical octahedral Mg^{2+}. Indeed, a coordination geometry resembling a slightly distorted trigonal prism and involving nine oxygen atoms (four ribose hydroxyl groups and five waters) was observed for a Sr^{2+} ion in the crystal structure of the tRNA^{Ala} acceptor stem (Mueller et al., 1999). Taking into account that four hydroxyl groups are inner-sphere ligands of this Sr^{2+} ion, whereas inner-sphere coordination of 2'-OH ligands to Mg^{2+} seems to be rare (Juneau et al., 2001), it is an intriguing possibility that Sr^{2+} fails to support *E. coli* P RNA catalysis due to inner-sphere coordination to the 2-OH at nt −1 of the substrate. A role for this substituent in Sr^{2+} binding is indeed indicated by a weaker inhibitory effect of Sr^{2+} in the context of the ptRNA substrate with a 2'-F modification at nt −1 (Fig. 4.1.7 A).
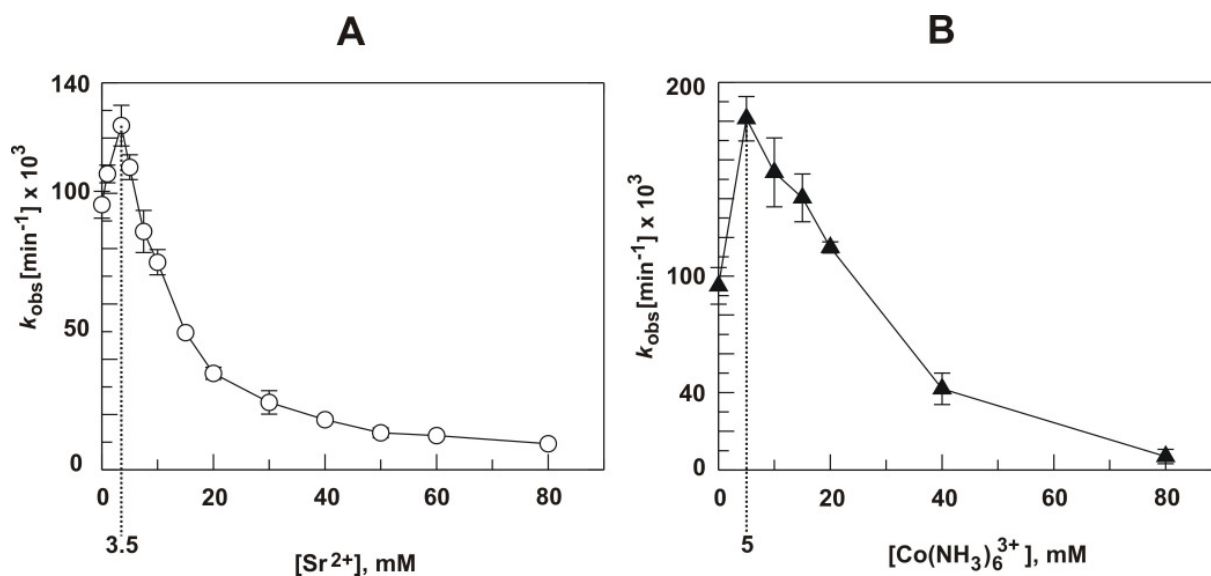

Fig. 4.1.3: Processing rates as a function of increasing concentrations of $SrCl_2$ (A) or $Co(NH_3)_6Cl_3$ (B); reaction conditions: 5 µM *E. coli* P RNA, < 1 nM ptRNA, 50 mM PIPES, pH 6.65, 1 M NH_4OAc, 20 mM $Zn(OAc)_2$; transition points between the stimulatory and inhibitory phases of the curves are marked by broken lines.

The inability of Zn^{2+} to mediate high affinity substrate binding suggested the potential to use Zn^{2+} as a specific tool to study catalysis apart from E•S complex formation. This, however, turned out to be difficult because saturating enzyme concentrations could only be reached when a second non-catalytic metal ion was present that promotes substrate binding but does not support catalysis, such as Sr^{2+}. Unfortunately, Sr^{2+} also inhibited catalysis (Fig. 4.1.3 A). Analysis of ptRNA processing under single turnover conditions by *E. coli* P RNA in the presence of Zn^{2+} and increasing concentrations of Sr^{2+} resulted in complex velocity versus $[Sr^{2+}]$ curves with ascending and descending sections (Fig. 4.1.3 A; Fig. 4.1.7 and Fig. 4.1.8). This suggested that two different Sr^{2+} ions (or classes of ions) affected the cleavage reaction under these experimental conditions. Similar results were observed with $Co(NH_3)_6^{3+}$ instead of Sr^{2+} (Fig. 4.1.3 B).
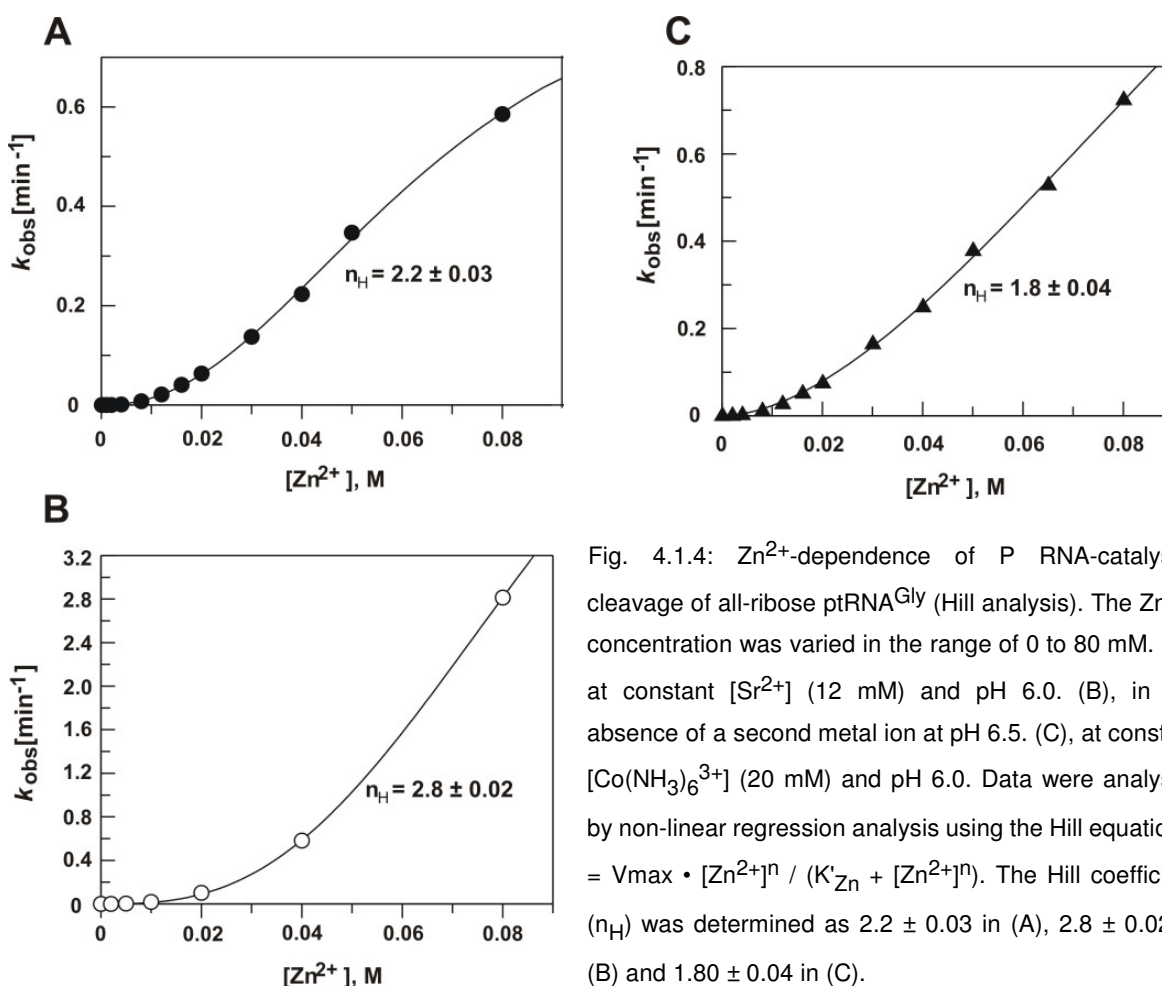

Fig. 4.1.4: Zn^{2+}-dependence of P RNA-catalysed cleavage of all-ribose ptRNA^{Gly} (Hill analysis). The Zn^{2+}-concentration was varied in the range of 0 to 80 mM. (A), at constant $[Sr^{2+}]$ (12 mM) and pH 6.0. (B), in the absence of a second metal ion at pH 6.5. (C), at constant $[Co(NH_3)_6^{3+}]$ (20 mM) and pH 6.0. Data were analysed by non-linear regression analysis using the Hill equation $v = V_{max} \cdot [Zn^{2+}]^n / (K'_{Zn} + [Zn^{2+}]^n)$. The Hill coefficient ($n_H$) was determined as 2.2 ± 0.03 in (A), 2.8 ± 0.02 in (B) and 1.80 ± 0.04 in (C).

Hill analyses of *E. coli* P RNA-catalysed cleavage in the presence of Zn^{2+} alone or Zn^{2+} / Sr^{2+} or Zn^{2+} / $Co(NH_3)_6^{3+}$ combinations revealed an involvement of two or more

Zn^{2+} ions or classes of Zn^{2+} ion binding sites (Fig. 4.1.4). This result is similar to those obtained with Mg^{2+} as the metal ion cofactor (Smith and Pace, 1993). These authors concluded that at least three Mg^{2+} ions take part in the catalytic step.

4.1.2 Zn^{2+}/ Sr^{2+} dependence of substrate binding to *E. coli* P RNA

Binding of ptRNA[Gly] to *E. coli* P RNA was analysed as a function of Zn^{2+} and Sr^{2+}. K_d measurements (Fig. 4.1.5) were performed with trace amounts of ^{32}P-labelled ptRNA and varying excess amounts of enzyme using a gel filtration spin column assay (Warnecke et al., 1999; Beebe & Fierke, 1994). The results are summarised in Table 4.1.1.

Table 4.1.1 Influence of Zn^{2+}, Sr^{2+} and/or $Co(NH_3)_6^{3+}$ on ptRNA binding

metal ion(s)		K_d (nM)	average endpoint
transition Me^{2+}	other		
--	--	10,000 ± 3,000	0.66
20 mM Zn^{2+}	--	≥ 20,000	n. d. [*]
20 mM Cd^{2+}	--	2,100 ± 400	0.75
--	5 mM Sr^{2+}	240 ± 15	0.93
20 mM Zn^{2+}	5 mM Sr^{2+}	700 ± 300	0.59
--	80 mM Sr^{2+}	4 ± 0.5	0.98
20 mM Zn^{2+}	80 mM Sr^{2+}	9 ± 0.5	0.92
20 mM Zn^{2+}	5 mM $Co(NH_3)_6^{3+}$	2,486 ± 400	0.55
--	20 mM $Co(NH_3)_6^{3+}$	751 ± 200	0.75
20 mM Zn^{2+}	20 mM $Co(NH_3)_6^{3+}$	350 ± 120	0.65
--	80 mM $Co(NH_3)_6^{3+}$	79 ± 35	0.26
20 mM Zn^{2+}	80 mM $Co(NH_3)_6^{3+}$	53 ± 6	0.28

K_d and endpoint values (n. d. = not determined) could not be determined with reasonably low errors due to very low ribozyme-substrate affinity; the K_d of 20000 nM in the presence of 20 mM Zn^{2+} alone is a lower limit estimate.
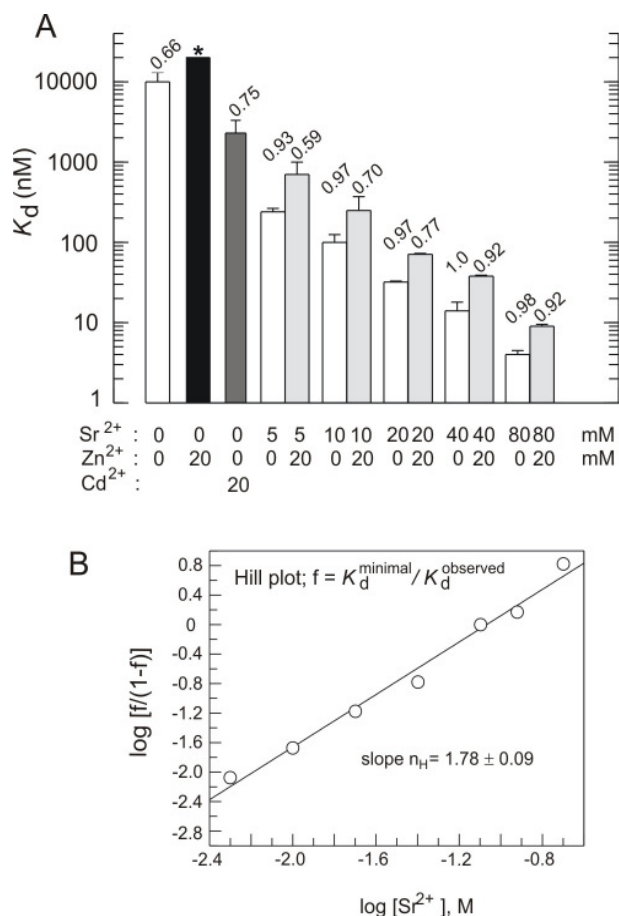
Fig. 4.1.5: K_d values for ptRNA^{Gly} binding to *E. coli* P RNA determined by the spin column assay (Beebe and Fierke, 1994; Warnecke et al., 1999). Assay buffers contained 50 mM MES, pH 6.0, 1 M NH$_4$OAc and indicated concentrations of Sr^{2+} and/or Zn^{2+} (or Cd^{2+}). (A) Bar diagram of log K_d dependence on Sr^{2+} and/or Zn^{2+} (or Cd^{2+}) concentration as indicated below the diagram. Values above bars represent the proportion of ptRNA^{Gly} that was able to form a complex with P RNA at the theoretical endpoint (P RNA saturation), normalised to conditions of 40 mM Sr^{2+}. Asterisk above the black bar for conditions of 20 mM Zn^{2+} alone: the experimental endpoint could not be reached due to very weak complex formation, which resulted in high errors for K_d determinations; the K_d of $\geq$ 20 µM is therefore only an estimate. Error bars indicate errors obtained from the average of four independent experiments. (B) Hill plot analysis of K_d dependence on Sr^{2+} concentration. f = (minimal K_d) / (observed K_d); the minimal K_d at saturating Sr^{2+} concentrations was determined to be 2 nM.

In the absence of any divalent metal ion, a K_d of about 10 µM was measured under standard assay conditions. The K_d increased to $\geq$ 20 µM in the presence of 20 mM Zn^{2+}, demonstrating that Zn^{2+} destabilises substrate ground state binding. Another transition metal ion, Cd^{2+}, supported E•S formation poorly as well, although more efficiently than Zn^{2+}. In contrast to these transition metal ions, Sr^{2+} or Co(NH$_3$)$_6$$^{3+}$ support substrate binding, with Sr^{2+} being more efficient than Co(NH$_3$)$_6$$^{3+}$. K_d values in the presence of 20 mM Zn^{2+} progressively decreased with increasing Sr^{2+} concentrations (Fig. 4.1.5 A). However, at all tested Sr^{2+} concentrations (5, 10, 20, 40 and 80 mM), addition of 20 mM Zn^{2+} resulted in a constant 2 to 3-fold increase in K_d, indicating that Sr^{2+} is unable to displace Zn^{2+} (or to compensate its deleterious effects) at some sites where it directly or indirectly impairs high affinity substrate binding. Moreover, the proportion of substrate that is able to form a stable complex under conditions of enzyme saturation (Fig. 4.1.5 A, numbers above bars) decreased with increasing ratios of [Zn^{2+}] to [Sr^{2+}], for example the binding-

proficient substrate fraction at 20 mM Zn^{2+} increased from 0.59 to 0.92 (normalised to 1.0, measured for 40 mM Sr^{2+} alone, Fig. 4.1.5 A) at 5 and 80 mM Sr^{2+}, respectively. Hill analysis of K_d in the presence of varying concentrations of Sr^{2+} and in the absence of Zn^{2+} gave a slope of $n_H = 1.8$ (Fig. 4.1.5 B), suggesting that binding of at least two Sr^{2+} ions contributes to enzyme-substrate complex formation under the applied conditions.

Since K_d reflects structural properties of enzyme and substrate, the Zn^{2+} binding sites responsible for this K_d increase may be located on the substrate and/or enzyme. To understand the structural effects of Zn^{2+} observed in the presented study, it is instructive to inspect the Zn^{2+} binding sites detected in yeast $tRNA^{Phe}$ crystals (Rubin et al., 1983). Five bound Zn^{2+} ions were identified, two of which, Zn (1) and Zn (2), replaced tightly bound Mg^{2+} ions in the U8-U12 region and in the D loop (corresponding to the Mg^{2+} binding sites 1 and 3 in Jovine et al., 2000), one, Zn (3), overlapped with the weak Mg^{2+} binding site 7 of Jovine et al., and the remaining two, Zn (4, 5), being Zn^{2+}- or transition metal ion-specific sites in base-paired regions. All five Zn^{2+} ions were coordinated tetrahedrally, and four of them were bound by direct coordination to a guanine N7 at positions where the G residue is flanked by a purine residue on its 5' side. Based on these observations, Zn^{2+} may well cause specific changes of tRNA conformation or may occupy novel Zn^{2+}-specific sites that disturb ptRNA interaction with *E. coli* P RNA. The preference of Zn^{2+} for purine-guanine dinucleotides also in paired regions implies that (a) some Zn^{2+} binding sites may directly perturb E•S contacts involving acceptor and T stems regions and (b) that effects of Zn^{2+} will be to some extent sequence-specific and thus specific for every individual RNA under investigation.

$Co(NH_3)_6^{3+}$ also decreased the K_d (Table 4.1.1), but substrate affinity was lower relative to equal concentrations of Sr^{2+}, suggesting that $Co(NH_3)_6^{3+}$ is a rather inefficient substitute for hexahydrated Mg^{2+} in this system. Whereas K_d values in the presence of Sr^{2+} were generally increased by addition of 20 mM Zn^{2+} (Fig. 4.1.5 A), addition of 20 mM Zn^{2+} to 20 or 80 mM $Co(NH_3)_6^{3+}$ (Table 4.1.1) tended to lower K_d to some extent compared with the corresponding $Co(NH_3)_6^{3+}$ alone conditions. This suggests that Zn^{2+} and $Co(NH_3)_6^{3+}$ weakly complement each other in promoting E•S complex formation. Remarkably, higher concentrations (e.g. 80 mM) of $Co(NH_3)_6^{3+}$ substantially lowered the proportion of ptRNA capable of complex formation (compared to Sr^{2+}) under saturating enzyme concentrations (0.26 for 80 mM $Co(NH_3)_6^{3+}$ versus 0.98 for 80 mM Sr^{2+}; Table 4.1.1).

4.1.3 Processing of substrates with 2'-ribose modifications at nt –1 in the presence of Zn^{2+}/ Sr^{2+}

A model of the P RNA cleavage mechanism (Chen and Gegenheimer, 1997; Fig. 4.1.6, model I) proposes that one Mg^{2+} ion (Mg[B]) simultaneously interacts with the OH⁻ nucleophile and the 2'-OH at position –1 of the substrate and directly coordinates to the *pro-R*p phosphate oxygen at the cleavage site. In an alternative model (Fig. 4.1.6, model II), two metal ions (Mg[A] and Mg[B]) directly coordinate to the *pro-R*p oxygen, but Mg[A] instead of Mg[B] coordinates the OH⁻ nucleophile (Warnecke et al., 1996; Kuimelis & McLaughlin, 1998). In both models, Mg[B] interacts with the 2'-OH group at nt –1 of the substrate. The possibility that Sr^{2+} displaces catalytically important Zn^{2+} at the aforementioned metal ion binding site B was addressed in this study, assuming that the binding sites for the two different metal ions overlap to such an extent that their binding is mutually exclusive. Recently it was shown that 2'-substitutions at nt –1 of ptRNA decreased cleavage efficiency by *E. coli* P RNA in the order 2'-H ≤ 2'-N < 2'-F < 2'-OH under conditions of rate-limiting chemistry (Persson et al., 2003). Assuming that Sr^{2+} indeed displaces a Zn^{2+} ion that is bound to site B involving the 2'-OH at nt –1 of ptRNA (Fig. 4.1.6), one would expect that
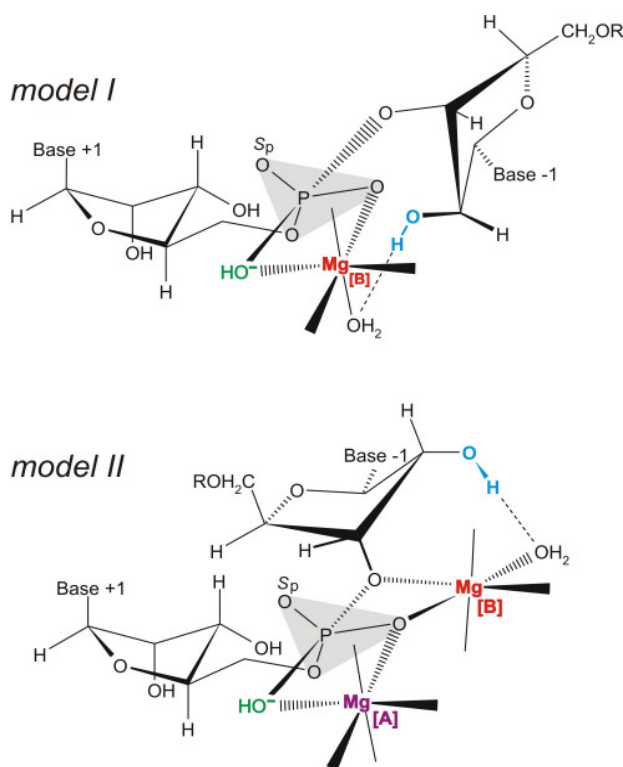

Fig. 4.1.6: Transition state models for phosphodiester hydrolysis by *E. coli* P RNA. The single 2'-hydroxyl at nt –1 (in blue) was replaced with a 2'-deoxy, 2'-amino or 2'-fluoro group in the modified substrates analysed in Fig. 4.1.7. Putative, catalytically important Mg^{2+} ions are shown in red and magenta; metal ion site B was in the focus of the present study. The transition state model for hydrolysis of the scissile phosphodiester connecting nt +1 and –1 is derived from that proposed in Chen and Gegenheimer, 1997, according to which the Mg^{2+} ion at site B (Mg[B]) directly coordinates to the *pro*-Rp phosphate oxygen and simultaneously interacts with the OH⁻ nucleophile (in green) and the 2' OH at position –1 (model I). Alternatively, two magnesium ions Mg[A] and Mg[B] may directly coordinate to the *pro*-Rp oxygen, but Mg[A] instead of Mg[B] coordinates the OH⁻ nucleophile (Warnecke et al., 1996; Kuimelis & McLaughlin, 1998; model II).

these 2'-modifications change the affinities of Zn^{2+} and Sr^{2+} (which largely differ in their electronic properties and the details of their coordination spheres) to different extents. In contrast, the competition profile should be much less affected if Sr^{2+} displaces catalytic Zn^{2+} at another than site B, where metal ion coordination is not directly dependent on the 2'-hydroxyl at nt −1.
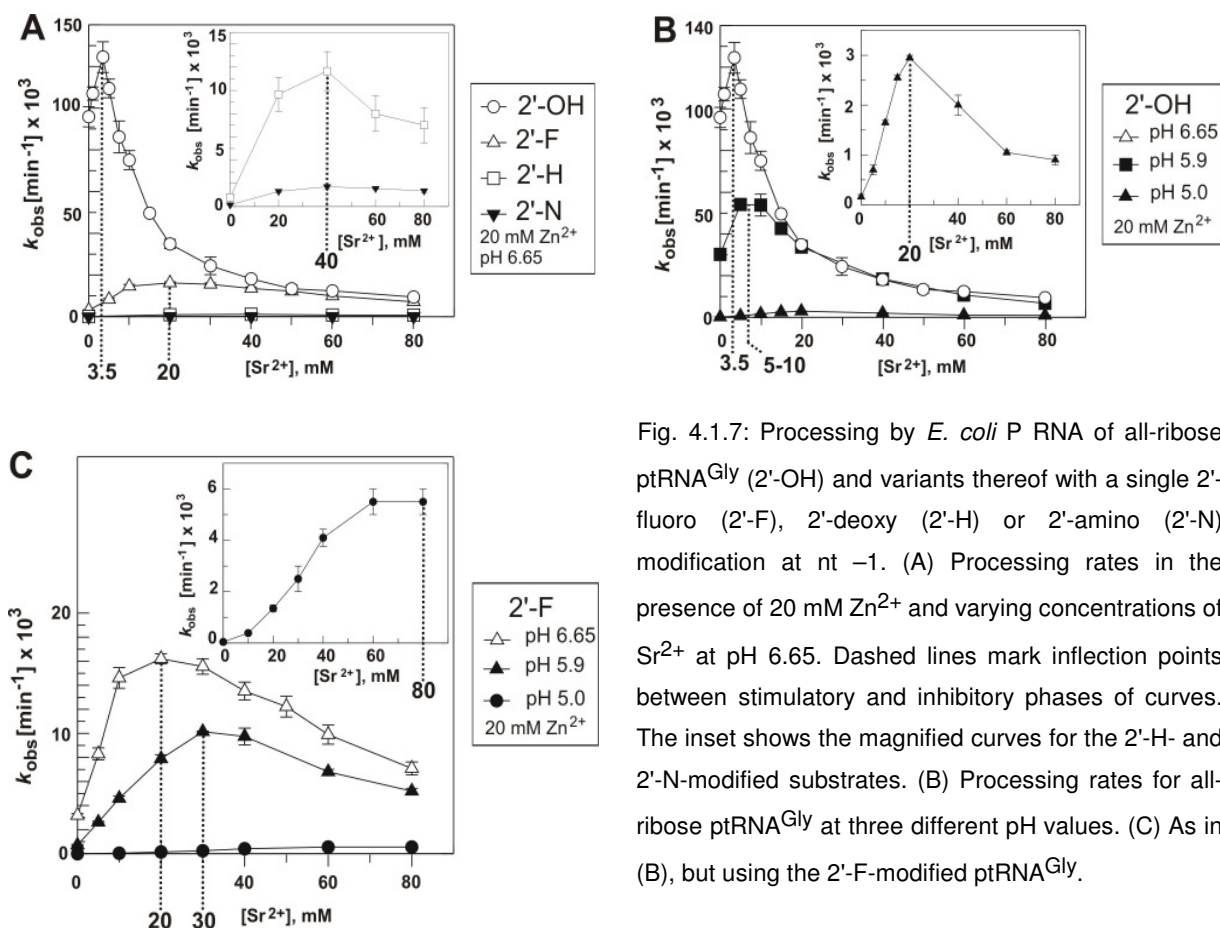

Fig. 4.1.7: Processing by *E. coli* P RNA of all-ribose ptRNA^{Gly} (2'-OH) and variants thereof with a single 2'-fluoro (2'-F), 2'-deoxy (2'-H) or 2'-amino (2'-N) modification at nt −1. (A) Processing rates in the presence of 20 mM Zn^{2+} and varying concentrations of Sr^{2+} at pH 6.65. Dashed lines mark inflection points between stimulatory and inhibitory phases of curves. The inset shows the magnified curves for the 2'-H- and 2'-N-modified substrates. (B) Processing rates for all-ribose ptRNA^{Gly} at three different pH values. (C) As in (B), but using the 2'-F-modified ptRNA^{Gly}.

In fact, the concentration of Sr^{2+} at the transition point between the stimulatory and inhibitory phases of the curve was substantially shifted towards higher Sr^{2+} concentrations (20 to 40 mM versus 3.5 mM, Fig. 4.1.7 A) when the 2'-OH at nt −1 was replaced with a 2'-F, 2'-N or 2'-H substituent. To determine if this shift in the inflection point of the curve is a specific feature associated with the 2'-ribose modifications at nt −1 rather than a general effect, for example related to a reduction in the rate of the chemical step (k_{chem}), the Sr^{2+} dependence of cleavage rate was analysed for the all-ribose substrate at two lower pH values to reduce the rate of the chemical step (k_{chem}). When the changes in the inflection point observed are exclusively due to the ribose modifications at nt −1, one would expect the same inflection point for all pH values. However, the inflection point of these curves shifted

toward higher Sr^{2+} concentrations with decreasing pH (Fig. 4.1.7 B), which also holds for cleavage of the 2'-F ptRNA measured at the same pH values (Fig. 4.1.7 C). These findings suggested that it might be difficult to extract metal ion-specific information based on changes of the inflection point between the stimulatory and inhibitory phases.

4.1.4 The effect of enzyme concentration on the inhibition by Sr^{2+}

The affinity measurements (Fig. 4.1.5 A) showed that an enzyme concentration of 5

Fig. 4.1.8: Sensitivity of Sr^{2+}-dependent processing rates to differences in [E]. (A), all-ribose ptRNA^{Gly} (2'-OH); (B), 2'-F-ptRNA^{Gly}; (C, D) Secondary v_0/v_i plots of the data ($v_0 = k_{obs}$ in the absence of Sr^{2+}; $v_i = k_{obs}$ at the respective Sr^{2+} concentration) from (A) and (B). Data fitting was best with the model depicted in Fig. 4.1.9 A, using equation 4.1.1 (see below); curve fits yielded the following values for $\alpha K_{I(a)}$ and βK_I: 1.46 ± 0.46 mM and 0.72 ± 0.025 mM (panel C, 1.4 µM *E. coli* P RNA, 2'-OH), 1.49 ± 0.45 mM and 0.72 ± 0.005 mM (panel C, 5 µM *E. coli* P RNA, 2'-OH), 3.5 ± 0.4 mM and 9.1 ± 2.1 mM (panel D, 1.4 µM *E. coli* P RNA, 2'-F) and 2.2 ± 0.2 mM and 11 ± 0.8 mM (panel D, 5 µM *E. coli* P RNA, 2'-F); estimates for K_S were 50 and 120 µM in panels C and D, respectively.

µM was subsaturating at 20 mM Zn^{2+} and < 5 mM Sr^{2+}. Since the stimulatory effect of Sr^{2+} at low concentrations was attributed to its stabilisation of E•S complexes, changes in enzyme concentration [E] were also expected to affect the inflection point between the stimulatory and inhibitory phases. Indeed, Sr^{2+}-dependence of processing rate displayed changes in the inflection point between the two phases for the all-ribose as well as the 2'-F ptRNA when monitored at enzyme concentrations of 5 versus 1.4 µM (Fig. 4.1.8 A, B).

4.1.5 Mode of inhibition and stimulation by Sr^{2+}

In this study a kinetic model that describes both the inhibition and stimulation of *E. coli* P RNA catalysis by Sr^{2+} ions was proposed. As discussed previously, the Hill plot analysis in Fig. 4.1.5 B and the biphasic curves obtained by plotting the reaction velocity (k_{obs}) versus [Sr^{2+}] suggested that at least two Sr^{2+} ions contribute to E•S complex

Fig. 4.1.9: (A) Equilibria for the *E. coli* P RNA-catalysed processing reaction in the presence of constant [Zn^{2+}] as the catalytic cofactor and varying concentrations of [Sr^{2+}] that activate the reaction at low but inhibit at higher concentrations. The model involves two Sr^{2+} ions (or two classes of Sr^{2+} ions) that both improve substrate affinity in a cooperative manner (see Fig. 4.1.5), but one of the two inhibiting substrate conversion noncompetitively with respect to the substrate. I(a) = Sr^{2+} ion that activates processing by decreasing K_S to αK_S; I = inhibitory Sr^{2+} ion that inhibits cleavage chemistry but also decreases K_S to βK_S. (B) Dixon plot of the *E. coli* P RNA-catalysed ptRNA cleavage rate at 37 °C as a function of [Sr^{2+}] in the presence of four different fixed Zn^{2+} concentrations and 5 µM *E. coli* P RNA, < 1 nM ptRNA, 50 mM PIPES, pH 6.65, and 1 M NH_4OAc; open circles, 8.1 mM Zn^{2+}; filled circles, 10 mM Zn^{2+}; open squares, 15 mM Zn^{2+}; filled triangles, 20 mM Zn^{2+}. All four data sets fit to straight lines intersecting on the x-axis, indicating that Sr^{2+} acts as a noncompetitive inhibitor with respect to Zn^{2+}

formation. This model (Fig. 4.1.9 A) assumes that there are two Sr^{2+} ions involved, both mediating substrate binding to *E. coli* P RNA and one of these two inhibiting substrate conversion.

According to this model the following formula (the derivation of this formula is described in appendix 1) was obtained:

$$\frac{v_0}{v_i} = \frac{K_S + [E] \cdot (1 + (\frac{1}{\beta \cdot K_I} + \frac{1}{\alpha \cdot K_{I(a)}}) \cdot [I] + \frac{1}{\alpha \cdot \beta \cdot K_I \cdot K_{I(a)}} \cdot [I]^2)}{(K_S + [E]) \cdot (1 + \frac{1}{\alpha \cdot K_{I(a)}} \cdot [I])} \qquad (4.1.1)$$

The data of Fig. 4.1.8 A and B were then replotted as v_0 / v_i (v_0 and v_i correspond to k_{obs} in the absence and presence of Sr^{2+}, respectively; Fig. 4.1.8 C and D). The best fit of the data was obtained utilising equation 4.1.1 (see above) based on the model outlined in Fig. 4.1.9 A. The two Sr^{2+} ions involved may well be those suggested by the Hill coefficient of the binding data in Fig. 4.1.5 B. The fact that both Sr^{2+} ions contribute to formation of high affinity E•S complexes is accounted for by introducing the interaction factors α and β in the scheme of Fig. 4.1.9 A. Other models, for example assuming the involvement of two "activating" and one inhibitory Sr^{2+} ion or predicting that E•I•S and E•S•I(a)•I complexes retain residual reactivity, failed to give satisfactory curve fits of the data.

In order to investigate the inhibition type of Sr^{2+} with respect to Zn^{2+}, kinetic experiments were performed by varying the Sr^{2+} concentration between 10 and 40 mM at four different Zn^{2+} concentrations. Under these conditions, the enzyme concentration (5 μM) was assumed to be saturating at all variations of Sr^{2+} and Zn^{2+}, even at the combination 10 mM Sr^{2+} and 20 mM Zn^{2+}, where a K_d of about 250 nM was determined (Fig. 4.1.5 A). Thus, cleavage chemistry was expected to limit the rate of substrate turnover. The Dixon plot of the data (Fig. 4.1.9 B) suggests that Sr^{2+} inhibition is noncompetitive with respect to Zn^{2+}, arguing against a direct displacement of catalytic Zn^{2+} by a Sr^{2+} ion at the aforementioned metal ion site [B] (Fig. 4.1.6).

4.2 Chemical modification studies: the role of 2'-hydroxyls at the cleavage site and neighbouring positions

The presence of the 2' OH group on the RNA pentose sugar ring is at the origin of the profound structural and dynamical differences observed between RNA and DNA molecules. Structural and biophysical studies have led to the conclusion that the additional 2' OH group stabilises the C 3' -endo pucker (Fig. 4.2.1 B) typical of RNA, compared with the C 2' -endo pucker prevalent in DNA (Sanger, 1984; Fig. 4.2.1 A). Yet, a precise knowledge of the orientation and dynamics of the 2' OH substituent, which is an important RNA recognition element, is essential to clarify its specific structural contribution to the stabilisation of helical regions, complex RNA tertiary folds and RNA / protein interactions. This knowledge will be useful in the study of the mechanisms of catalytic RNA molecules, which all depend on direct or indirect contributions from 2' OH groups (Gesteland & Atkins, 1993; Eckstein & Lilley, 1996).

A   **B**
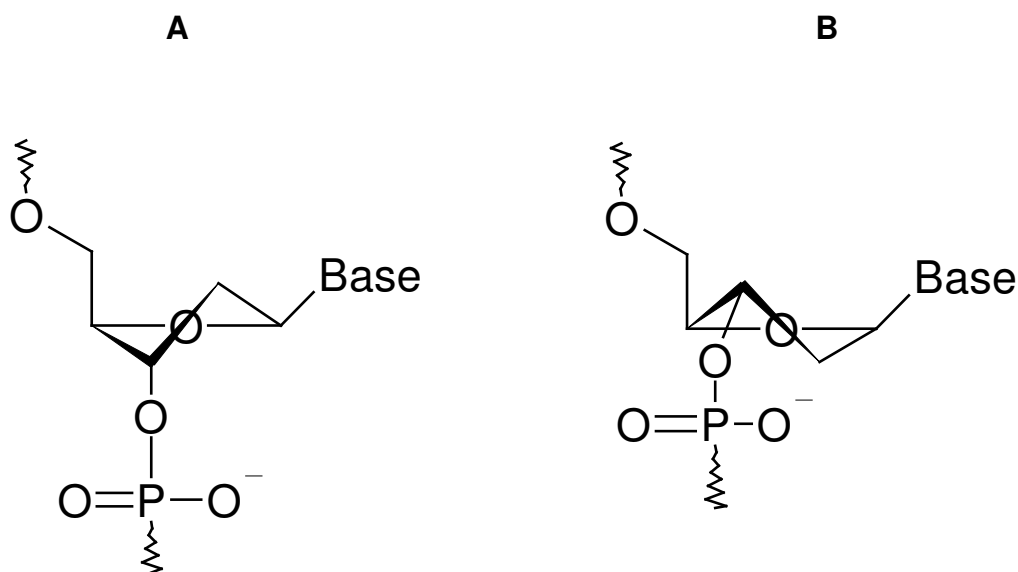
Fig. 4.2.1: The conformations of sugar rings found in nucleic acids; (A) C 2' -endo (type S) conformation typical of DNA that form B-type helices; (B) C 3' -endo (type N) conformation typical of RNA forming A-type helices

In this work the role of the 2' OH groups within the ptRNA substrate in the RNase P - catalysed cleavage was examined. The studies required modification of this group followed by analysis of the modified RNAs. Chemical modifications were introduced by ligation of chemically synthesised 24-mer oligoribonucleotides to the 3' portion of a glycine tRNA (tRNA$_{18-79}$) starting with position +18 according to the tRNA numbering system. The ligation site was in the tRNA D loop, marked by the red circle (Fig. 4.2.2). The following modified

ptRNAs were analysed: variants with locked nucleic acid (LNA; see Fig. 4.2.2 left) modifications at nucleotide (nt) positions −2 (T_{LNA} −2), −1 (T_{LNA} −1) and +1 (G_{LNA} +1), 2'-deoxy modifications at nt −1 (2' H −1) and +1 (2' H +1), 2'-fluoro at nt −1 (2' F −1) and 2'-methoxy at −1 (2' OCH_3 −1) and +1 (2' OCH_3 +1). An unmodified ptRNA [r (T −1, T −2)] was used as reference. The ptRNA variants 2' H −1 and 2' F −1 contained a uracil (U) and cytosine (C) at nt −2 and −1 (see Fig. 4.1.1) while all other substrates mentioned above had a ribo-thymine at both positions (Fig. 4.2.2). Therefore, for these two variants a second substrate with U at nt −2 and C at nt −1 [r (C −1)] was used as reference.
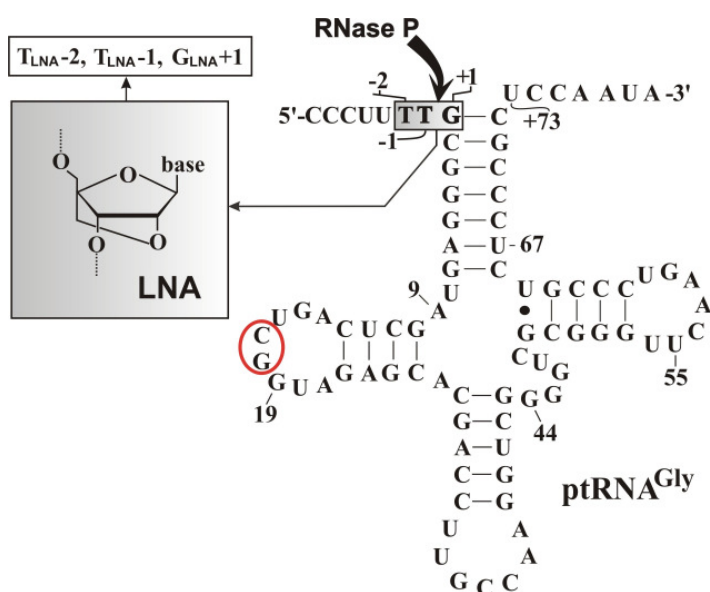
Fig. 4.2.2: Secondary structure of the ptRNA^{Gly} substrate. Modified bases at and around the canonical RNase P cleavage site (between nt −1 and +1, marked by the arrow) are illustrated by the grey-shaded box. In the grey box on the left an LNA modification is illustrated. Please note that the sequence of the ptRNA variants r (C − 1), 2' H −1 and 2' F −1 differs at nt −1 and −2 from that shown here; compare with Fig. 4.1.1.

LNA monomers (2'-O,4'-C-methylene-,-D-ribofuranosyl nucleotide) are nucleotide analogues with a bicyclic furanose unit locked in an RNA-mimicking C 3' -endo sugar conformation (Obika et al., 1997; Singh et al., 1998; Koshkin et al., 1998). Duplexes involving LNA's (hybridised with either DNA or RNA) display an unprecedented increase of the melting temperature, ranging from 4℃ to 9.3℃ per modification compared to the corresponding unmodified reference duplex. In contrast to nucleotides with a flexible ribose ring which exist in a fast equilibrium between C 3'- and C 2' -endo conformation (the N, S two-state model; Altona & Sundaralingam 1972; 1973), the LNA-modified nucleotides adopt a rigid C 3' -endo conformation. The positions flanking an LNA modification adopt sugar conformations with a significantly increased population of the N-type (C 3' -endo) conformer (Nielsen et al., 1999; 2000; Petersen et al., 2000; 2002). The 2' substituent of the LNA - modified nucleoside is a good H-bond acceptor but lacks an H-bond donor function. Some sterical effects caused by the methylene bridge of LNA have to be taken into consideration as well.

In contrast to LNA, 2' fluoro nucleosides have a flexible sugar conformation and similar to LNA lack the H-bond donor function, but may retain some acceptor activity, although weaker than LNA.

2' deoxy nucleosides have neither an H-bond donor nor acceptor function, while the conformation of the sugar moiety is flexible, although the deoxynucleosides show a preference for the C 2' -endo conformation.

2' methoxy nucleosides have properties similar to LNA. They lack the H-bond donor function but can accept H-bonds with similar strength as LNA. In contrast to LNA, the ribose conformation of 2' methoxy nucleosides is flexible. The location of the methyl group is similar but not identical to that of the methylene group in LNA. Therefore, sterical effects caused by these groups are not necessarily identical but may overlap to some extent.

4.2.1 Ground state binding of ptRNAs carrying 2'-ribose modifications

The affinity of ptRNA to *E. coli* P RNA was investigated using the gel filtration spin column assay (see 3.5.3; Warnecke et al., 1999; Beebe & Fierke, 1994) in the presence of Sr^{2+} (5 or 80 mM) or Ca^{2+} (15 mM). These metal ions were selected in order to avoid significant cleavage by *E. coli* P RNA during binding experiments. K_d measurements (Fig. 4.2.3) were performed with trace amounts of ^{32}P-labelled ptRNA variants and varying excess amounts of enzyme. The results are summarised in Table 4.2.1.
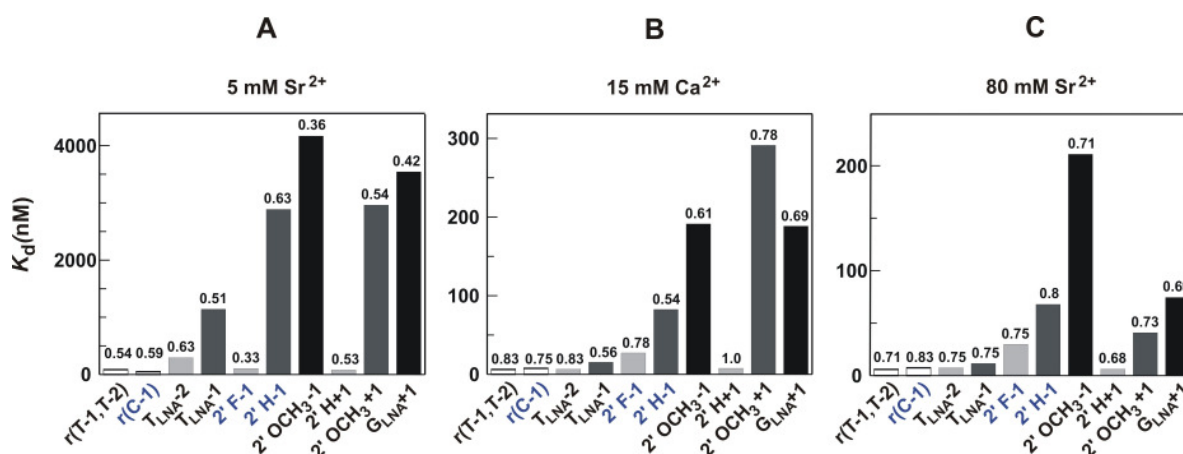
Fig. 4.2.3: Ground state binding of 2'-ribose modified ptRNAs to *E. coli* P RNA in the presence of 1 M NH_4OAc, 0.1 % SDS, 0.05 % Nonidet P40, 50 mM MES, pH 6.0 and 5 mM Sr^{2+} (A), 15 mM Ca^{2+} (B) and 80 mM Sr^{2+} (C). The binding experiments were performed according to 3.5.3. The numbers above the columns indicate the fraction of substrate able to bind under enzyme saturation conditions normalised to the fraction measured for 2' H +1 at 15 mM Ca^{2+}. The variants highlighted in blue represent those with a C at nt −1 and a U at nt −2, while those shown in black correspond to substrates with a ribo T at nt −1 and −2.

Table 4.2.1 Influence of the ribose modifications on ptRNA binding to E. coli P RNA.

divalent metal ion	ptRNA substrate	K_d (nM)	average endpoint
5 mM Sr^{2+}	r(T −1, T −2)	86 ± 22	0.54
	r(C −1)	48 ± 20	0.59
	T$_{LNA}$ −2	295 ± 70	0.63
	T$_{LNA}$ −1	1143 ± 232	0.51
	2' F −1	103 ± 49	0.33
	2' H −1	2887 ± 874	0.63
	2' OCH$_3$ −1	4168 ± 733	0.36
	2' H +1	80.4 ± 11	0.53
	2' OCH$_3$ +1	2960 ± 931	0.54
	G$_{LNA}$ +1	3544 ± 1100	0.42
	r(T −1, T −2)	6.1 ± 2.3	0.83
	r(C −1)	7.6 ± 1.3	0.75
	T$_{LNA}$ −2	6.7 ± 3	0.83
	T$_{LNA}$ −1	15.5 ± 3.7	0.56
	2' F −1	27.1 ± 3.7	0.78
	2' H −1	82.5 ± 11.3	0.54
	2' OCH$_3$ −1	191.4 ± 4	0.61
	2'H +1	7.6 ± 2.7	1.00
	2' OCH$_3$ +1	188 ± 21	0.78
	G$_{LNA}$+1	291 ± 84	0.69
	r(T −1, T −2)	5.9 ± 2.9	0.71
	r(C-1)	7.4 ± 2	0.83
	T$_{LNA}$ −2	7.4 ± 2.4	0.75
	T$_{LNA}$ −1	11.5 ±4.2	0.75
	2'F −1	29.9 ±8.3	0.75
	2'H −1	67.9 ± 16.4	0.80
	2' OCH$_3$ −1	211 ± 61	0.71
	2'H +1	6.2 ± 1.2	0.68
	2' OCH$_3$ +1	46.7 ± 18.5	073
	G$_{LNA}$ +1	74.4 ± 25.6	0.69

The average endpoints (right column) represent the fraction of substrate able to bind under enzyme saturation conditions and were normalised to 1, measured for 2' H +1 at 15 mM Ca^{2+}. The red numbers correspond to ptRNA variants with reduced endpoints compared with the corresponding reference substrate. The variants shown in blue (second column from left) carry C at nt −1 and a U at nt −2, while in all other variants a ribo T is incorporated at these positions.

The modifications introduced into ptRNA substrates at nt −1 and +1 affected ptRNA binding. The T$_{LNA}$ −2 variant had a slightly reduced binding affinity (3.4-fold, relative to the reference substrate) at 5 mM Sr^{2+}, but not at 15 mM Ca^{2+} and 80 mM Sr^{2+}.

Effects of ribose modification at nt −1 on ptRNA ground state binding

The 2' modifications introduced at nt −1 had different effects on ptRNA binding affinity. The substrate affinity decreased in the order r(C −1) ~ r(T −1, T −2) > 2' F −1 > T$_{LNA}$ −1 >> 2' H −1 > 2' OCH$_3$ −1 at 5 mM Sr^{2+} and r(T −1, T −2) ~ r(C −1) > T$_{LNA}$ −1 > 2' F −1 > 2' H −1 > 2' OCH$_3$ −1 at 15 mM Ca^{2+} and 80 mM Sr^{2+} (Table 4.2.1; Fig. 4.2.3). The two

reference substrates r (T −1, T −2) and r (C −1) showed similar binding affinity to *E. coli* P RNA, although slight differences were observed (factor of 1.2 to 1.8; see Table 4.2.1). A significant reduction in binding affinity (compared to the corresponding reference substrate) was observed for the following ptRNA variants: T_{LNA} −1 (13-fold at 5 mM Sr^{2+}), 2' H −1 (60-fold at 5 mM Sr^{2+}, 11-fold at 15 mM Ca^{2+} and 9-fold at 80 mM Sr^{2+}) and 2' OCH_3 −1 (48-fold at 5 mM Sr^{2+}, 31-fold at 15 mM Ca^{2+} and 36-fold at 80 mM Sr^{2+}). The observed reduction in the binding affinity of T_{LNA} −1 at 15 mM Ca^{2+} and 80 mM Sr^{2+} (K_d increased 2 to 2.5-fold compared to the corresponding reference substrate) as well as for 2' F −1 in all tested conditions (K_d increased 1.4 to 5-fold compared to the corresponding reference substrate) was considered as marginal. Taken together, these results suggest that formation of E•S complexes is supported by a H-bonding interaction that involves the 2' OH group at nt −1. The stronger reduction in the binding affinity of T_{LNA} −1 (at 5 mM Sr^{2+}) and 2' OCH_3 −1 (in all tested conditions) is probably caused by an additional sterical effect of the methylene bridge and the 2' methoxy group, respectively, found at nt −1 of these substrates.

Moreover, the proportion of substrate that was able to form stable E•S complexes under enzyme saturation conditions (the binding-proficient substrate fraction; Fig. 4.2.3, numbers above columns; Table 4.2.1, right column) was reduced by all modifications at nt −1. While the binding affinity constant (K_d) reflects the effect of the ribose modifications on enzyme and substrate, the binding-proficient substrate fraction is a characteristic of substrate only and indicates if the analysed modification induces changes in the substrate conformation, partially converting it to a non-functional form. The binding-proficient substrate fraction (compared to the corresponding reference substrate) was reduced (Table 4.2.1, right column, red numbers) by ~ 44 % for 2' F −1 and ~ 33 % for 2' OCH_3 −1 at 5 mM Sr^{2+} or ~ 28 % for 2' H −1, ~ 33 % for T_{LNA} −1 and ~ 26 % for 2' OCH_3 −1 at 15 mM Ca^{2+}, indicating that all modifications introduced at nt −1 have a significant effect on the conformation of ptRNA, reducing the fraction of substrate able to bind to the enzyme. This suggests a role of the 2' OH group at nt −1 in ptRNA folding, stabilising its functional conformation.

Effects of ribose modification at nt +1 on ptRNA ground state binding

When an LNA or 2' methoxy modification was introduced at position +1, a strong defect in ground state binding was observed. K_d increased by a factor of 41 (G_{LNA} +1) or 34 (2' OCH_3 +1) at 5 mM Sr^{2+} and 48 (G_{LNA} +1) or 31 (2' OCH_3 +1) at 15 mM Ca^{2+}, relative to the unmodified substrate (Fig. 4.2.3 A and B; Table 4.2.1). This binding defect could be rescued to some extent by increasing the divalent metal ion concentration: the K_d ratio to r

(T −1, T −2) was reduced to a factor of 13 (G_{LNA} +1) or 7 (2' OCH_3 +1) at 80 mM Sr^{2+} (Fig. 4.2.3 C; Table 4.2.1). Moreover, the binding-proficient substrate fraction was reduced 17 % (15 Ca^{2+} mM) to 22 % (5 mM Sr^{2+}) by an LNA at nt +1 (Fig. 4.2.3, numbers above columns; Table 4.2.1, right column). Neither reduction in binding affinity nor changes in the fraction of substrate able to bind to the enzyme were observed when a 2' deoxy modification was introduced at this position (2' H +1; Fig. 4.2.3; Table 4.2.1). These results suggest that the 2' OH group at nt +1 is involved neither in an H −bonding interaction during substrate binding in the ground state nor in stabilisation of ptRNA functional conformation. Therefore, the effects observed with G_{LNA} +1 (on K_d and binding-proficient substrate fraction) and 2' OCH_3 +1 (only on K_d) at relative low Me^{2+} concentration (5 mM Sr^{2+} and 15 Ca^{2+}; Table 4.2.1) can be attributed to sterical effects caused by the methylene bridge and methyl group at nt +1 of these substrates. Since these effects are compensated by higher Me^{2+} concentration (80 mM Sr^{2+}; Table 4.2.1) it is likely that these modifications disrupt binding of Me^{2+} ion required for E•S complex formation. Fore more detailed analyses, see 4.2.5.

4.2.2 Influence of ribose modifications on cleavage site selection

The active site of P RNA enzymes consists of a network of inter- and intramolecular interactions that are the basis for substrate recognition and catalysis. Disruption of one or more of these interactions by mutation or chemical modification can lead to complex effects due to more or less locally confined conformational changes. In addition to changes in the affinity and catalytic rate, deletion or modification of important functional groups can result in miscleavage (cleavage at a site different from the canonical one). Miscleavage can occur at different sites, and loss of fidelity can result in processing within the acceptor stem, the 5′ leader sequence, or sometimes both. Accordingly, this study aimed to determine whether modifications within ptRNA at and around the cleavage site result in miscleavage. Processing of all ptRNA variants analysed here except T_{LNA} −1 resulted in single cleavage products (Fig. 4.2.4). The T_{LNA} −1 variant was processed at two consecutive sites (Fig. 4.2.4, lane 3).

The ptRNA variants T_{LNA} −2, G_{LNA} +1, 2' OCH_3 +1 and 2' H +1 were processed by *E. coli* P RNA at identical site (canonical site; c_0) as the reference substrate [r (T −1, T −2); Fig. 4.2.4]. The cleavage site identity for ptRNA variants r (C −1), 2' H −1 and 2' F −1 was previously analysed (Persson et al., 2003); they were processed at the canonical site as well. The differences observed in the electrophoretic mobility of these variants (Fig. 4.2.4, lanes 7, 8 and 9) are due to the modification located in the 5' flank (for details see Persson et al., 2003).
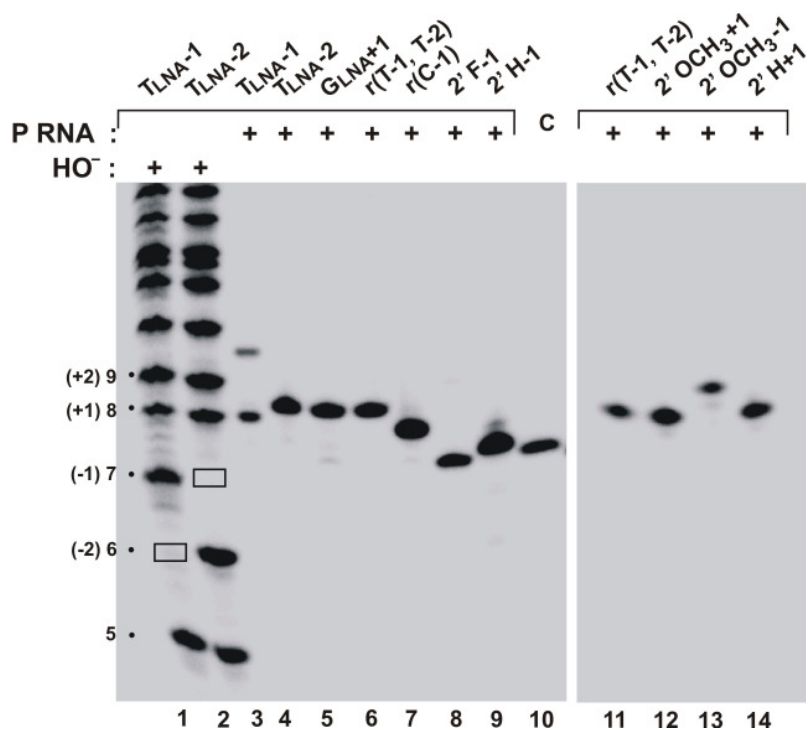
Fig. 4.2.4: Cleavage analysis of ptRNA variants. Lanes 1 to 10 and 11 to 14 represent two individual experiments. The first two lanes represent the cleavage pattern of alkaline hydrolysis of ptRNA substrates carrying an LNA residue at nt −2 (first lane) and −1 (second lane). The missing bands marked by rectangles represent the LNA modified positions that could not be hydrolysed by alkaline due to the absence of the 2' OH. Please note that alkaline hydrolysis generates cleavage products with 2', 3'-cyclic phosphates at the 3' -end, while RNase P generates 3' OH termini. Therefore, products with the same number of nucleotides obtained by alkaline hydrolysis run faster during PAGE than RNase P cleavage products due to an additional negative charge. In the third lane the two products obtained by *E. coli* P RNA cleavage of ptRNA with an LNA at nt −1 can be seen. The lanes 4-9 and 11-14 show products of *E. coli* P RNA cleavage using the variants indicated above each lane. Lane 10 labeled as C above, corresponds to a 7-mer oligoribonucletide with a 2' deoxy modification at nt 7 (pCCCUUUdC). This fragment is identical to the *E. coli* P RNA cleavage product obtained using the 2' H −1 substrate (lane 8). *E. coli* P RNA cleavage was performed at 37°C, pH 7, 1 M NH$_4$OAc and 20 mM Mg(OAC)$_2$. The incubation time was 10 min (lane 4, 6, 7 and 11), 20 min (lane 8, 12 and 14), 1 h (lane 5 and 9) and 22 h (lane 3 and 13). Alkaline hydrolysis was performed as described (3.4.6) with the 24-mer oligoribonucleotides from the ligation reaction used to create the full-length ptRNA substrate (Fig. 4.2.2).

The identity of the P RNA cleavage site for the unmodified substrate [r (T-1, T-2)] and the 2' OCH$_3$ −1 and T$_{LNA}$ −1 variants was further analysed by co-electrophoresis with nuclease P1 hydrolysis ladders (P1, like RNase P (RNA), generates 5´-phosphate termini) along with the *E. coli* P RNA cleavage products (Fig. 4.2.5).

Subsequent analysis of the cleavage pattern obtained by P1 hydrolysis compared with that obtained with P RNA indicate that the unmodified ptRNA [r(T −1, T −2)] was processed by *E. coli* P RNA at the canonical site (c$_0$; lanes 5 and 6). Surprisingly, the 2' OCH$_3$ −1 variant was processed only at site m$_{+1}$ (between nt +1 and +2; compare lanes 3 and 4) while the T$_{LNA}$ −1 variants at both sites (m$_{+1}$ and c$_0$; lanes 1 and 2).
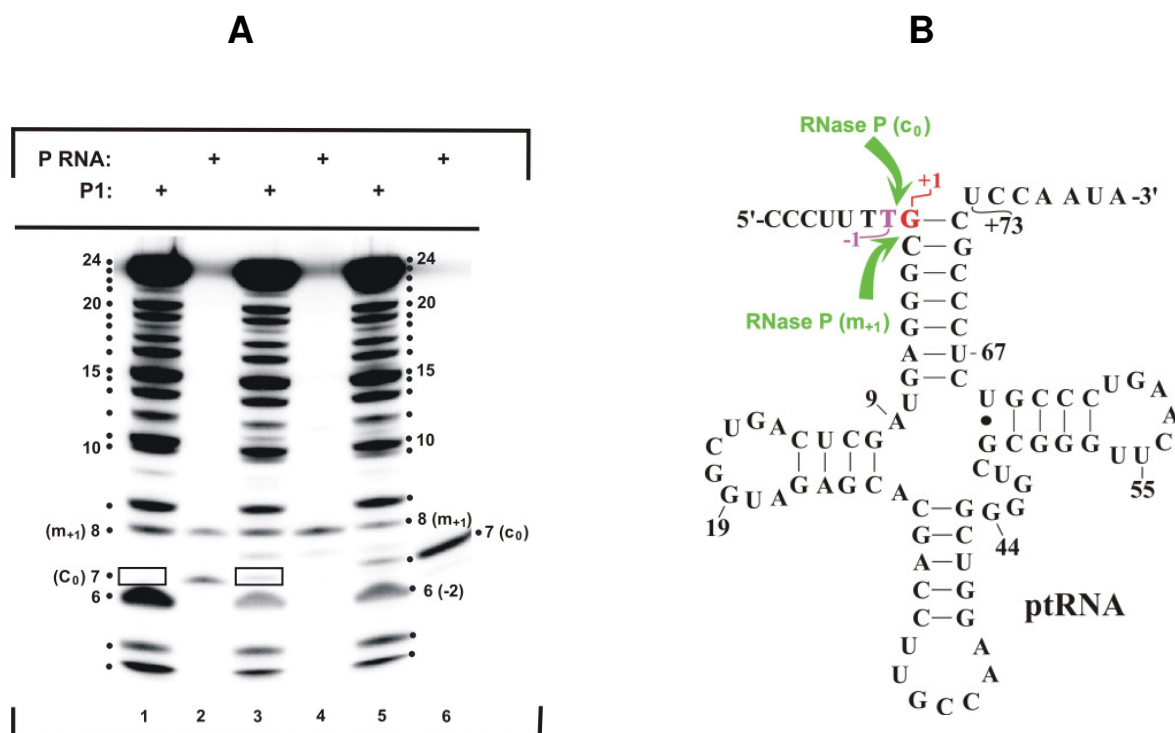
75

A

B

Fig. 4.2.5: Analysis of the P RNA cleavage site. (A) P RNA (lane 2, 4 and 6) and P1 nuclease (lanes 1, 3 and 5) cleavage pattern of T_{LNA} −1, 2' OCH_3 −1 and r (T −1, T −2) variants, respectively. Numbers on the left and right side indicate the fragment length (nt) generated by nuclease P1; P RNA cleavage sites are indicated in parentheses. The rectangles mark the missing P1 fragments due to the absence of a 2' OH at the corresponding position. Hydrolysis by P1 was performed as described (3.4.7), using as substrate the 24-mer oligonucleotide (the same as in the ligation reaction to generate the full-length ptRNA). For P RNA cleavage reaction conditions, see legend to Fig. 4.2.4; incubation times were 8 h (lane 2), 22 h (lane 4) and 10 min (lane 6). (B) The secondary structure of ptRNA; the green arrows show the two RNase P (RNA) cleavage sites. The nt −1 is shown in violet and nt +1 in red.

In a previous study (Zahler et al., 2005), a single mutation in the P RNA (A 248 to U) led to miscleavage at site $m_{−2}$ (one nucleotide upstream the canonical cleavage site) of ptRNA^{Asp} with a 2' deoxy at nt −1. This miscleavage was almost completely abolished when an additional 2' deoxy modification at nt −2 was introduced, but simultaneously miscleavage at site m_{+1} was obtained. These results suggest that altering the cleavage reaction at site c_0 (e.g. by disrupting the interaction of nt −1 with A 248 and removing the 2' OH group at nt −1) favours miscleavage at site $m_{−2}$; additional blockage of cleavage at site $m_{−2}$ (e.g. by introducing a second 2' deoxy modification at nt −2) results in miscleavage at site m_{+1}, a site normally masked owing to its slow rate of cleavage. According to this hypothesis, it seems that an LNA or 2' OCH_3 residue at nt −1 alters not only the cleavage at site c_0, but also at site $m_{−2}$. Since miscleavage at m_{+1} was obtained with both modified ptRNA variants (2' OCH_3 −1 and T_{LNA} −1), it is likely that the bulky methyl or methylene group found at the 2'

position of nt −1 within the two variants induces sterical effects (e.g. repulsion of catalytic metal ions) that affect catalysis at c_0 as well as $m_{−2}$. The different positioning and flexibility of the methyl / methylene group at nt −1 of the two substrates might explain why one substrate was processed exclusively (2' OCH_3 −1) and the other partially (T_{LNA} −1) at the m_{+1} site.

4.2.3 Effect of ribose modifications on ptRNA cleavage rate

The cleavage experiments were performed under single turnover conditions (5 µM *E. coli* P RNA and < 1 nM ptRNA; 3.5.2) in the presence of 1 M NH_4OAc. A pH of 5.5 was

Table 4.2.2 Cleavage rates and endpoints of ptRNA variants

ptRNA variant	pH 5.5			pH 7	
	10 mM Mg^{2+}	20 mM Mg^{2+}	120 mM Mg^{2+}	20 mM Mg^{2+}	120 mM Mg^{2+}
r (T -1,T -2) (c_0)	0.47 ± 0.09 0.86	0.84 ± 0.2 0.84	3.0 ± 0.9 0.91	6.3 ± 1.7 0.92	17 ± 4 0.96
r(C −1) (c_0)	0.23 ± 0.01 0.75	1.33 ± 0.14 0.85	4.5 ± 0.7 0.97	-	
T_{LNA} −2 (c_0)	0.52 ± 0.02 0.73	-	2.3 ± 0.2 0.86	-	-
T_{LNA} −1 (c_0)	-	-	0.0008 ± 0.0 0.73	$0.0012 ± 10^{-4}$ 0.52	$0.024 ± 10^{-4}$ 0.81
T_{LNA} −1 (m_{+1})	-	-	0.003 ± 0.0 0.12	$0.003 ± 10^{-4}$ 0.17	0.022 ± 0.001 0.13
2' F −1 (c_0)	-	0.03 ± 0.01 0.74	0.5 ± 0,07 0.96	1.2 ± 0.1 0.84	6.7 ± 2.5 0.92
2' H −1 (c_0)	-	$[6 ± 3] x 10^{-4}$ 0.76	0.04 ± 0.006 0.86	0.03 ± 0.006 0.88	0.6 ± 0.1 1.0
2'OCH_3 −1 (m_{+1})	-	-	0.002 ± 0.0 0.22	$0.003 ± 10^{-4}$ 0.34	$0.003 ± 10^{-4}$ 0.67
2' H +1 (c_0)	0.4 ± 0.05 0.98	1.23 ± 0.2 1.0	3.8 ± 0.1 0.97	-	-
2' OCH_3 +1(c_0)	$0.004 ± 10^{-4}$ 0.94	0.09 ± 0.05 0.93	3.6 ± 0.25 0.92	-	-
G_{LNA} +1 (c_0)	0.005 ± 0.002 0.87	0.07 ± 0.006 0.84	1.3 ± 0.2 0.91	-	-

The black numbers are cleavage rates in $[min^{-1}]$, the red numbers below designate the average endpoints normalised to the 2' H +1 variant at 20 mM Mg^{2+}, pH 5.5. The endpoint represents the maximum fraction of substrate that could be cleaved (time → ∞). The variants with C at nt −1 are shown in blue (left column) while all other ptRNAs (with a ribo T at this position) are in black. c_0 indicates canonical cleavage (between −1 and +1), m_{+1} miscleavage (between nt +1 and +2).

chosen to allow for substantial substrate turnover under conditions where the rate of cleavage is determined by the chemical step (Warnecke et al., 1996). The results are summarised in Table 4.2.2.

The effect of the 2' OH substitution at nt −1 on E. coli *P RNA catalysis*

Several functions for the 2' OH at nt −1 have been proposed so far. Smith and Pace analysed the effect of a 2' deoxy modification at nt −1 on Mg^{2+} binding. This modification reduced the affinity for Mg^{2+} ions, suggesting that the 2' OH at nt −1 might be involved in binding and positioning of Mg^{2+} ions required for the chemical step (Smith & Pace, 1993). Pan and coworkers, when reanalysing the role of 2' OH at nt −1, proposed a model according to which different cleavage sites are the result of the formation of distinct E•S complexes. Here the substitution of 2' OH by 2' H at nt −1 of a yeast tRNA[Phe] changed the reaction kinetics for all cleavages to a similar extent, suggesting that the ribozyme interaction with this 2' OH group is universal for all E•S complexes (here referred to as the 2' OH model; Loria & Pan, 1998). According to this model, the 2' OH at position −1 could be still involved in binding of a Mg^{2+} ion necessary for maximal efficiency in chemistry, but a Mg^{2+} of this kind may be distinct from the two other Mg^{2+} ions proposed to act as the base and the electrophile in the transition state (Steitz & Steitz, 1993). Kirsebom and colleagues, analysing the role of the 2' OH at the cleavage site using a model RNA hairpin substrate mimicking the architecture of a ptRNA[His] cleavage site, concluded that the presence of the 2' OH at the immediate vicinity of the scissile bond is crucial for efficient cleavage by P RNA, contradicting the 2' OH model (Loria & Pan, 1998). Here, introducing a 2' H at the canonical cleavage site did not affect cleavage at an alternative site to any significant extent (Brannvall & Kirsebom, 2005). Similarly, the importance of the 2' OH at the immediate vicinity of the scissile bond in RNase P-mediated cleavage was shown for ptRNA[Phe] (Zahler et al., 2005). Here, the substitution of the 2' OH at nt −2 affected the cleavage reaction at the corresponding site. These studies (Brannvall & Kirsebom, 2005; Zahler et al., 2005) favour the model proposed by Smith and Pace (Smith & Pace, 1993) where the 2' OH at the cleavage site influences Mg^{2+} binding in its immediate vicinity. To address the question of a potential direct metal interaction with the 2' substituent at nt −1, we analysed cleavage of a ptRNA substrate carrying a 2' N substitution at nt −1 in the presence of Mg^{2+} vs. Mn^{2+}. Since Mn^{2+} is able to form stable inner-sphere complexes with nitrogen-containing compounds, a Mn^{2+} rescue effect could indicate a direct metal coordination to the 2' N substituent. A Mn^{2+} rescue was indeed observed, but a rescue of similar strength was also observed for the substrate carrying a 2' H modification at nt −1, arguing against a direct metal ion coordination (Persson et al., 2003).

The substitution of 2' OH by 2' H at nt −1 led to a reduction in RNase P catalysis by several hundred-fold (Loria & Pan, 1997; Smith & Pace, 1993; Persson et al., 2003). When the 2' OH at nt −1 was replaced with 2' F, a 13-fold increase in catalysis (relative to the 2' H-modified substrate) was observed, but this was still 10-fold less effective relative to the unmodified substrate, suggesting a hydrogen bonding function for the 2' OH at nt −1 during catalysis (Persson et al., 2003). Alternatively, the 2' OH at nt −1 may be involved in lowering the pKa of the neighbouring 3'-oxygen leaving group, analogous to the mechanism proposed for the group I ribozyme reaction (Herschlag et al., 1993; Smith & Pace, 1993).

The results presented in this work are in agreement with previous studies (see above). All modifications introduced at nt −1 significantly affected the cleavage reaction. The rate corresponding to canonical site cleavage (c_0) decreased in the order r (T −1,T −2) ~ r(C −1) > 2' F −1 > 2' H −1 > T_{LNA} −1 (c_0) by a factor of 9 (2' F −1), 100 (2' H −1) and 3300 (T_{LNA} −1; c_0) at 120 mM Mg^{2+} / pH 5.5 relative to the corresponding reference substrate (Table 4.2.2). These results indicate that there is a H-bonding interaction involving the 2' OH group at nt −1 during catalysis. Since a 2' H substituent at nt −1 is not able to form any H-bonding interactions, while LNA is a good H–bond acceptor, one might expect a higher cleavage rate for the T_{LNA} −1 than the 2' H −1 variant. However, the LNA at nt −1 had a huge detrimental effect on *E. coli* P RNA-catalysed cleavage at site c_0 (cleavage rate reduced by a factor of ~ 3300 at 120 mM Mg^{2+} / pH 5.5, ~ 5300 at 20 mM Mg^{2+} / pH 7.0 and ~ 700 at 120 mM Mg^{2+} / pH 7.0 relative to the unmodified substrate; Table 4.2.2), suggesting sterical hindrance caused by the methylene bridge of LNA at nt −1. Moreover, the proportion of substrate able to be cleaved at the canonical site was significantly smaller at low Mg^{2+} concentration but similar at high Mg^{2+} concentration for the T_{LNA} −1 substrate compared to the reference substrate. Interestingly, a small proportion of the T_{LNA} −1 substrate (~ 12 to 17 %) was processed at another than the canonical site (m_{+1}; miscleavage between nt +1 and +2). Similarly, the 2' OCH_3 −1 variant was completely processed at the site of miscleavage (m_{+1}). The rate of miscleavage of the 2' OCH_3 −1 variant was similar (at 120 mM Mg^{2+} / pH 5.5 and 20 mM Mg^{2+} / pH 7.0) to or 8-fold lower (120 mM Mg^{2+} / pH 7.0) than that obtained for the T_{LNA} −1 variant (see Table 4.2.2), suggesting that the sterical effects leading to miscleavage of both substrates are of the same kind. The different positioning and flexibility of the methyl / methylene group at nt −1 of the two substrates might explain why one substrate was processed exclusively (2' OCH_3 −1) and the other only partially (T_{LNA} −1) at the m_{+1} site. Miscleavage one nucleotide downstream from the canonical cleavage site was also detected previously when analysing a substrate with a 2' OCH_3 at nt −1 (Smith & Pace,

1993). The presence of the methyl / methylene group at the canonical cleavage site might (completely or partially) hinder binding of a catalytic Mg^{2+} ion or disrupt an intimate contact to the ribozyme, therefore shifting the cleavage site one nucleotide downstream of the canonical site. Further analysis (NMR experiments) might explain the kind of sterical effects induced by the methylene / methyl group and their effect on catalysis by *E. coli* P RNA. The canonical cleavage and miscleavage of the T_{LNA} −1 variant were further analysed for their dependence of Mg^{2+} concentration and pH (see 4.2.4).

In a previous study (Zuleeg et al., 2001), model substrates mimicking the acceptor stem of a tRNA and carrying three nucleotides extension at the 5' -end and the 3' –CCA terminus were analysed by NMR. Hre it was shown that the ribose at nt −1 is found in a C 2' –endo conformation. Using LNA modification the importance of the C 2' endo conformation at nt −1 in the P RNA catalysed cleavage can be inferred. In this part of my work it is demonstrated that the transition state can be achieved even with a C 3' –endo conformation at nt −1, since the substrate with an LNA modification at nt −1 that fixes the ribose in a C 3' –endo conformation, was still processed by P RNA at the canonical site, although with a lot reduced efficiency compared to the unmodified substrate.

The effect of the 2' OH substitution at nt +1 on E. coli P RNA catalysis

Modifications introduced into the ptRNA substrate at nt +1 had different effects on the cleavage reaction. The 2' H +1 ptRNA variant was processed with similar efficiency (even faster) as the reference substrate. When an LNA or $2'OCH_3$ modification was introduced at position +1, a strong deleterious effect was observed for *E. coli* P RNA cleavage at low Mg^{2+} concentrations (~ 100-fold decrease in the cleavage rate relative to the reference substrate at 10 mM Mg^{2+} and pH 5.5; Table 4.2.2). This effect could be largely rescued in the case of the G_{LNA} +1 variant (only 2.5-fold decreased cleavage rate compared to the reference substrate) or completely for the $2'OCH_3$ +1 variant by increasing the metal ion concentration (Table 4.2.2, 120 mM Mg^{2+} and pH 5.5). A similar effect was observed in the binding experiments (4.2.1); the affinity to *E. coli* P RNA of these two substrates was 30- to 50-fold lower at 5 mM Sr^{2+} / 15 mM Ca^{2+} and only 8- to 12-fold lower at 80 mM Sr^{2+} (see Table 4.2.1). The results suggest that the effect of these modifications on *E. coli* P RNA cleavage at low Mg^{2+} concentration can be attributed to a decreased affinity between substrate and enzyme, as it has been observed in the binding experiments. For further analyses see 4.2.5.

Cleavage by and affinity binding to the RNase P holoenzyme of single LNA modified ptRNA variants

In order to determine if the RNase P protein subunit (P protein) can rescue the effects seen in P RNA alone studies (see above and 4.2.2), the LNA-modified ptRNA variants were tested for cleavage by and affinity to the RNase P holoenzyme (*E. coli* and / or *B. subtilis*). The cleavage experiments were performed under single turnover conditions at 100 mM KCl, 50 mM MES, pH 6.0 and 2 or 10 mM Mg^{2+} according to the protocol described in Materials
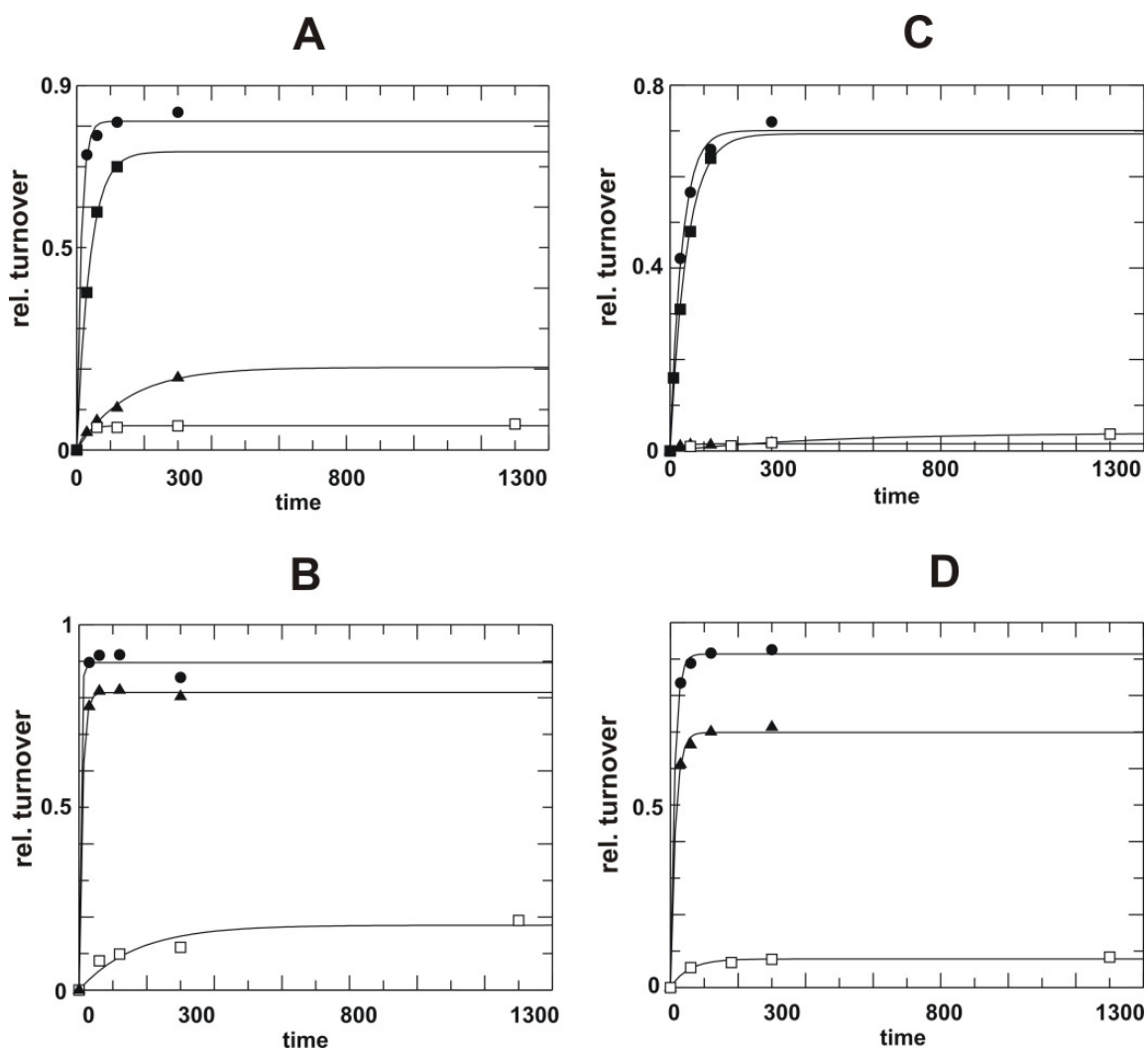
Fig. 4.2.6: Cleavage experiments of ptRNA substrates: r(T −1,T −2): filled circles; G_{LNA} +1: filled triangles; T_{LNA} −1: empty squares and T_{LNA} −2: filled squares. The cleavage reaction was catalysed by the *E. coli* (A and B) or *B. subtilis* (C and D) P holoenzyme. The experiments were performed at two Mg^{2+} concentrations, 2 (A and C) and 10 (B and D) mM. Assays were performed as follows: P RNA (100 nM) was preincubated for 5 min at 55 °C and 25 min at 37 °C in 100 mM KCl, 50 mM MES, pH 6.0 and Mg^{2+} as indicated above. After preincubation the P protein was added in excess over P RNA (4-fold for *B. subtilis* or 10 fold for *E. coli* P protein). The entire mix was incubated for 5 min at 37 °C. Then the substrate (preincubated for 30 min at 37 °C in the same buffer as the P RNA) was added. Aliquots were withdrawn at different time points (between 0 and 1300 min). For more details see 3.5.2.

and Methods (3.5.2).

The results show the same huge detrimental effect on catalysis, that was observed in the *E. coli* P RNA alone reaction (see above) for an LNA modification at nt −1; no significant canonical cleavage (c_0) of the T_{LNA} −1 substrate was obtained under all tested conditions (Fig. 4.2.6 A, B, C and D; open squares). Also, cleavage at site m_{+1} was detected like in the *E. coli* P RNA alone reaction. The rate of both cleavage and miscleavage could not be determined reliably due to a very slow substrate conversion.

The cleavage of the $G_{LNA}+1$ substrate was poor at 2 mM Mg^{2+} (Fig. 4.2.6 A and C; filled triangles) compared with the unmodified substrate (filled circles). The cleavage efficiency substantially increased with both holoenzymes at 10 mM Mg^{2+} (Fig. 4.2.6 B and D; filled triangles), but was still reduced (1.2- to 2.5-fold) compared to the unmodified substrate).

The LNA modification at nt −2 had only a marginal effect on cleavage catalysed by both holoenzymes (Fig. 4.2.6 A and C, filled squares). These results correlate with those obtained in cleavage experiments with the *E. coli* P RNA alone, suggesting that the protein subunit is not able to compensate for deleterious effects caused by LNA modifications at nt −1 and +1.

In a further experiment, ptRNA affinity to the *B. subtilis* holoenzyme was analysed. The binding experiments were performed as described (3.5.3) at 200 mM NH_4OAc, 0.1 % SDS, 0.05 % Nonidet P40, 50 mM MES, pH 6.0 and in the presence 15 mM $Ca(OAc)_2$. The obtained results (Fig. 4.2.7) are similar to those obtained for binding to *E. coli* P RNA alone (4.2.1). The LNA modification at nt −1 and −2 had a minor effect on ptRNA binding to the *B.*
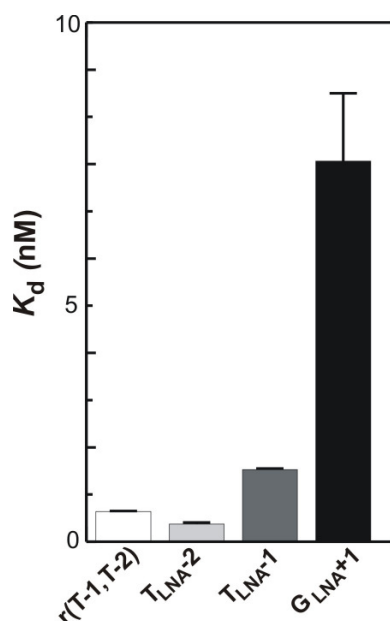

Fig. 4.2.7: High affinity binding of ptRNA substrates carrying LNA modifications to the *B. subtilis* RNase P holoenzyme. Spin column assays were performed as described in 3.5.3 under the following conditions: 200 mM NH_4OAc, 0.1 % SDS, 0.05 % Nonidet P40, 50 mM MES, pH 6.0 and in the presence 15 mM $Ca(OAc)_2$. Error bars indicate standard deviations obtained in 3 independent experiments.

subtilis holoenzyme (Fig. 4.2.7). A significant loss of affinity was observed when the LNA modification was introduced at nt +1 (12-fold; Fig. 4.2.7).

4.2.4 Kinetic analysis of canonical cleavage and miscleavage of ptRNA substrate carrying an LNA modification at nt –1

Deletion or modification of important functional groups can result in miscleavage within the acceptor stem and / or the 5' leader sequence. Although the factors that govern miscleavage are not entirely understood, structure-function studies using miscleavage as an indicator provide important insights into P RNA–ptRNA interactions. Substrate features proximal to the cleavage site that contribute to affinity and catalysis include the 3' RCCA sequence, the G(+1)-C(+72) base pair, the interaction of nt –1 with the conserved base A 248 (*E. coli* numbering system) and the 2' OH at nt –1 (Fig. 4.2.8).
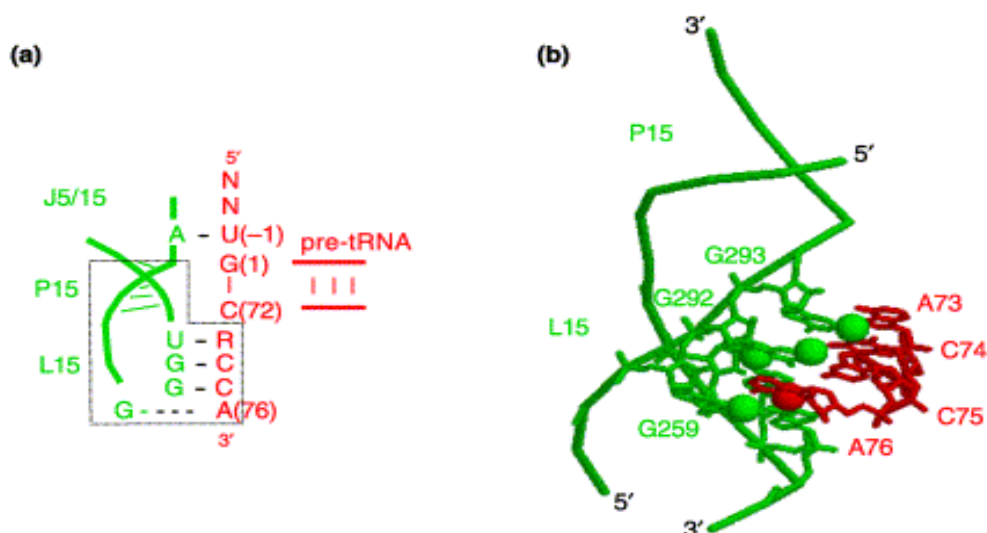
Fig. 4.2.8: Contacts between the ptRNA cleavage site and the C-domain of P RNA. (a) Diagram of active site pairing interactions between P RNA and the ptRNA substrate. The base of the acceptor stem, the 5´ leader sequence and the 3´ RCCA sequence of ptRNA are shown in red. Helix P15 in P RNA and adjoining structures involved in substrate interactions are indicated in green; such interactions include the pairing interaction between the 3´ end of ptRNA and L15, and between J5/15 and nt –1 in the 5´ leader sequence. The portion of the structure depicted in the model (b) is indicated by a dashed box. (b) Three-dimensional structure derived from computer modelling of the L15–RCCA interaction from the *E. coli* ribozyme. The phosphodiester backbones of P15 and L15 are depicted in green; only the individual nucleotides involved in substrate contacts are shown. Functional groups identified by NAIM as important for binding are indicated by spheres.

As an important example, analysis of the effect of compensatory mutations on cleavage fidelity demonstrated an interaction between the substrate's 3′ RCCA sequence

and the loop of helix P15 (L15) of P RNA (Kirsebom & Svard, 1994). The importance of understanding interactions with functional groups flanking the cleavage site is underscored by the observation that removal or substitution of the 2' OH at nt −1 decreases the rate of substrate cleavage by 100- to 1000-fold (Smith & Pace, 1993; Loria & Pan, 1998; 1999; Persson et al., 2003; this work, see Table 4.2.2). In the context of a substrate that is cleaved at multiple sites (ptRNA^{Phe}), Pan and colleagues showed that a 2' deoxy modification at nt −1 affects the rate of cleavage at both correct and incorrect sites. In contrast, substitution of 2' OH groups at neighbouring sites had no effect. These and other observations led to a model in which cleavage at correct and incorrect sites involves formation of distinct enzyme–substrate complexes, which differ in their interactions with the 5' leader, but involve similar recognition of the T stem-loop and the 2' OH group at the correct cleavage site (Loria & Pan, 1998; 1999). In contrast to these studies, Harris and colleagues studying miscleavage of ptRNA^{Asp} by P RNA with a mutation at nt 248 (U instead of A) showed that the 2' OH at nt −2 is an important enzyme-substrate contact for miscleavage at the m$_{-2}$ site (Zahler et al., 2005). By removing this 2' OH group, the miscleavage at the m$_{-2}$ site was essentially abolished. Similarly, Kirsebom and colleagues observed that the 2' OH at nt −1 did not influence cleavage at an alternative cleavage site to any significant extent, suggesting that the presence of the 2' OH at the immediate vicinity of the scissile bond is crucial for efficient P RNA cleavage (Brannvall & Kirsebom, 2005). In the context of weakened interactions with the RCCA motif, cleavage site selection is dependent on the identity of nt −1 (Brannvall et al., 1998; 2002) and the presence of a 2' OH at nt −1 (Persson et al., 2003). In addition, in the context of a minimal substrate representing only the acceptor stem of a tRNA, changes in nt −1 identity influence the rate of cleavage (Zuleeg et al., 2001). Similarly, changing the identity of nt −1 in a full-length ptRNA alters the rate of catalysis by the RNase P holoenzyme and results in miscleavage of certain substrates (Crary et al., 1998; Loria et al., 1998; Loria & Pan, 1998). Photocrosslinking and compensatory mutation studies suggest that the conserved adenosine (A 248; *E. coli* numbering system) in the J5/15 region of the ribozyme is involved in interactions with substrate elements proximal to the scissile phosphate (Burgin & Pace, 1990; Kufel & Kirsebom, 1996; Christian et al., 1998; Christian & Harris, 1999; Zahler et al., 2003). Mutation of the conserved nucleotide A 248 in addition to a 2' deoxy modification at nt −1 led to miscleavage between nt −1 and −2 (Zahler et al., 2005). Titration studies demonstrated that metal ion identity and concentration as well as reaction pH can also influence cleavage site selection (Brannvall & Kirsebom, 1999; 2001; Persson et al., 2003). Moreover, changes in active site architecture due to changes in the nature of the 3′ RCCA and 5′ nt −1 interactions can affect the extent to which different combinations of metal ions lead to miscleavage.

Processing of the T_{LNA} −1 variant occurs via two parallel pathways leading to canonical cleavage and miscleavage

In addition to a large reduction in the catalytic rate and a moderate decrease of substrate affinity, a single LNA modification at nt −1 leads to miscleavage of ptRNA within the acceptor stem between positions +1 and +2 (4.2.2; Fig. 4.2.5). Previous studies of RNase P miscleavage have shown that cleavage at the canonical site as well as at the site of miscleavage arises from structurally distinct E•S complexes (Zahler et al., 2003; Branvall et al., 2002). A simple model for formation of distinct E•S complexes under single turnover conditions involves two parallel pseudo-first-order reactions as illustrated in Fig. 4.2.9 (Zahler et al., 2005).
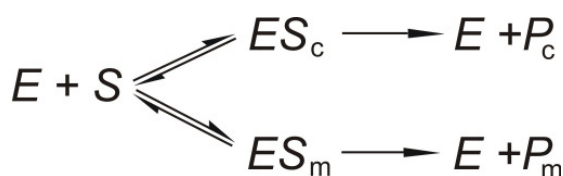
Fig. 4.2.9: Model for formation of distinct enzyme-substrate complexes (E•S) under single turnover conditions involving two parallel pathways of RNase P cleavage. ES_c is the complex that results in cleavage at the canonical site, generating product P_c. ES_m is the complex that generates miscleaved product P_m.

To characterise the kinetics of product formation for correctly cleaved and miscleaved ptRNAs, *E. coli* P RNA cleavage experiments were performed as described (3.5.2). An example result of this analysis is shown in Fig. 4.2.10; the results are consistent with the scheme presented in Fig. 4.2.9.
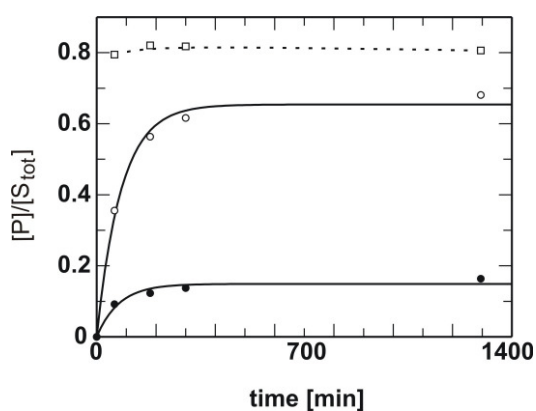
Fig. 4.2.10: Kinetic analyses of canonical and miscleavage of T_{LNA} −1 variant. Cleavage experiments were performed under single turnover conditions in the presence of 1 M NH_4OAc, 60 mM Mg^{2+}, pH 7. Plots show cleavage at the canonical site (open circles) and miscleavage in the acceptor stem (filled circles). The fraction of substrate reacted is expressed as the ratio of product at a given time [P] to the total amount of substrate [S_{tot}] at the start of the reaction. The relative amount of cleavage taking place at the canonical site (F_c; open squares) was calculated as the ratio between the amount of product obtained by cleavage at the canonical site and the sum of both cleavage products. Similar curves were obtained at all pH values and Mg^{2+} concentrations tested.

One can see that both cleavage pathways follow a single exponential decay and that the fraction of cleavage taking place at the canonical site (Fig. 4.2.10; open squares) remains constant over time. Given the observed rate constant (k_{obs}; determined from curve fitting; see 3.5.5) and $F_c = P_c / (P_m + P_c)$, it was possible to calculate the apparent rate of cleavage (k_{app}) at a particular site:

$$k_{app,c} = k_{obs,c} \times F_c \qquad (4.2.1)$$

$$k_{app,m} = k_{obs,m} \times (1 - F_c) \qquad (4.2.2)$$

where $k_{app,c}$, $k_{app,m}$ are the apparent rates of cleavage at the canonical and miscleavage site, respectively; and $k_{obs,c}$ and $k_{obs,m}$ are the observed rate constants for correct and miscleaved product formation. However, as F_c is dependent on equilibrium binding terms, the magnitude of these rate constants will not be entirely determined by the cleavage step. Thus, quantitative analysis of F_c and apparent rates of cleavage and miscleavage must be undertaken with caution, since it is not possible to fully distinguish between effects on substrate binding and catalysis. Nonetheless, evaluation of these parameters provides an overall measure of the relative difference in the kinetics of correct cleavage and miscleavage pathways.

Mg^{2+} dependence of cleavage site selection

Given the potential for structural differences between the two E•S complexes (Fig. 4.2.9), it seemed likely that they could differ with respect to Mg^{2+} binding. In such a case it would be possible to influence cleavage site selection by changing Mg^{2+} concentration. Fig. 4.2.11 shows plots of k_{app} and F_c as a function of Mg^{2+} concentration. The k_{app} corresponding to the canonical cleavage (c_0) increases with Mg^{2+} concentration in the range of 20 to 800 mM, while k_{app} corresponding to miscleavage (m_{+1}) increases at concentrations lower than 300 mM (Fig. 4.2.11 A). Using the program Grafit (3.0), this data was fitted to the equation

$$k_{app} = (k_{app,\ max} \times [Mg^{2+}]) / (K_{1/2} \times [Mg^{2+}]) \qquad (4.2.3)$$

where $k_{app,\ max}$ represents the maximum value at saturating Mg^{2+} concentration and $K_{1/2}$ the concentration of Mg^{2+} required to achieve half of the maximum rate ($k_{app,\ max}$). From data fits of $k_{app,\ max}$ and $K_{1/2}$, values for both reaction pathways were obtained:

$k_{app,\ max}$ (c_0) = 0.1 min^{-1}, $K_{1/2}$ (c_0) = 400 mM for canonical cleavage,

$k_{app,\ max}$ (m_{+1}) = 0.01 min^{-1}, $K_{1/2}$ (m_{+1}) = 150 mM for miscleavage.

A

B
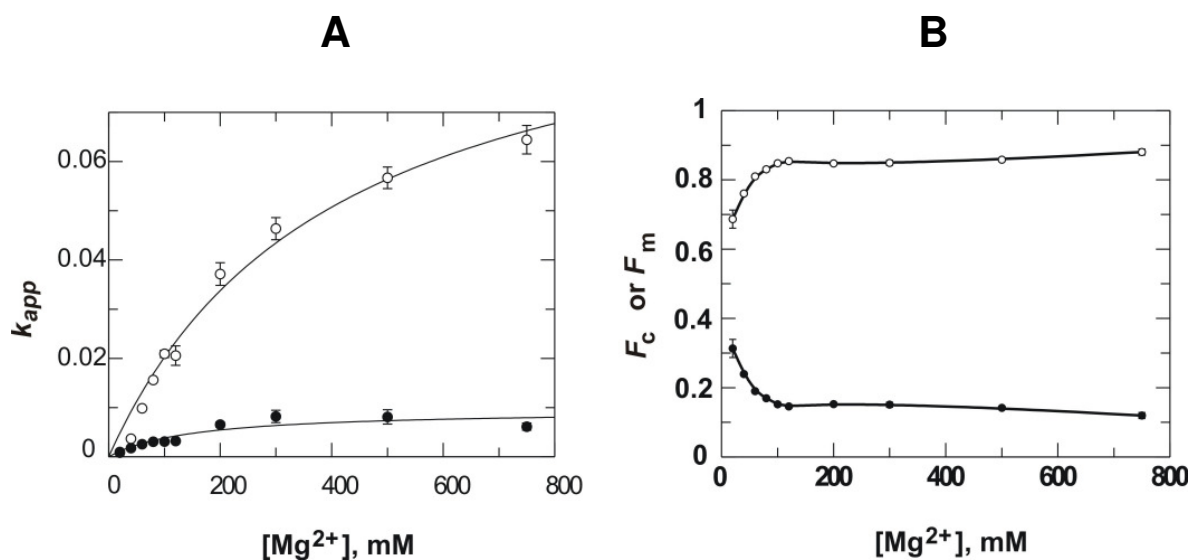
Fig. 4.2.11: Mg^{2+} influence on the cleavage reaction of ptRNA substrate with an LNA modification at nt -1. A: [Mg^{2+}] dependence of the apparent cleavage (k_{app}) at the canonical site (c_0; open circles) and the site of miscleavage (m_{+1}; filled circles). B: dependence of F_c (corresponding to canonical cleavage; open circles) and F_{m+1} (for miscleavage; filled circles) on Mg^{2+} concentration. For reaction conditions see legend to Fig. 4.2.10.

At relatively low Mg^{2+} concentrations, an increase in [Mg^{2+}] resulted in a larger fraction of correctly cleaved products (c_0), with F_c reaching its maximum value at approximately 100 mM Mg^{2+} (Fig. 4.2.11 B), suggesting that the pathway leading to cleavage at the canonical site (c_0) exhibits a higher dependency on Mg^{2+} than the pathway leading to miscleavage (m_{+1}). Further increases in the Mg^{2+} concentration did not have any influence on F_c (Fig. 4.2.11 B). Usually, cleavage at the c_0 site has a lower Mg^{2+} requirement than cleavage at sites m_{-2} or m_{+1} (Zahler et al., 2005). This observation together with the results shown here indicates a sterical hindrance of binding catalytic Mg^{2+} ions required for cleavage at the canonical site by the methylene group found at nt -1 of the ptRNA variant with an LNA at this position. The dependence on the Mg^{2+} concentration may be attributed to the structural differences between the two E•S complexes (ES$_c$ and ES$_m$; Fig. 4.2.8) if both reaction pathways share the same rate-limiting step. Alternatively, it is possible that the rate of miscleavage reflects different rate-limiting steps that display different metal ion concentration dependencies.

The canonical and miscleavage pathways have different rate-limiting steps

It is well established that the rate of cleavage by the RNase P ribozyme increases with increasing pH and displays log-linear dependence with a slope of about 1 (Smith &
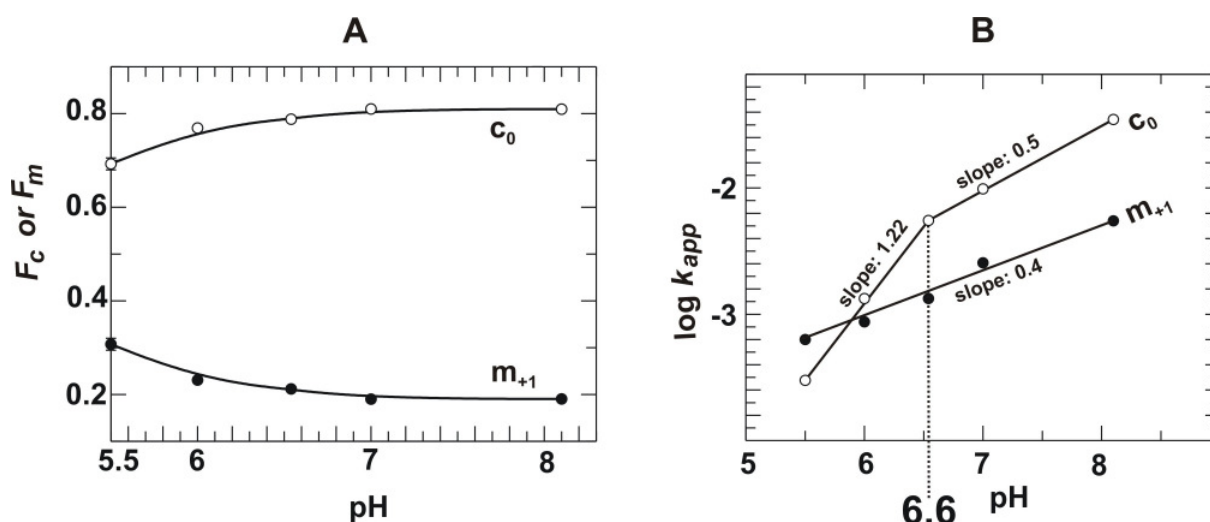
Fig. 4.2.12: pH dependence of cleavage site selection. (A) Effects of pH on F_c (open circles) and F_m (filled circles) indicate that the correct cleavage pathway has a higher pH dependency than the miscleavage pathway; (B) Plots of log $k_{app, c}$ (open circles) and log $k_{app, m}$ (filled circles). Curve fits indicate a slope of 1.22 for cleavage at the canonical site in the pH range of 5.5 to 6.6, consistent with the chemical step being rate-limiting in this pH range. Canonical cleavage at higher pH as well as miscleavage over the whole pH interval occurs with a slope of 0.5 and 0.4, respectively, suggesting that another slower step limits the cleavage rate under these conditions.

Pace, 1993). The pH dependence of P RNA-mediated catalysis is believed to arise from the dependence of phosphodiester hydrolysis on hydroxide concentration (Kirby & Younas, 1970; Cassano et al., 2002), and is therefore taken to indicate that chemistry is rate-limiting (Warnecke et al., 1996; Frank & Pace, 1998; Christian et al., 2002). However, the correct cleavage and / or miscleavage pathways observed with the LNA −1 substrate could involve limiting steps other than cleavage chemistry. If that is the case, changes in pH will differentially affect the rates of canonical cleavage and miscleavage pathways, altering the observed level of miscleavage.

In Fig. 4.2.12 A, the dependency of F_c and F_m on pH is shown. In the pH range studied (5.5 to 8.1), an increase of F_c with pH was observed, suggesting that the pathway leading to correct cleavage has a higher pH dependency than the miscleavage pathway. The difference in pH dependency between the two pathways could arise from different rate-limiting steps or differences in the structure or metal ion requirements for formation of the two E•S complexes (ES_c and ES_m; Fig. 4.2.9).

To extract useful information regarding the steps that limit the correct cleavage and miscleavage pathways, the pH dependence of k_{app} of both pathways ($k_{app,c}$ and $k_{app,m}$)

was analysed (Fig. 4.2.12 B). Both were log-linear, consistent with phosphodiester hydrolysis being at least partially rate-limiting for both pathways. In the case of canonical cleavage, a slope of 1.22 was obtained in the pH range from 5.5. to 6.6, suggesting that chemistry is rate-limiting in this range. The slope of 0.5 above pH 6.6 for canonical cleavage and 0.4 for the miscleavage pathway over the whole pH range tested indicates that an additional slow step (e.g. refolding) upstream from the hydrolytic step limits the cleavage rate under these conditions. Since the $K_{1/2}$ value (see above) determined for canonical cleavage is higher than that corresponding to the miscleavage pathway, it might be possible that LNA at nt −1 decreases the affinity of a catalytic Mg^{2+} ion at the canonical cleavage site. This hypothesis is also supported by the observation that increasing the Mg^{2+} concentration favours formation of E•S complexes leading to canonical cleavage (Fc increases with Mg^{2+} concentration; see Fig. 4.2.11 B). The complexes that are not able to bind the catalytic Mg^{2+} at the canonical site might change their conformation to allow binding of Mg^{2+} to the site of miscleavage, consistent with the notion that a refolding step limits the miscleavage pathway.

4.2.5 Analysis of the effect of an LNA modification at nt +1 on ptRNA ground state binding and cleavage by *E. coli* P RNA

The substrate carrying an LNA at nt +1 was analysed as well in cleavage experiments under single turnover conditions (3.5.2) and for affinity binding to *E. coli* P RNA by a gel filtration spin column assay (3.5.3). The binding experiments showed a significant reduction of the $G_{LNA}+1$ substrate's affinity (relative to the unmodified substrate) to *E. coli* P RNA at low Me^{2+} (5 mM Sr^{2+} or 15 mM Ca^{2+}; 4.2.1) concentrations. This effect could be rescued to some extent by a higher concentration of Me^{2+} (80 mM Sr^{2+}; 4.2.1). Consistent with these observations, a significantly reduced cleavage efficiency was observed for *E. coli* P RNA cleavage of the $G_{LNA}+1$ substrate at low Mg^{2+} concentrations (compared to the corresponding unmodified substrate), which, however, could be rescued at higher concentrations (Fig. 4.2.13 A; see also 4.2.3). This reduction of catalytic efficiency was attributed to poor E•S complex formation at low Me^{2+} ion concentrations and seems to be independent of the type of divalent cation, since a similar curve was obtained using Mn^{2+} instead of Mg^{2+} (Fig. 4.2.13 B) when plotting the relative reaction velocity (k_{rel}) as a function of Me^{2+} concentration; k_{rel}, calculated as the ratio between the observed rate constants (k_{obs}) for the unmodified substrate and the LNA +1 substrate (see legend to Fig. 4.2.13), decreased from ~100 at 10 mM Mg^{2+} to 2 at 60 mM Mg^{2+}, reaching a plateau at higher concentrations (Fig. 4.2.13 A). With Mn^{2+} instead of Mg^{2+}, k_{rel} decreased from 40 to 1.3 in
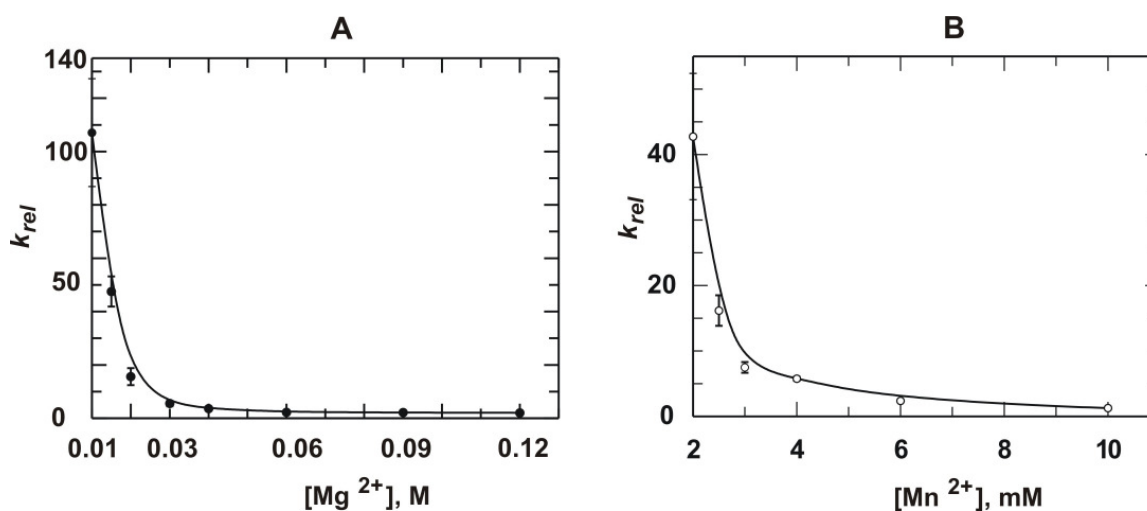
Fig. 4.2.13: *E. coli* P RNA cleavage experiments at different Me^{2+} concentrations, 1M NH_4OAc and pH 5.5; A: cleavage in the presence of Mg^{2+} in the concentration range of 10 to 120 mM; B: cleavage with Mn^{2+} between 2 to 10 mM. The k_{rel} represents the relative cleavage rate constant calculated as the ratio between the observed rate constants (k_{obs}) for the unmodified substrate [r(T −1, T −2)] and the LNA +1 substrate (G_{LNA} +1).

$$k_{rel} = k_{obs} \, [r(T\text{-}1, T\text{-}2)] \, / \, k_{obs} \, (G_{LNA}+1)$$

the concentration range of 2 to 10 mM Mn^{2+} (Fig. 4.2.13 B). Taken together, these results suggest that the observed catalytic deficiency caused by this modification is generated mainly by the low affinity of the modified substrate for *E. coli* P RNA.

Since neither changes in ground state binding (relative to the unmodified substrate; 4.2.1) nor significant reduction of catalysis (~ 1.2 fold decrease in cleavage rate at 10 mM Mg^{2+}; 4.2.3) was observed in the analysis of the 2' H +1 variant, it was concluded that the 2' OH at nt +1 is not involved in H-bonding interactions.

A hypothesis proposed by Altman and coworkers assumes that the ptRNA acceptor stem is denatured during or after binding to *E. coli* P RNA, but before catalysis occurs (Knap et al., 1990). This possibility was also addressed in this study. Since the LNA at nt +1 stabilises the acceptor stem helix, it should hinder its denaturation and thereby reduce ptRNA binding. A way to test this theory was to perform cleavage experiments by *E. coli* P RNA, using the unmodified and LNA +1 substrate at different temperatures (37°C, 50°C). One would expect a decrease of k_{rel} (see above) with increasing temperature. Interestingly, no significant differences between k_{rel} values obtained in cleavage experiments at different temperatures were observed at 15 mM Mg^{2+} (43 at 37°C, 47 at 50°C) or 20 mM Mg^{2+} (13 at 37°C, 15 at 50°C), arguing against the notion that helix stabilisation by the LNA +1 modification may impair catalytic efficiency by exacerbating ptRNA acceptor stem opening. It can also not be completely ruled out that two compensatory effects occur: the higher temperature might favour the denaturation of the acceptor stem but at the same time

destabilise Me^{2+} ion binding at the cleavage site.

A significant deleterious effect on ptRNA ground state binding and processing at low Me^{2+} ion concentration was obtained when an LNA or 2' OCH$_3$ modification was introduced at nt +1, suggesting sterical effects induced by the methylene bridge of G$_{LNA}$ +1 or CH$_3$ group of the 2' OCH$_3$ +1 variant. These bulky substituents at the 2' position of nt +1 within the two ptRNA variants might hinder binding of divalent metal ions or disrupt an important enzyme-substrate contact required for ptRNA binding to *E. coli* P RNA. Therefore, binding of the G$_{LNA}$ +1 variant vs. the unmodified substrate was analysed as a function of Me^{2+} (Ca^{2+}) ion concentration (Fig. 4.2.14). The K_d of both ptRNAs decreased with increasing Ca^{2+} concentration (Fig. 4.2.14 A). Hill analysis of K_d in the presence of varying concentrations of Ca^{2+} yielded slopes of n$_H$ = 1.8 for the unmodified substrate [r (T −1, T −2)] and 2.6 for the G$_{LNA}$ +1 variant (Fig. 4.2.14 B), suggesting that the two substrates bind to the P RNA via different mechanisms, involving at least two [r (T −1, T −2)] or three (G$_{LNA}$ +1) Ca^{2+} ions.

Since the slope of the Hill plot (Fig. 4.2.14 B) for the G$_{LNA}$ +1 ptRNA variant is higher than that determined for the unmodified substrate (2.6 vs. 1.8), it can be concluded that the E•S complexes with the G$_{LNA}$ +1 substrate bind at least one Ca^{2+} ligand more compared with the unmodified ptRNA. Two explanations are conceivable: (1) because G$_{LNA}$ +1 has a
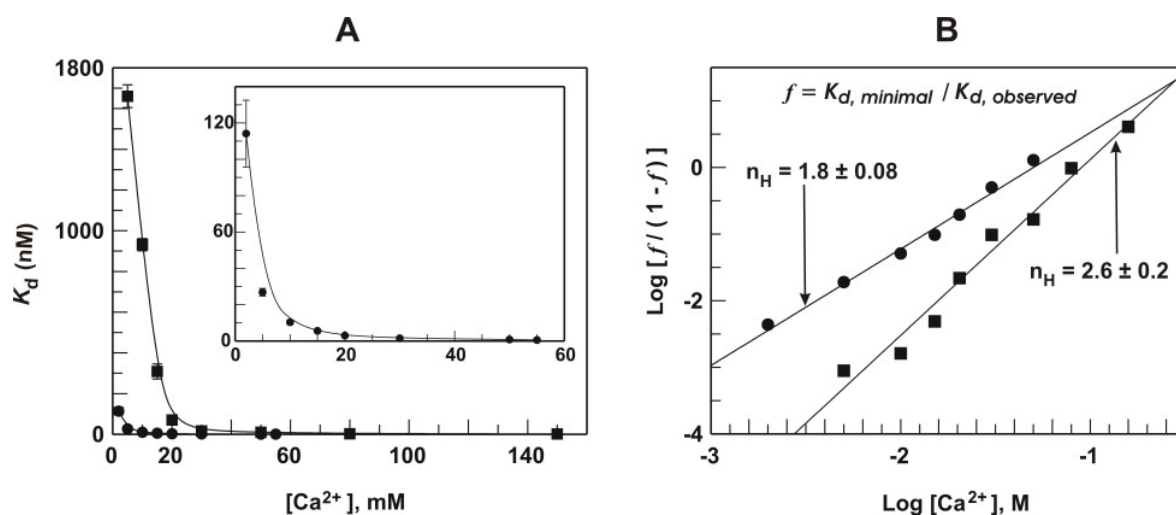
Fig. 4.2.14: Ca^{2+} dependence of ptRNA binding; unmodified (filled circles) and LNA at nt +1 modified (filled squares) ptRNA substrate. (A) K$_d$ dependence on Ca^{2+} concentration; the inset shows the magnified curve for the unmodified ptRNA. (B) Hill plot analysis of K_d dependence on Ca^{2+} concentration. $f = K_{d, minimal} / K_{d, observed}$; the $K_{d, minimal}$ at saturating Ca^{2+} concentrations was determined to be 0.5 nM for the reference (unmodified) substrate and 1.5 nM for G$_{LNA}$+1 variant.

lower binding affinity compared to the reference substrate, it is likely that the LNA modification blocks one of the two Ca^{2+} binding sites determined for the unmodified substrate to be involved in stable E•S complex formation (a direct displacement of a Ca^{2+} ion by LNA). To partially compensate for the loss of one important binding site, two other Ca^{2+} ions might be taken up at different low affinity sites into the E•S complexes with the G_{LNA} +1 variant. Both of them support complex formation, but with lower affinity than that displaced by the LNA modification. (2) Alternatively, it is possible that an LNA modification at nt +1 disrupts a direct enzyme – substrate contact, via sterical hindrance, inducing rearrangements in the substrate orientation with respect to the enzyme. As a consequence one of the two essential Ca^{2+} ions (see above) is not able to bind anymore (an indirect displacement of a Ca^{2+} ion by LNA). This might be partially compensated by binding of two different Ca^{2+} ions at other lower affinity sites [see (1)].

Both hypotheses are consistent with the results obtained in the ptRNA binding experiments and might explain the very slow E•S complex formation (with G_{LNA} +1 ptRNA) at low Me^{2+} concentration [~ 41-fold at 5 mM Sr^{2+} (4.2.1; Table 4.2.1; Fig. 4.2.3) or ~ 62-fold at 5 mM Ca^{2+} (Fig. 4.2.14 A) slower than the reference ptRNA] and the rescue effect at higher concentrations [~ 12-fold slower at 80 mM Sr^{2+} (4.2.1; Table 4.2.1; Fig. 4.2.3) or 50 mM Ca^{2+} (Fig. 4.2.14 A)].

4.3 Modification interference studies: an approach to identify functional groups that interfere with the cleavage reaction

4.3.1   Introduction to modification interference studies

The NAIM approach; Nucleotide analogue interference mapping (NAIM) is a specific and versatile chemogenetic approach which allows to probe the functional consequences of changes as minor as single atom substitutions in the base, sugar or phosphate moiety of nucleic acids. NAIM uses the potential of phosphorothioate modifications as reporters (Fig. 4.3.1, yellow), which permits to specifically cleave the nucleic acid chain by iodine exclusively

at the sites of analogue incorporation (Gish & Eckstein, 1998; 3.4.8). Phosphorothioate modifications are obtained by substitution of one of the two non-bridging phosphate oxygen atoms (*pro Sp* and *pro Rp*) with sulphur. For synthesis of modified RNA by run-off transcription, *Sp*-α-thio-NTP's are used. During polymerisation the phosphate group is converted to the *Rp*–configuration (Griffiths et al., 1987). The substitution with sulphur may affect the coordination of Mg^{2+} and the formation of hydrogen bonds while the secondary structure of RNA usually remains unaffected.

Fig. 4.3.1: Phosphorothioate as reporter for modification interference studies

At the onset of NAIM studies, a pool of RNA molecules with limited numbers of randomly distributed nucleotide analogues is synthesised. Such a pool of RNAs is then subjected to a selection procedure to separate active variants from those with impaired function due to modification at a particular location. Subsequent comparative analysis of the distribution of modifications in the active RNA fraction and a reference fraction (e.g. the fraction of molecules with impaired function or the original unselected pool) reveals positions critical for function.

The partial modification of RNA is achieved by the presence of nucleoside α-thiotriphosphate analogues during *in vitro* transcription by T7 RNA polymerase, resulting in the aforementioned pool of RNA molecules, each carrying a low number of randomly

distributed modifications. The elegance of the method lies in the capacity to simultaneously screen for the functional contribution of a particular chemical group at almost every A, C, G or U position in an RNA chain. The analogues available for NAIM studies can be divided into three categories (Strobel, 1999), according to their main attribute: (a) if they primarily change the chemical properties of the substitutent, (b) delete a functional group or (c) introduce a bulky substituent.

Depending on the type of modification introduced, NAIM experiments have the potential to reveal the following information:

- An *Rp*-phosphorothioate (Fig. 4.3.1, yellow) modification *per se* (AMPαS, GMPαS, CMPαS, UMPαS) may identify crucial coordination sites for Mg^{2+} ions. Substitution of sulfur for a non-bridging phosphate oxygen essentially abolishes inner-sphere coordination to Mg^{2+}, because Mg^{2+}, a "hard" Lewis acid, prefers to bind oxygen, a "hard" Lewis base, relative to the much more polarisable and thus "softer" sulfur (Pearson, 1963). However, addition of more thiophilic metal ions ("softer" Lewis acids) such as Mn^{2+} or Cd^{2+} may restore, to varying extent, metal ion binding to the thiophosphate, leading to a (partial) rescue of the functional defect (Warnecke et al., 1996).

- C7-deaza (the nitrogen marked in red replaced by a C-H group; Fig. 4.3.1) purine analogues (c7-AMPαS, c7-GMPαS) are employed to reveal N7 positions involved in hydrogen binding or metal ion coordination. The latter aspect may be particularly relevant if RNA structure and function is probed in the presence of transition metal ions, such as Mn^{2+} or Zn^{2+}, which form inner-sphere complexes with the N7 of purines (Sigel & Song, 1996; Rubin et al., 1983).

- 2'-deoxy (removal of the 2'-OH group highlighted in green; Fig. 4.3.1) modifications allow probing of the hydrogen donor and acceptor functions of 2' hydroxyls.

- IMPαS (the amino group highlighted in magenta replaced with hydrogen; Fig. 4.3.1), incorporated by T7 RNA polymerase instead of G nucleotides is suited to probe the role of guanine exocyclic amino groups in hydrogen bonding. For *E. coli* P RNA, relatively few inosine interference effects were detected in regular helices, suggesting that helix destabilisation by this modification is of minor importance for the function of the RNase P ribozyme (Heide et al., 1999). However, destabilisation of secondary structure can become important if inosines are part of a short intermolecular hybrid helix required to bind the substrate to the ribozyme, particularly under conditions where ribozyme molecules compete for a limited amount of substrate RNAs (Ortoleva–Donnely et al., 1998). For such cases, combined analysis of IMPαS and N2-methyl-GMPαS interference patterns was reported as a strategy to

differentiate between helix destabilisation and loss of important tertiary interactions as the cause of interference (Strobel, 1999; Ortoleva–Donnely et al., 1998). The N2-methyl group can still form a hydrogen bond with the O2 of cytosine in Watson-Crick base pairs, but has lost its capacity to participate in a bifurcated hydrogen bonding frequently observed in tertiary contacts that involve the 2-amino group of paired G residues (Heide et al., 1999; Ortoleva–Donnely et al., 1998; Cate et al., 1996; Pley et al., 1994).

Nucleotide analogue interference suppression (NAIS) is an extension of NAIM to determine whether an observed interference effect is caused by disruption of a direct contact between two particular functional groups of two interacting molecules. In NAIS, the partially analogue-modified RNA pool (RNA 1) is analysed for interference effects in two parallel setups: one employing the interacting RNA (RNA 2) in its unmodified form, as in NAIM, and the second one using RNA 2 with a point mutation or a single chemical group altered at a location suspected to interact directly with RNA 1. If a functional group in RNA 2 that normally interacts with the functional group in RNA 1 has been changed by the aforementioned mutation or modification, the interference effect observed in the first experimental setup corresponding to the disruption of this particular interaction should disappear, since the contact has already been abolished by the mutation or modification introduced into RNA 2, and a modification in RNA 1 at the corresponding position remains without effect. A critical point of such NAIS experiments is to adapt the functional assay with the mutant or modified RNA 2 in such a way that the extent of reaction or complex formation is the same as in the reference assay with unmodified RNA 2. For a more detailed description and illustration of NAIM and NAIS, see Cuzic & Hartmann, 2005 and Fedorova et al., 2005.

4.3.2 Construction of *E. coli* P RNA – tRNA conjugates

In order to identify functional groups that are important for substrate cleavage by RNase P RNA, NAIM and NAIS experiments have to be performed with a self-cleaving RNA conjugate (P RNA - tRNA; Fig. 4.3.2). In this experimental setup, functional, self-cleaving conjugates can be separated from inactive ones according to size, employing denaturing PAGE (Harris & Pace, 1995). In this study two types of RNA conjugates were used:

P RNA – tRNA 5' -half

The P RNA – tRNA 5' -half conjugate (Fig. 4.3.2) is based on a transcript consisting of *E. coli* P RNA (black), a linker region (green) and the 5' -half of a bacterial tRNA^{Gly} (blue). To generate a functional substrate, an excess of tRNA 3' -half (red, Fig. 4.3.2) was annealed

to this construct, creating a self-cleaving P RNA – tRNA conjugate. This bipartite system prevents premature self-cleavage at the tRNA 5' -end during RNA preparation and furthermore enables NAIS-studies using modified functional groups in the 3' -half region of tRNA.
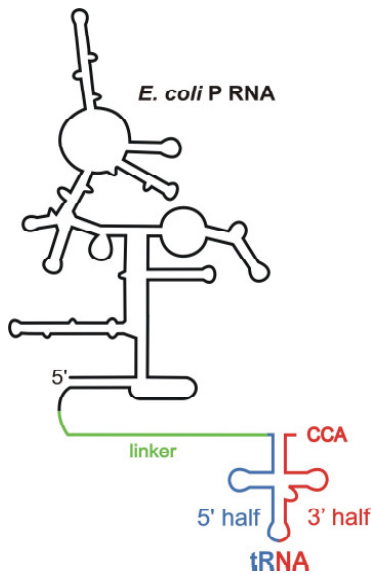
Fig. 4.3.2: *E coli* P RNA – tRNA conjugate; with the P RNA in black, linker in green, tRNA 5' half in blue and 3' half in red. The tRNA 3' -half is either only annealed to the 5' -half part of the conjugate (P RNA – tRNA 5' -half conjugate) or directly connected to the 5' half (P RNA – tRNA conjugate).

The sequence encoding the P RNA – tRNA 5' -half was constructed in three steps (Fig. 4.3.3). To create a homogenous end, a hammerhead sequence was attached to the 3' - end of the DNA construct; the hammerhead self – cleaves during RNA transcription.

Fig. 4.3.3: Construction of the P RNA – tRNA 5' -half conjugate; For simplification the primers have been numbered: primer 1 in magenta (Eco M1 5' Eco R I T7), 2 in green (3' M1 Gly spacer), 3 in blue (3' Gly spacer 2 compl) and 4 in red (3' Gly spacer 3). The sequence corresponding to each primer and their direction is indicated.

Please note that the primer sequence is complementary to (primer 2 and 4) or identical with (primer 1 and 3) the given sequence (see also appendix 2). A part of the sequence not shown here is indicated by the broken line.

(1) A standard PCR (3.3.4), using primers 1 (magenta) and 2 (green) and plasmid pFL 117 (encoding the sequence of P RNA from *E. coli*) as template;

(2) A primer elongation reaction (3.3.6) using primers 3 (blue) and 4 (red);

(3) A fill up reaction (3.3.7) using the double-stranded DNA products of step (1) and (2).

The DNA product obtained in step (3) was digested with Eco RI and Bam HI and ligated into the vector pUC 19 which was previously linearised using the same two restriction endonucleases and dephosphorylated at the 5' end. *E coli* XL2 blue cells were transformed with the ligation product, and ampicillin resistant colonies were analysed (analytical plasmid preparation, restriction digest and sequencing [the latter being performed by MWG-Biotech]). The desired plasmid (called pXX) was isolated (3.3.1), linearised with Bam HI and subjected to *in vitro* transcription (3.4.1).

The tRNA 3' -half (Fig 4.3.2; red) encoding sequence was constructed by standard PCR (3.3.4), using the primers 9 (tgly 3' -half 5' T7 EcoR I) and 10 (tgly 3' -half 3' Mfe I-Bahm HI) and the plasmid pSBpt3'HH (encoding the ptRNA^{Gly} sequence) as template. The PCR product was cloned into the vector pUC 19 using the restriction sites Eco RI and Bam HI. *E coli* XL2 blue cells were transformed with the ligation product, and ampicillin resistant colonies were analysed (see above). The desired plasmid (ptgly 3' -half) was isolated (3.3.1), linearised with Mfe I (Mun I) and subjected to *in vitro* transcription (3.4.1). Linearisation with Mfe I enzyme ensured that CCA termini (important for P RNA catalysis) were generated during the run-off transcription.

P RNA – tRNA conjugate

The sequence encoding the P RNA–tRNA conjugate (Fig. 4.3.2) was constructed by PCR using as template the plasmid containing the P RNA–tRNA 5' -half sequence (pXX; see above). The PCR method applied in this case differed from the standard method (3.3.4) regarding the number and the amount of primers used (Fig. 4.3.4). Instead of one antisense primer, three overlapping ones were used in this special case, in order to generate the sequence for the tRNA 3' -half (which is not encoded by the template). The amount (1 nM) of
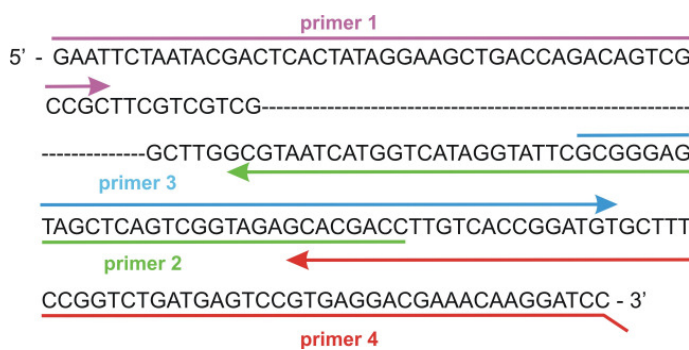

Fig. 4.3.4: Construction of the P RNA – tRNA conjugate; For simplification the primers have been numbered: primer 5 in light green (Eco M1 5' Eco RI T7 short), 6 in yellow (ptRNA loops), 7 in blue (3' ptRNA Mun I-Bam HI) and 8 in red (3' ptRNA short). The sequence corresponding to each primer and their orientation is indicated. Please note that the primer sequence is complementary to (primer 6, 7 and 8) or identical with (primer 5) the given sequence (see also appendix 2). A part of the sequence not shown here is indicated by the broken line.

short primers (5 in light green and 8 in violet; Fig. 4.3.4) added to the PCR mix corresponded to the standard PCR method (3.3.4). The concentration of the long primers (6 in yellow and 7 in dark blue; Fig. 4.3.4) was ten times lower.

The PCR product was cloned into the Eco RI and Bam HI sites of a pUC 19 derivative (pUC 19 Hind III to Eco 147I), containing a point mutation (introduced by PCR mutagenesis; 3.3.5) that transforms the Hind III recognition site into an Eco 147 I recognition site. The resulting plasmid was termed pXY. Absence of the Hind III site from the original vector was necessary for the construction of P RNA – tRNA conjugates with different linker lengths (Fig. 4.3.2; linker shown in green):

(1) The plasmid encoding the P RNA – tRNA conjugate sequence (pXY), containing a linker of 53 nt and constructed as described above, was digested with Hind III (2 recognition sites within the linker region) and religated, resulting in a conjugate with a linker of 33 nt;

(2) By annealing of a self – complementary deoxyoligonucleotide with 5' phosphate termini, creating a recognition site for Eco 47 III (enzyme generating blunt ends) in the middle of the helix as well as appropriate overhangs, and ligating this short DNA duplex into the Hind III linearised vector [see (1)], a 43 nt linker was obtained;

(3) The plasmid obtained in (2) was linearised with Eco 47 III, and bluntend double - stranded DNA fragments of different size obtained from a 10 bp DNA ladder by separation on an agarose gel were ligated into the vector. The resulting products contained linkers between 54 and 375 nt.

For run - off transcription all templates, obtained as described above, were linearised with Mfe I (Mun I). Transcription was performed using the protocol for internally labelled RNA as described in 3.4.1 with one exception: the Mg^{2+} concentration was 7 instead of 33 mM. At this Mg^{2+} concentration, *cis*–cleavage of the conjugate during transcription was avoided.

4.3.3 Characterisation of P RNA – tRNA conjugates by kinetic experiments

Cis-cleaving P RNA - tRNA conjugates open up the perspective to identify functional groups that are crucial for cleavage chemistry, either applying NAIM or NAIS. In previous related approaches, the tRNA substrate was tethered to internal positions of *E. coli* P RNA (Harris & Pace, 1995; Kazantsev & Pace, 1998; Kaye et al., 2002). However, these constructs required 3 M monovalent salt for efficient self-cleavage, and such conditions may suppress informative interference effects to an unwanted extent. Therefore, a somewhat different strategy was pursued: a transcript consisting of *E. coli* P RNA, a linker region and the 5' -half of a bacterial $tRNA^{Gly}$ was annealed to an oligomer representing the tRNA's 3' -half (added in excess over the P RNA - tRNA 5' -half construct), thereby creating a self-cleaving P RNA - tRNA conjugate (see Fig. 4.3.2). Using this bipartite system, premature

self-cleavage during RNA preparation is prevented by the absence of a functional substrate. Furthermore, it permits the use of tRNA 3' halves with single-site modifications for NAIS experiments.

Before conducting NAIM experiments, it was essential to analyse the kinetic behaviour of the conjugate in order to determine the conditions under which *cis*-cleavage occurs exclusively. Moreover, the step limiting the reaction rate, for example cleavage chemistry or a refolding step, had to be identified.

Conditions for cis-*cleavage only*

Employing conditions that exclude *trans*-cleavage is essential for the separation of active ribozymes from less active and inactive RNA variants. To check for *cis*-cleavage, kinetic experiments were performed at increasing concentrations of P RNA - tRNA 5' -half conjugate with a linker of 53 nt. If *trans*-cleavage occurs, a proportional increase of cleavage rate (or product formation) with ribozyme conjugate concentration is to be expected. The finding that the cleavage rate remained constant (after 20 minutes 55 to 60 % of the RNA conjugate was cleaved; Fig. 4.3.5) in the tested range of P RNA - tRNA 5' -half concentrations (0.5 to 40 nM; Fig. 4.3.5) demonstrated that this type of ribozyme acts only *in cis* and not *in trans* under dilute conditions.
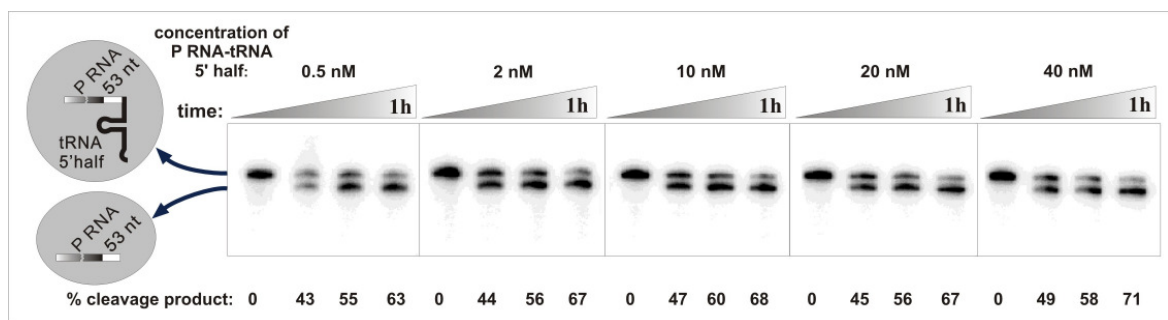
Fig. 4.3.5: *cis*-cleavage of P RNA - tRNA conjugate at different complex concentrations. This figure documents that no significant *trans* - cleavage occurred under the conditions tested, since the cleavage rate was constant for different concentrations of P RNA - tRNA 5' -half (0.5 to 40 nM). Assays were performed as follows: the P RNA - tRNA complex was formed by annealing the tRNA 3' -half to 5' -end-labelled P RNA - tRNA 5' -half in the presence of 100 mM NH_4Cl and 5 mM $CaCl_2$ to avoid self-cleavage. The P RNA - tRNA 5' -half concentration was 80 nM and that of tRNA 3' -half 5 µM. The annealing mixture was heated to 95 °C for 2 min, then cooled down to 50 °C in a heating block and preincubated for 30 min at 50 °C. After preincubation, the mixture was diluted to 0.5 to 40 nM P RNA - tRNA 5' -half and 30 to 2500 nM tRNA 3' -half by adding NH_4Cl, urea and $CaCl_2$ to final concentrations of 100, 100 and 5 mM, respectively. The reaction was started by adding $MgCl_2$ to a final concentration of 36 mM. Samples were withdrawn at different time points and analysed by 8% denaturing PAGE.

Kinetic analysis of P RNA - tRNA conjugate

Kinetic experiments using P RNA - tRNA 5' -half and tRNA 3' -half were performed to characterise the behaviour of this chimeric RNA. It was observed that the curve obtained by single exponential fitting [rel. turnover = Limit x $(1 - e^{-kt})$] did not mirror the course of the reaction as defined by the data points (Fig. 4.3.6 A). Assuming two independent types of turnover (a fast one and a slow one) for the self-cleavage of the complex, each obeying the kinetic of a single exponential decay, and employing the corresponding formula [rel. turnover = Limit 1 x $(1 - e^{-k_1 t})$ + Limit 2 x $(1 - e^{-k_2 t})$], a better fitting was obtained (Fig. 4.3.6 B). This finding suggests that there are at least two populations of ribozymes reacting with different velocities: the presumably correctly folded population (ca. 20%, see Limit 1 in Fig. 4.3.6 B) that reacts fast, and a fraction of slower reacting conjugates (ca. 50 %; see Limit 2 in Fig. 4.3.6 B) that either have to change their conformation before *cis*-cleavage can occur or use an alternative, albeit slower reaction pathway.

A

single exponential fit

Variable	Value	Std. Err.
Limit	0.6	0.04
k	0.2	0.04

B

double exponential fit

Variable	Value	Std. Err.
k_1	1.55	0.48
Limit 1	0.20	0.03
k_2	0.07	0.01
Limit 2	0.49	0.03
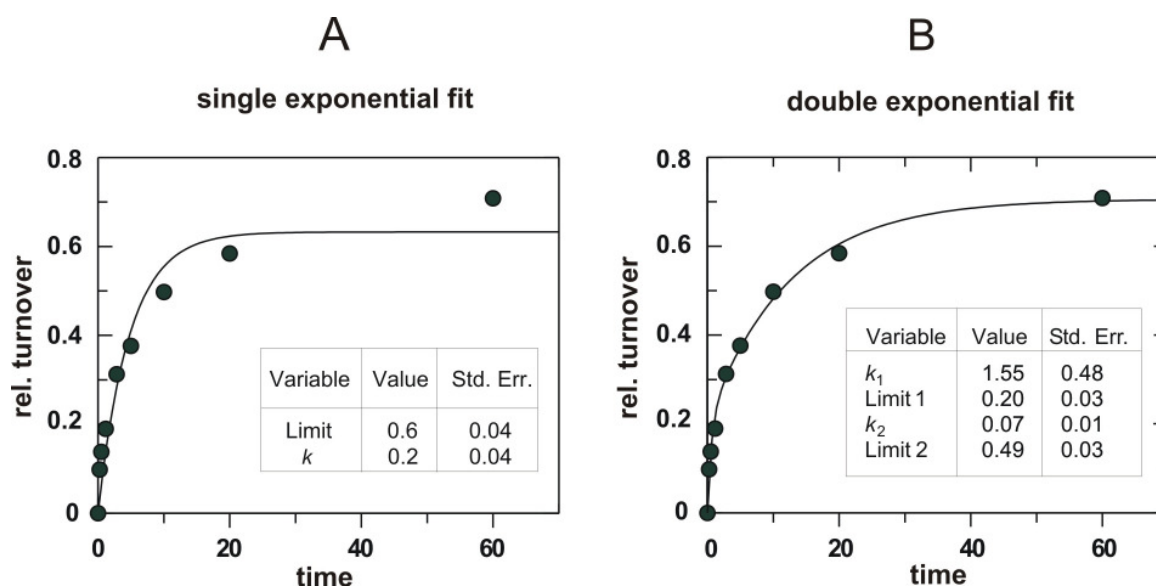
Fig. 4.3.6: *cis*-cleavage of the P RNA - tRNA conjugate equipped with a 53-nt long linker. Assays were performed as follows: the P RNA - tRNA^{Gly} complex was formed by annealing the tRNA 3' -half to 5' -end-labelled P RNA - tRNA 5' -half in the presence of 100 mM NH_4Cl and 5 mM $CaCl_2$ to avoid self-cleavage. The P RNA - tRNA 5' -half concentration was 0.3 nM and that of tRNA 3' -half 300 nM. The annealing mixture was heated to 95 °C for 2 min, then cooled down to 50 °C in a heating block and preincubated for 30 min at 50 °C. After preincubation, the mixture was diluted to 0.1 nM P RNA - tRNA 5' -half and 100 nM tRNA 3' -half by adding NH_4Cl, urea and $CaCl_2$ to final concentrations of 100, 100 and 5 mM, respectively. The reaction was started by adding $MgCl_2$ to a final concentration of 36 mM. Samples were withdrawn at different time points and analysed by 8% denaturing PAGE. The time course was fitted to either a single first - order (A) or two simultaneously occurring first - order reactions (B).

The saturation concentration of the tRNA 3' -half

For further kinetic analysis, one concentration of the P RNA - tRNA 5' -half conjugate was selected (0.3 nM during the annealing step and 0.1 nM in the cleavage reaction). In order to define the saturating concentration of tRNA 3' -half, cleavage experiments were performed at increasing tRNA 3' -half concentrations (up to 1 µM in the cleavage reaction) in the presence of 0.1 nM ribozyme conjugate. Transfer RNA 3' -half concentrations exceeding that of P RNA - tRNA 5' -half by a factor of 800 did not increase k_1 (Fig. 4.3.7).
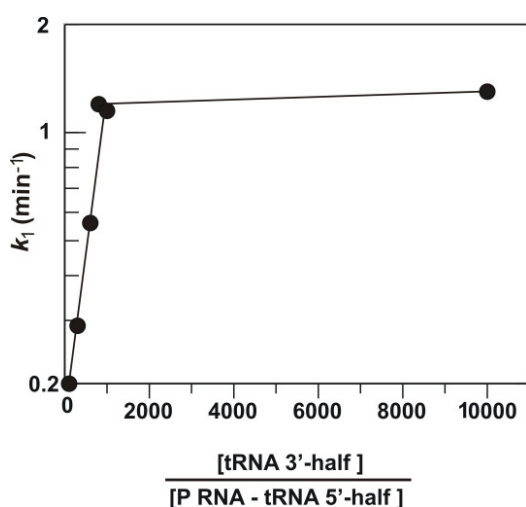
Fig. 4.3.7: Determination of the saturation limit for tRNA 3' -half, by varying its concentration up to a 10000-fold excess over P RNA - tRNA 5' -half (53 nt linker), whose concentration was 0.1 nM; tRNA 3' -half concentrations exceeding that of P RNA - tRNA 5' -half by more than a factor of 800 did not further increase the cleavage rate constant k_1. For reaction conditions see legend to Fig. 4.3.6.

The fast and the slow turnover have different rate limiting steps

The pH dependence of the rate of cleavage by P RNA is believed to arise from the dependence of phosphodiester hydrolysis on metal-bound hydroxide concentration (Kirby & Younas, 1970; Cassano et al., 2002), and is therefore taken to indicate that chemistry is rate limiting (Frank & Pace, 1998; Christian et al., 2002). The linear relationship observed for log k_1 versus pH with a slope of about 1 in the range of pH 5.2 to 6.5 (Fig. 4.3.8, A) indicates that the chemical step is rate-limiting in this pH range (Warnecke et al., 1996; Persson et al., 2003) for the fast turnover, predominant in the initial phase of the reaction. In contrast, the cleavage rate constant k_2 describing the slow turnover (Fig. 4.3.8, B) was independent of pH, supporting the idea that k_2 may reflect the rate of a slow refolding step.
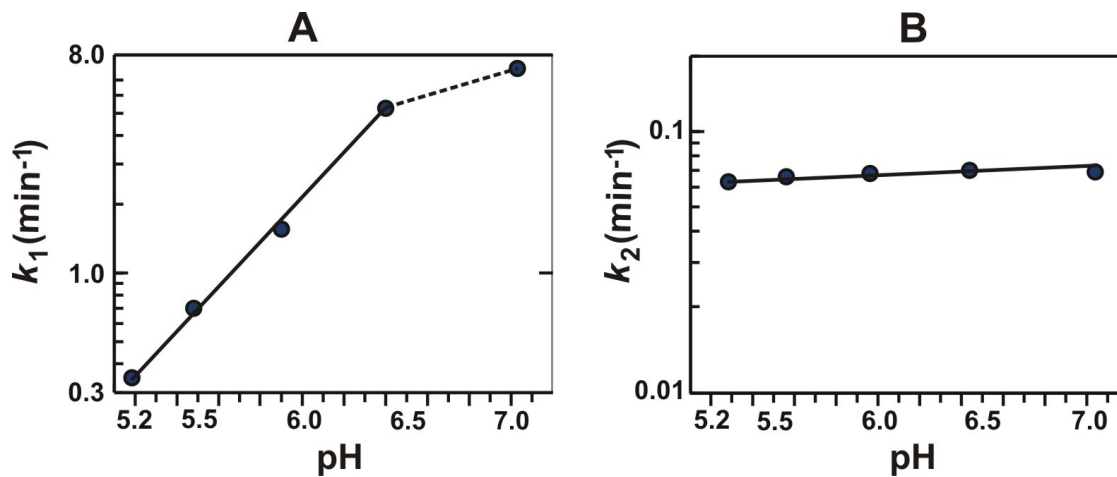
Fig. 4.3.8: pH dependence of k_1 (the rate constant of the fast initial phase of the reaction, panel A) and k_2 (the rate constant of the second slower phase of the reaction; see panel B). For reaction conditions see legend to Fig. 4.3.6.

The length of the linker that connects the P RNA to the tRNA has no effect on the cis-cleavage reaction of the fast reacting conjugates

For analysing the influence of the linker length on *cis*-clevage of P RNA–tRNA complexes, variants with different linkers were constructed as described in 4.3.2. The linker
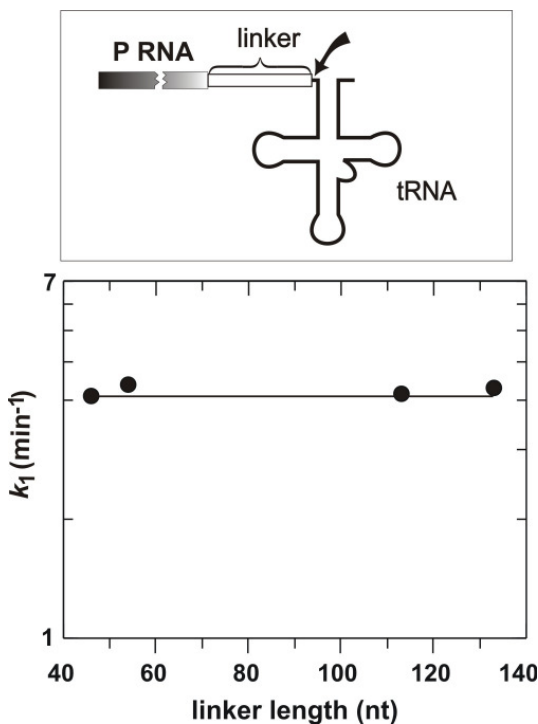
Fig. 4.3.9: Influence of the linker length on the cleavage rate constant k_1. No significant differences were observed in the cleavage rate constant k_1 among complexes with linker lengths between 43 and 133 nt. The P RNA - tRNA complex was preincubated for 10 minutes at 50 °C in the presence of 100 mM NH_4Cl and 100 mM urea at pH 7.0. The concentration of the RNA conjugate was 0.3 nM. After preincubation the mixture was diluted to 0.1 nM RNA conjugate at constant 100 mM NH_4Cl and 100 mM urea. The reaction was started by adding $MgCl_2$ to a final concentration of 36 mM. Samples were withdrawn at different time points and analysed by 8% denaturing PAGE.

length was defined as the number of nucleotides that separate the P RNA 3' -end from the tRNA 5' -end. The rate constant k_1 was shown to be independent of the linker length in the range of 43 to 133 nt (Fig. 4.3.9).

4.3.4 NAIM and NAIS: the concept of the method

The experimental setup proposed in this study was designed for identifying enzyme-substrate contacts and/or functional groups involved in binding of metal ions that are important for the cleavage reaction. Optimal conditions for the cleavage reaction were established by kinetic analyses (4.3.3): (1) a concentration of 24 nM for the P RNA - tRNA 5' -half conjugate was selected to combine an optimal yield of RNA in a small reaction volume with conditions under which *trans*-cleavage is negligible (Fig. 4.3.5); (2) a reaction time of 2 min where the fast turnover is predominant was chosen. During this time about 20 % of the RNA complexes, corresponding to the limit of the fast turnover (Limit 1 in Fig. 4.3.6 B), self-cleave. Thus, the cleaved fraction (pool of active molecules) predominantly consists of fast - cleaving complexes. (3) Moreover, a pH of 5.9 was chosen, at which cleavage chemistry limits the fast turnover (Fig. 4.3.8 A).

IMPαS modification experiments using the *E. coli* P RNA - tRNA conjugate with a 53 nt long linker connecting the P RNA and tRNA moieties are outlined below. The experimental procedure involved the following steps, illustrated in Fig. 4.3.10:

1. Transcription of P RNA - tRNA 5' -half carrying a low degree (2.5 %) of randomly distributed IMPαS modifications (3.4.1); 5' -^{32}P-end labelling of a small fraction of this RNA pool (3.4.2) for the detection of cleaved and uncleaved molecules after separation by denaturing PAGE; transcription of tRNA 3' -half (unmodified for NAIM; 3.4.1). The concept for NAIS experiments is illustrated as well. Experimental steps for NAIS are identical to those of NAIM, except that the reaction conditions have to be adapted for a modified 3' -half oligomer to yield a similar amount of cleaved conjugates as could be obtained with the unmodified tRNA 3' -half.

2. Formation of the P RNA - tRNA complex by annealing the tRNA 3' -half (8.8 μM) to the P RNA - tRNA 5' -half (91 nM; containing trace amounts of the 5'-radiolabelled pool) in the presence of 100 mM NH_4Cl and 5 mM $CaCl_2$ at pH 5.9, conditions that prevent premature self-cleavage; the annealing mix was heated to 95°C for 2 min, then cooled down to 50°C in a heating block and preincubated for 30 min at 50°C.

1. *Synthesis of partially modified RNA pool (IMPαS)*

Including trace amounts of 5'-^{32}P end-labeled pool

RNase P RNA   linker (~ 50 nt)

CCANNN-3'

▷ unmodified only: NAIM

▷ unmodified only
▶ 100 % modified } NAIS

2. *annealing*

RNase P cleavage site

CCANNN-3'

ptRNA

3. *dilution (to prevent trans - cleavage)*

4. *addition of Mg^{2+} to start cis -cleavage reaction*

a   *partial self-cleavage: low [Mg^{2+}] , short incubation time*

b   *complete cleavage: long incubation time (+ high [Mg^{2+}])*

CCANNN-3'

CCANNN-3'

CCANNN-3'

5. *Denaturing PAGE*

CCANNN-3'

CCANNN-3'

6. *3' end labelling and gel purification*

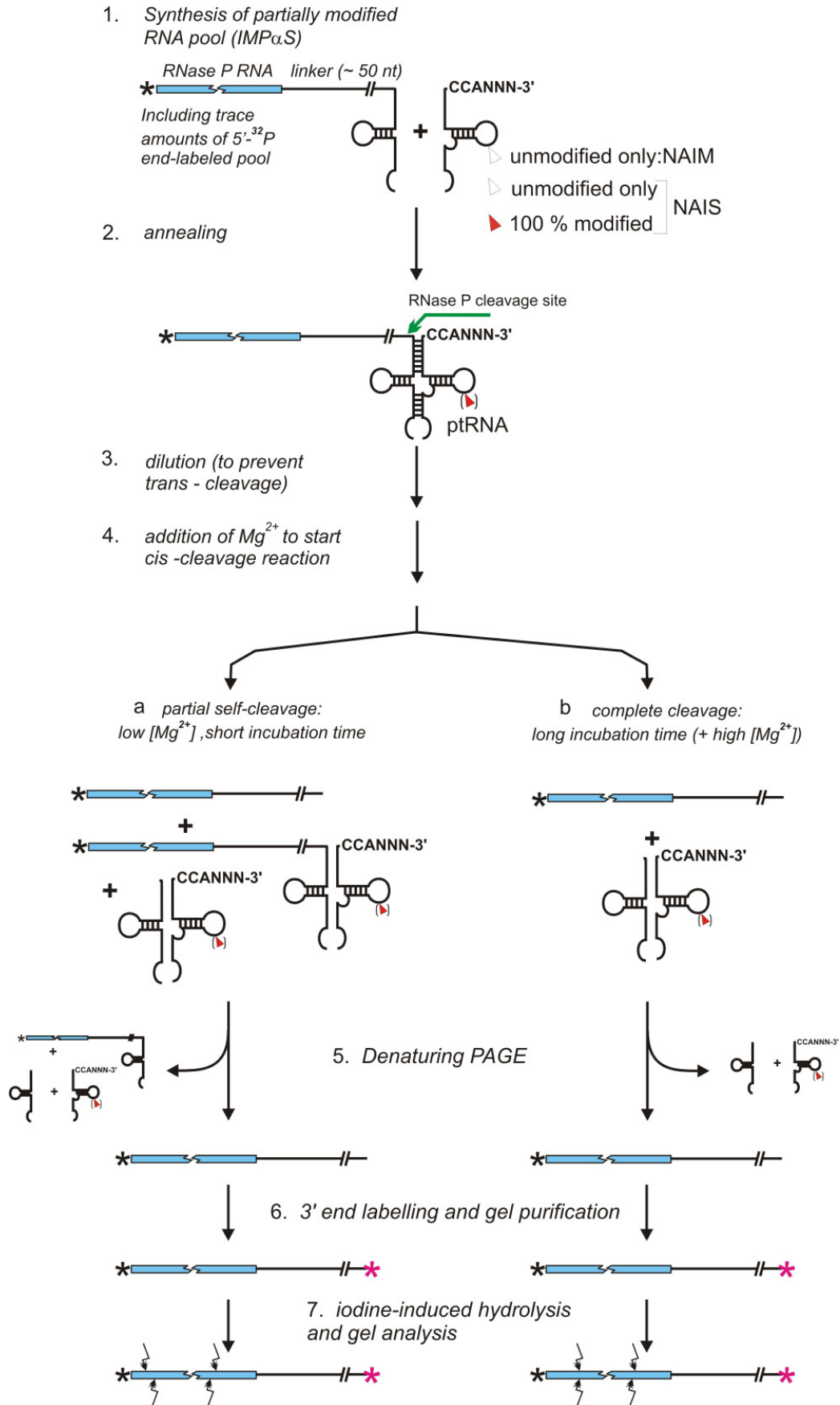7. *iodine-induced hydrolysis and gel analysis*

Fig. 4.3 10: Flow diagram for NAIM (NAIS) analysis of a *cis*-cleaving P RNA – tRNA conjugate. For details see the text (4.3.4).

3.   3.8-fold dilution of the annealing mix to 24 nM P RNA - tRNA 5' -half and 2.3 µM tRNA 3' -half by addition of NH$_4$Cl, urea and CaCl$_2$ to final concentrations of 100, 100 and 5 mM, respectively.

4.   Start of the *cis*-cleavage reaction by addition of MgCl$_2$ to a final concentration of 36 mM.

    (a) Stop of the reaction after 2 min at 50°C, resulting in 20 to 30 % product formation, and ethanol precipitation (3.2.2).

    (b) Incubation of a parallel reaction for 2 h, resulting in essentially complete substrate conversion. The products generated in this fashion serve as a reference RNA pool for NAIM analysis.

5.   Separation of cleaved P RNA conjugates from uncleaved fractions by denaturing PAGE (3.2.1) and elution by diffusion in elution buffer 2 (3.2.5).

6.   3' -end labelling (3.4.3) of the complete pool of eluted RNAs, resulting in an about 100 -fold higher specific radioactivity than that present at the 5' -end.

7.   Iodine hydrolysis (3.4.8) and denaturing PAGE analysis (3.2.1).

4.3.5 Application example

In a previous study, the NAIM method had been applied to locate positions within *E. coli* P RNA important for substrate recognition by employing a gel retardation assay to separate active ribozyme molecules from those with impaired function (Heide et al., 1999). The method described here, employing the *cis*-cleavage assay, was designed to identify positions that interfere with catalysis itself. It seems possible that functional groups in P RNA important for substrate binding are likewise important for substrate turnover, since binding is a prerequisite for cleavage. Therefore, interference effects observed in NAIM experiments investigating binding and cleavage are expected to overlap at least partially. Thus, the results obtained here with the *cis*-cleavage assay were compared with those obtained in the previous study using the gel retardation approach (Heide et al., 1999). In both approaches, the contribution of guanosine 2-NH$_2$ groups was investigated. Randomly distributed IMPαS modifications were introduced into P RNA – tRNA 5' -half conjugates by *in vitro* transcription. A low extent of modification (2.5 %) was chosen to avoid the possibility that an RNA molecule carries more than one modification at a functionally important position, which may otherwise mask weak interference effects.
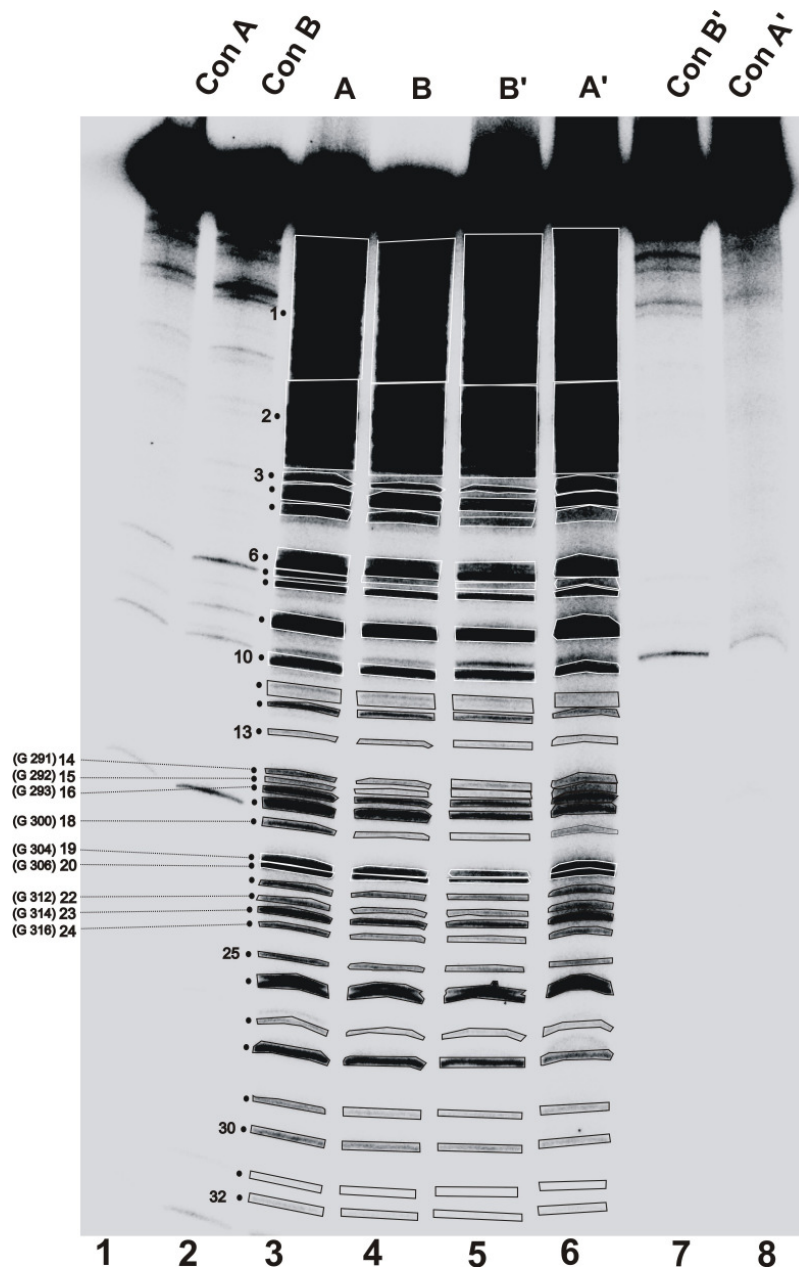
Fig. 4.3.11: NAIM experiment to identify IMPαS modifications that interfere with *cis*-cleavage of an *E. coli* P RNA - tRNA conjugate. 3' -end labelled RNA samples, either treated with iodine (lanes A, A', B, B') or not treated (lanes Con A, A', B, B') were loaded onto a 10 % PAA / 8 M urea gel and separated by electrophoresis until xylene cyanol reached the bottom of the gel. Radioactive bands were visualised as described (see paragraph "*Evaluation of NAIM data*"). Lane A: pool of RNA molecules after 2 h of incubation, representing the entire pool of modified RNA (Fig. 4.3.10, step 4 b); lane B: fraction of fast - reacting conjugates *cis*-cleaved in the initial fast phase of the reaction (within 2 min; Fig. 4.3.10, step 4 a). Lanes A' and B': same as lanes A and B, respectively, but representing a second individual experiment.

Evaluation of NAIM data

Iodine hydrolysis bands were visualised and quantified using a phosphorimage analyser (Bio-Imaging Analyser FLA 3000-2R; FUJIFILM) and the analysis software PCBAS/AIDA (Raytest). An application example is illustrated in Fig. 4.3.11, representing two individual experiments run in parallel (lanes 1-4 and 5-8) on a high resolution polyacrylamide gel. The quantification boxes positioned within the program AIDA are outlined in black or white lines (white when black lines are masked by high band intensities). In the case of insufficient separation of individual bands (e. g. boxes 1 and 2), two or more bands were enclosed by a single box. Some bands, such as those of boxes 31, are hardly discernible in Fig. 4.3.11 due to loss of resolution, but can be clearly differentiated from the background within the analysis program AIDA. The calculated parameters are given in table 4.3.1 and the results illustrated in Fig. 4.3.12.
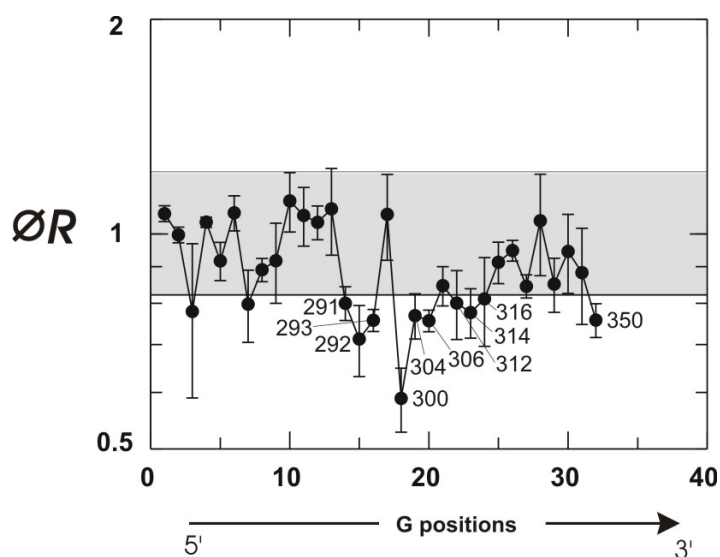
Fig. 4.3.12: Quantification and statistical analysis of IMPαS modifications that interfere with *cis*-cleavage of an *E. coli* P RNA - tRNA conjugate, based on three independent experiments. (**A)** Mean *R*-values (ØR; error bars: standard deviation of the mean) were plotted against the numbers (No.) of quantification boxes according to Table 4.3.1 (see next paragraph for data evaluation). Effects with *R*-values between 0.82 and 1.2 were arbitrarily considered insignificant (grey-shaded area). At positions where data points correspond to individual G residues for which interference effects were observed, the position according to the *E. coli* P RNA numbering system (see secondary structure in Fig. 4.3.13) is indicated next to the corresponding circle.

First the total band intensities per each lane were calculated ($\Sigma\ I_A$ and $\Sigma\ I_B$). The next step was to determine the normalisation factor κ to compensate for differences in total radioactivity in lanes A versus B, where A represents the pool of completely cleaved RNA conjugates (i.e. after 2 h) and B the fraction of fast reacting conjugates *cis*-cleaved during the initial phase of the reaction (within 2 min). A' and B' represent data from another

individual experiment; data from a third experiment (A" and B") were also included in the calculation of the average *R*-value, but are not given in Table 4.3.1.

Table 4.3.1: Analysis of NAIM data obtained upon selection of fast-cleaving (within 2 min) E. coli P RNA conjugates (fraction B and B') and comparison with the IMPαS-modified pool of RNA molecules obtained after exhaustive cleavage (fraction A and A')

No	position	fraction A	fraction B		fraction B'	fraction A'		R	R'	§R"	ØR	SD
		I$_A$	I$_B$	I$_B$ x κ	I$_{A'}$	I$_{B'}$	I$_{B'}$ x κ'					
1		267325,7	268508,1	285370,41	205632,4	247931,9	229510,56	1,07	1,16	1,02	1,07	0,03
2		99128,7	97563	103689,96	93011,7	96683,2	89499,64	1,06	0,96	0,98	0,10	0,03
3		5103,5	4019,6	4272,03	8152,5	3743,8	3465,64	0,84	0,43	1,08	0,78	0,19
4		11505,4	11559,2	12285,12	8920,8	9722,3	8999,93	1,07	1,01	1,04	1,04	0,02
5		6894,3	6143,4	6529,21	6028,7	5262,1	4871,13	0,95	0,81	0,99	0,92	0,06
6		16869,3	15114,1	16063,27	11072	13779,9	12756,05	0,96	1,15	1,11	1,07	0,06
7		5823,9	3511,6	3732,13	3464,9	2963,2	2743,03	0,65	0,79	0,96	0,8	0,09
8		6918,6	5624,5	5977,72	5825,2	5363,9	4965,36	0,86	0,85	0,96	0,89	0,03
9		20596,9	16283,7	17306,32	17227,6	14217,7	13161,32	0,85	0,76	1,15	0,92	0,12
10	271+270	9981,1	8461,5	8992,88	6623,5	8808	8153,57	0,90	1,23	1,21	1,11	0,11
11	275+276	4298,9	4396,8	4672,92	4542,9	4306,1	3986,16	1,09	0,88	1,22	1,06	0,10
12	280	3472,3	3499,8	3719,59	2768	3338	3089,99	1,07	1,12	0,93	1,04	0,06
13	285	1660,9	1402,6	1490,68	1699,1	1788,3	1655,43	0,90	0,97	1,38	1,09	0,15
14	291	2395,1	1871,8	1989,35	3471,2	2678,9	2479,84	0,83	0,71	0,86	0,80	0,04
15	292	2225,7	1535	1631,40	3451,9	2099,5	1943,51	0,73	0,56	0,84	0,71	0,08
16	293	5352,9	3555,6	3778,89	5085,5	4225,7	3911,73	0,71	0,77	0,80	0,76	0,027
17	297+296	8472,7	7253,3	7708,81	5296,3	5313,3	4918,52	0,91	0,93	1,36	1,07	0,15
18	300	3822,9	1686,3	1792,20	2301,7	1650,6	1527,96	0,47	0,66	0,63	0,59	0,06
19	304	6238,6	4291,2	4560,69	4714,8	3548,7	3285,03	0,73	0,70	0,88	0,77	0,06
20	306	7388,6	5131,3	5453,55	5342,3	4166,4	3856,84	0,74	0,72	0,81	0,76	0,03
21	310	3425,2	2531	2689,95	3154,1	2732,1	2529,10	0,79	0,80	0,95	0,85	0,05
22	312	2973	2091,6	2222,95	3304	2428,8	2248,34	0,75	0,68	0,97	0,80	0,09
23	314	5925,1	3661	3890,91	4617,2	4307,2	3987,17	0,66	0,86	0,81	0,78	0,06
24	316	2856,3	2112,4	2245,06	2818	1905,8	1764,20	0,79	0,63	1,02	0,81	0,12
25	320	2667,7	2265,8	2408,09	2014,7	2228,7	2063,11	0,90	1,02	0,81	0,91	0,06
26	323+324	10050,2	9544,4	10143,79	10304,4	10058,5	9311,15	1,01	0,90	0,93	0,95	0,03
27	329	1942,9	1449,4	1540,42	1867,6	1696,1	1570,08	0,79	0,84	0,90	0,85	0,03
28	332	6697,3	6058,8	6439,29	3723,5	5509,8	5100,42	0,96	1,37	0,80	1,04	0,17
29	336	2334,2	2167,8	2303,94	2261,5	1788,6	1655,71	0,99	0,73	0,83	0,85	0,07
30	340	2966	2978,4	3165,44	2224,3	2556,2	2366,27	1,07	1,06	0,71	0,95	0,12
31	346	1264,6	804,2	854,70	702,1	632,2	585,23	0,68	0,83	1,14	0,88	0,14
32	350	1944,3	1486,7	1580,06	1461,1	1236,6	1144,72	0,81	0,78	0,68	0,76	0,04
	sum	540522,8	508563,9		443085,5	478672,1						

κ = 1.06284146; κ' = 0.92565558

I = intensity; κ = normalisation factor (see text).

Position: according to the *E. coli* P RNA numbering system (see secondary structure in Fig. 4.3.13);

R = I$_B$ x κ / I$_A$; *R'* = I$_{B'}$ x κ' / I$_{A'}$; *R"*: calculated like *R* or *R'*, §primary data (I$_{A"}$, I$_{B"}$, I$_{B"}$ x κ") not included in the table;

ØR = mean of *R, R'* and *R"*; *SD* = standard deviation of the mean

The normalisation factor κ was calculated from the ratio of the sum of all band intensities in lane A versus B ($\Sigma\, I_A / \Sigma\, I_B$). Interference and enhancement effects for individual bands (or two or more bands if quantified as one due to low gel resolution) are then determined by calculating the ratio $R = (\kappa \times I_B) / I_A$. Interference effects are associated with R-values below 1.0, whereas enhancement effects will result in R-values above 1.0. In a previous study (Rox et al., 2002), only R-values below 0.82 and above 1.2 were considered significant, but these cutoff values are arbitrary and depend on the quality of the data, such as the number of and fluctuations between individual experiments as well as the selection stringency inherent to the experimental setup. In the example shown in Table 4.3.1, the data are based on three individual experiments, which we consider to be the absolute minimum for such studies. Fig. 4.3.12 shows a graphical representation of the mean R-values (including errors).

Comparing NAIM results obtained with the cis-cleavage assay of E. coli P RNA - tRNA conjugates (this study) with results obtained for tRNA binding (previous study)

Usually, one compares IMPαS with GMPαS interference patterns to be able to ascribe effects to the thioate and/or additional base modification. However, the idea behind the strategy employed here was to determine to which extent IMPαS interference patterns obtained with the *cis*-cleaving conjugate overlap with those observed in a gel retardation assay selecting for high affinity tRNA binding to *E. coli* P RNA (Heide et al., 1999). Generally, the amount of information derived from NAIM experiments can be significantly increased by comparing NAIM results obtained for the same system but using different functional assays. Comparison of NAIM results shown in Fig. 4.3.12 with those obtained for high affinity tRNA binding to *E. coli* P RNA by a gel retardation assay (Heide et al., 1999) reveals substantial overlap (Fig. 4.3.13). In the region of nucleotides 291 – 350, IMPαS modifications at G 291 – 293, G 300, G 304, G 306 and G 314 caused interference effects in both functional assays (marked by red circles in Fig. 4.3.13), although with different amplitudes. The interference effect at position G 300 obtained in the tRNA binding assay (Heide et al., 1999) was predominantly a phosphorothioate effect already observed with GMPαS modification alone, which, however, was not analysed in the *cis* – cleavage assay. The positions G 291 – 293 normally interact with the 3' -CCA terminus of tRNA (Heide et al., 1999; Busch et al., 2000). By introducing inosine modifications at these three positions, the interaction with the tRNA's CCA terminus is weakened, explaining why inosine interference effects at these positions were detected in both functional assays. Modifications at position G 300, G 304, G 306 and G 316 apparently destabilise substrate binding to the ribozyme, either directly or by inducing conformational changes of ribozyme structure. In the tRNA binding assay, two additional interference effects caused by IMPαS modifications were detected at positions G 329 and G

356 (highlighted in blue in Fig. 4.3.13). Interference effects at G 312, G 316 and G 350 (green; Fig. 4.3.13) were detected only in the *cis* – cleavage assay. G 350 may represent a position essential for the catalytic step, as evidence was provided that G 350 contributes to the binding of catalytically important Mg^{2+} near the active site of P RNA (Rasmussen & Nolan, 2002). According to the graphical representation shown in Fig. 4.3.12, IMPαS interference effects at G 312 and G 316 are borderline cases due to their weakness.
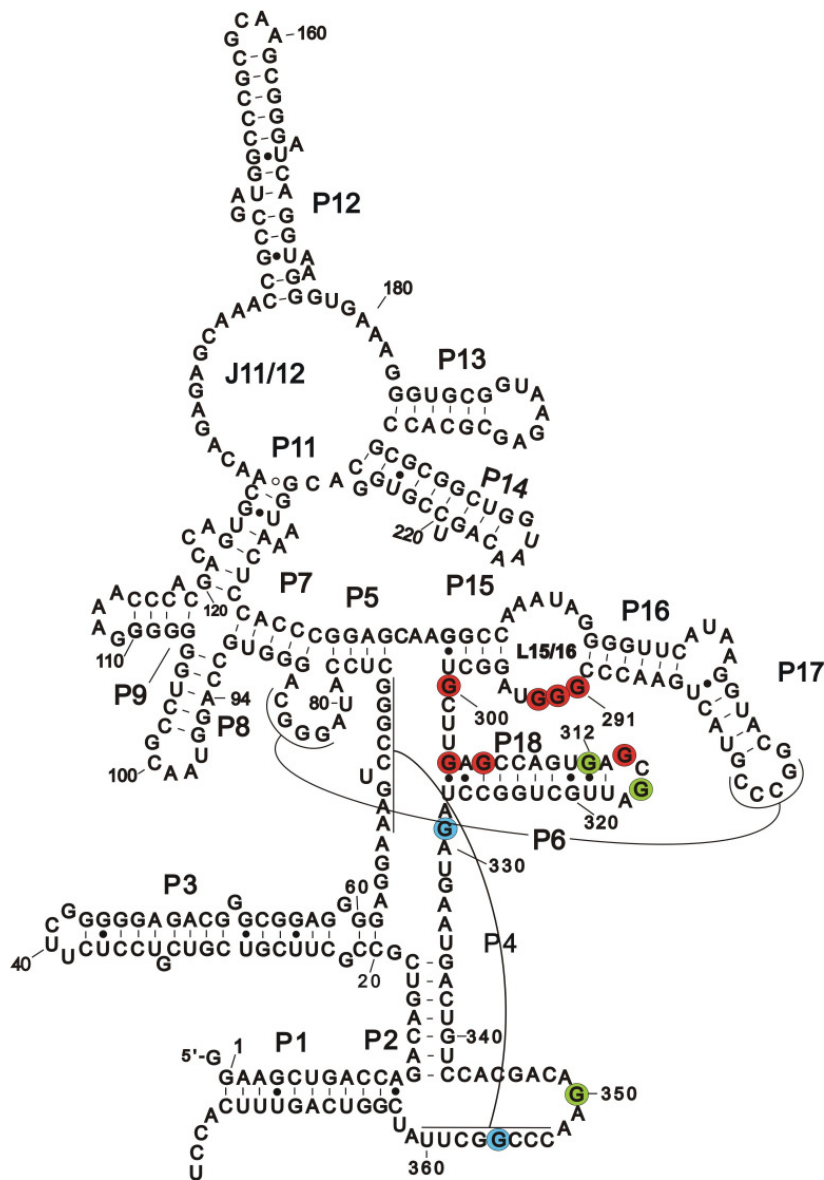
Fig. 4.3.13: Secondarry structure of *E. coli* P RNA. Positions where IMPαS interference effects were detected are marked by colored circles: red corresponds to interference effects detected in binding as well as cleavage assays; positions highlighted in green are those where interference effect were detected only in the *cis*-cleavage assay, blue corresponds to positions that interfere with tRNA binding only.

Outlook

NMR analyses of 2' ribose modified model substrates

Based on the biochemical approaches applied in this work, different assumptions were proposed, but these approaches did not totally clarify the role of the 2' OH at the cleavage site or the effect of the analysed modifications on ptRNA ground state binding and

```
        -1 ┐       +73
5'-U T T ─ U C C A -3'
    +1 ┐  G ─ C
        C ─ G
        G ─ C
        G ─ C
        G ─ C
        A ─ U
        G ─ C
```
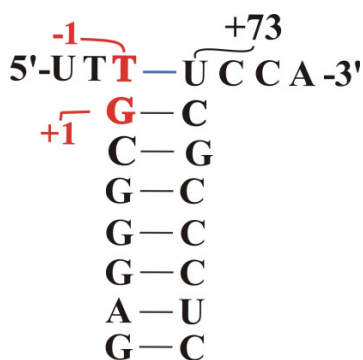
catalysis by P RNA. Structural analyses (NMR) using model substrates (see illustration on the left), consisting of a short 5' – leader sequence, the acceptor stem and the 3' –CCA termini, carrying 2' ribose modifications at the P RNA cleavage site (nt – 1 and +1 highlighted in red; see illustration) might give some more information regarding the divalent metal ion binding sites located in the vicinity of these positions. Preliminary NMR analyses (Imino-proton 1D-spectrum) indicated that the ribo T at position –1 forms a base pairing interaction (indicated by the blue line) with U 73. This base pairing interaction was very weak for the unmodified RNA substrate, very strong for the substrate with an LNA modification at nt –1 and intermediate for the variant with an LNA at nt +1. Mg^{2+} titration experiments revealed a Me^{2+} ion binding site located in the vicinity of this base pair, but this Me^{2+} might be not the one involved in the catalytic step. The biochemical data supports the hypothesis that an LNA at nt –1 destabilises binding of catalytic metal ions and LNA at nt +1 displaces (directly or indirectly) an Ca^{2+} ion essential for E•S complex formation. By applying other NMR techniques (COSY and NOESY spectra) Mg^{2+} / Mn^{2+} ion binding site can be inferred. Due to its paramagnetism, Mn^{2+} binding to RNA can be monitored by NMR , since manganese (II) ions cause specific line-broadening of 1D NMR signals of nuclei close to a bound Mn^{2+} ion.

NAIS experiments; proof of principle

The NAIM experiments using an RNA pool which carried randomly distributed IMPαS modifications revealed positions that interfere with P RNA cleavage. The strongest interference effects were observed in the region G 291 – 293 located in L 15 / 16 of *E. coli* P RNA. Since it is known that G 292 – 293 form base pairs with C 75 - 76 of the 3' –CCA terminus of tRNA, in a further NAIS experiment, using a point mutation in the CCA sequence (e.g. C 75 to G) is expected to suppress the interference effect observed in the NAIM experiment, an observation that would confirm the direct contact of the P RNA via the two G's in L 15 / 16 with 3' -CCA of the tRNA.

<u>Summary</u>

The ribonucleoprotein enzyme ribonuclease (RNase) P is an endonuclease that generates the mature 5' -ends of tRNA. Bacterial RNase P enzymes are composed of a catalytic RNA subunit of about ~400 nucleotides (nt) in length and a single small protein of typically 120 amino acids. Under physiological conditions, both subunits are essential for the catalysis. The RNA subunit is catalytically active in the absence of the protein at high divalent metal ion concentrations. This work focused on the catalytic mechanism of RNase P, and different aspects of RNase P processing are illustrated in three main chapters:

The role of divalent cations in RNase P RNA catalysis: studies with Zn^{2+} as catalytic cofactor

Studies with P RNA from *Escherichia coli* (structural P RNA subtype A) and *Bacillus subtilis* (subtype B) have implied a specific role for two or more metal ions in substrate binding and cleavage chemistry (Smith & Pace, 1993; Warnecke et al., 1996; 1999; Kurz & Fierke, 2002). Mg^{2+} and Ca^{2+} were shown to be the only earth alkaline divalent cations that support P RNA cleavage under standard assay conditions, Ca^{2+} being significantly less efficient than Mg^{2+}. Among the transition metal ions, only Mn^{2+} alone and Zn^{2+} in combination with Sr^{2+} or Ba^{2+} mediated RNase P cleavage.

This study demonstrated, for the first time, catalysis by *E. coli* P RNA with Zn^{2+} as the sole divalent metal ion cofactor in the presence of ammonium, but not sodium or potassium salts. Hill analysis suggests a role for two or more Zn^{2+} ions in catalysis. Zn^{2+} destabilises substrate binding even more than Cd^{2+}. In contrast, $Co(NH_3)_6^{3+}$ and Sr^{2+} in particular, both unable to support catalysis by themselves, promote high substrate affinity. Hill analysis suggests the uptake of at least two additional Sr^{2+} ions upon E•S complex formation. Zn^{2+} and $Co(NH_3)_6^{3+}$ substantially reduce the fraction of ptRNA molecules able to bind to *E. coli* P RNA at saturating enzyme concentration. Stimulating and inhibitory effects of Sr^{2+} could be rationalised by a model involving two Sr^{2+} ions (or two classes of Sr^{2+} ions), both improving substrate affinity in a cooperative manner, but one of the two inhibiting substrate conversion in a noncompetitive mode with respect to substrate. Kinetic analyses further suggest that the inhibition mode of Sr^{2+} is noncompetitive with respect to Zn^{2+}. A single 2'-fluoro modification at nt −1 of the substrate substantially weakened the inhibitory effect of Sr^{2+}, although the precise role of the 2'-OH at nt −1 in this context remains to be elucidated.

Chemical modification studies: the role of 2'-hydroxyls at the cleavage site and neighbouring positions

2' OH groups within the structural context of ptRNA can serve as H-bond donors or acceptors for specific residues in the P RNA and they could be involved in binding of catalytic metal ions. In this work, the role of the 2' OH groups was analysed at and around the cleavage site of a ptRNA in *E. coli* P RNA - catalysed cleavage. Towards this goal, single modifications were introduced into the ptRNA at the cleavage site (nt −1) and neighbouring positions (nt −2 and +1) and their effect on binding and processing efficiency by *E. coli* P RNA was analysed.

Analyses of ptRNA variants carrying 2' ribose modifications at nt −1 suggest that the 2' OH group of nt −1 is involved in a H-bonding interaction during the cleavage reaction. Removal or modification of this group led to a significant reduction in cleavage efficiency by *E. coli* P RNA, while the effect on ptRNA binding was moderate. In addition to a huge reduction of the catalytic rate, an LNA or 2' OCH_3 modification at nt −1 induced partial (LNA) or exclusive (2' OCH_3) miscleavage of the corresponding ptRNA at a site one nucleotide downstream from the canonical cleavage site. Analyses of pH dependence of canonical cleavage and miscleavage for LNA −1 substrates indicate that the two reaction pathways have different rate limiting steps; chemistry limits the rate for canonical cleavage in the pH range 5.5 to 6.5, while a refolding step seems to limit the rate of canonical cleavage at a pH above 6.5 as well as the rate of miscleavage over the entire pH range investigated. Mg^{2+} titration experiments indicate that the pathway leading to canonical cleavage has a higher requirement for Mg^{2+} than the pathway leading to miscleavage. These notions suggest that the LNA at nt −1 interferes with binding of catalytic metal ions at the canonical site; the E•S complexes that are not able to bind the catalytic Mg^{2+} at the canonical site might change their conformation to allow binding of the catalytic Mg^{2+} to the site of miscleavage, consistent with the observation that a refolding step limits the miscleavage pathway.

Analysis of ptRNA substrate carrying a deoxy modification at nt +1 indicates that E•S complex formation is not supported by a H-bonding interaction involving the 2' OH at nt +1 since this modification neither had an effect on ptRNA binding to nor on processing by *E. coli* P RNA. An LNA or 2' OCH_3 modification at nt +1 significantly decreased ptRNA affinity to *E. coli* P RNA at low divalent cations concentration. This binding defect was compensated to some extent by higher Me^{2+} concentrations. A similar effect, observed in the cleavage reaction of this substrate at low Me^{2+} concentrations, was independent of the type of divalent cation and attributed to poor E•S complex formation under these conditions. These results suggest that these two modifications interfere with substrate binding via sterical hindrance by

the bulky methyl or methylene group found at nt +1 of these variants. Hill analysis of ptRNA binding with LNA at nt +1 compared to the unmodified variant in the presence of Ca^{2+} indicates a higher Ca^{2+} cooperativity for the modified ptRNA variant, since a higher slope of the Hill plot for the G_{LNA} +1 variant compared to the one determined for the unmodified substrate was obtained. Two hypotheses consistent with these results were proposed, suggesting a direct or indirect displacement of Ca^{2+} by an LNA modification at nt +1.

Modification interference studies: an approach to identify functional groups that interfere with the cleavage reaction

Nucleotide analogue interference mapping (NAIM) and nucleotide analogue interference suppression (NAIS) are two powerful methods to identify important functional groups in nucleic acids. RNA (DNA) pools randomly modified with nucleotide analogues are separated into functional (e.g. binding or catalytically active) and defective fractions. Subsequent analysis of the respective modification patterns obtained by iodine-induced hydrolysis allows the identification of functionally important groups.

The focus of this study was to develop a method suitable for identifying residues important for the interaction of a ribozyme (P RNA) with its substrate (ptRNA) during the cleavage reaction. To address this issue, a chimeric RNA consisting of *E. coli* P RNA and the 5' -half of a ptRNA linked by a spacer was constructed. A functional substrate was reconstituted by annealing the 3' -half of the tRNA to the 5' -half contained within the chimeric RNA. After annealing, a *cis*-cleaving RNA complex was obtained. Reaction parameters for optimal cleavage and insuring the absence of *trans*-cleavage under conditions where chemistry limits the cleavage rate were established.

Kinetic analysis of the *cis*-cleavage reaction of the chimeric RNA showed that the course of the reaction is governed by a fast turnover dominating in the initial phase of the reaction and a slow one predominant in the second phase. The fast turnover was dependent of pH in the range from 5.2 to 6.5, suggesting that under this conditions cleavage chemistry is rate limiting. The slow turnover was pH independent, suggesting that other step than cleavage chemistry like a refolding step limits the second phase of the reaction. The length of the linker that connects the ribozyme to the reconstituted tRNA did not have an influence on the fast turnover in the range from 45 to 130 nucleotides.

For modification interference studies, a partially modified pool of this ribozyme chimera was synthesised by *in vitro* transcription. After separation of functional (*self-cleaving*) and non-functional molecules, positions within the 3' -half of the P RNA where modifications interfered with processing (cleavage reaction) could be identified. These positions are overlapping to some extent with those found in a previous study, where

interference with *E. coli* P RNA - tRNA binding was analysed (Heide et al. 1999). In the region of nucleotides 291 – 350, IMPαS modifications at G 291 – 293, G 300, G 304, G 306 and G 314 caused interference effects in both functional assays, although with different amplitudes. These results are to be expected because functional groups in P RNA important for substrate binding are likewise important for substrate turnover, since binding is a prerequisite for cleavage. Interference effects at G 312, G 316 and G 350 were detected only with the *cis* – cleavage assay. G 350 may represent a position essential for the catalytic step, as evidence was provided that G 350 contributes to the binding of catalytically important Mg^{2+} near the active site of P RNA (Rasmussen & Nolan, 2002), while G 312 and G 316 are borderline cases due to weak interference effects.

Appendix

Appendix 1: Derivation of the equation describing the inhibition and stimulation of *E. coli* P RNA catalysed cleavage by strontium

The velocity dependence equation is:

$$v_i = k_{chem} \cdot ([ES] + [ESI(a)]) \tag{1}$$

Dividing both sides of the velocity dependence equation (1) by $[S]_t$:

$$\frac{v_i}{[S]_t} = \frac{k_{chem} \cdot ([ES] + [ESI(a)])}{[S]_t} \tag{2}$$

$$[S]_t = [S] + [ES] + [ESI] + [ESI(a)] + [ESI(a)I] \tag{3}$$

Replacing $[S]_t$ in the right-hand side of equation (2):

$$\frac{v_i}{[S]_t} = \frac{k_{chem} \cdot ([ES] + [ESI(a)])}{[S] + [ES] + [ESI] + [ESI(a)] + [ESI(a)I]} \tag{4}$$

Expressing the concentration of each species in terms of [E]:

$$\frac{v_i}{[S]_t} = \frac{k_{chem} \cdot \left(\dfrac{[S] \cdot [E]}{K_S} + \dfrac{[S] \cdot [E] \cdot [I]}{\alpha \cdot K_S \cdot K_{I(a)}} \right)}{[S] + \dfrac{[S] \cdot [E]}{K_S} + \dfrac{[S] \cdot [E] \cdot [I]}{\beta \cdot K_S \cdot K_I} + \dfrac{[S] \cdot [E] \cdot [I]}{\alpha \cdot K_S \cdot K_{I(a)}} + \dfrac{[S] \cdot [E] \cdot [I]^2}{\alpha \cdot \beta \cdot K_S \cdot K_{I(a)} \cdot K_I}} \tag{5}$$

Multiplying the numerator and dominator with $\dfrac{K_S}{[S]}$ and simplifying:

$$\frac{v_i}{[S]_t} = \frac{k_{chem} \cdot [E] \cdot \left(1 + \dfrac{1}{\alpha \cdot K_{I(a)}} \cdot [I] \right)}{K_S + [E] \cdot \left(1 + \left(\dfrac{1}{\beta \cdot K_I} + \dfrac{1}{\alpha \cdot K_{I(a)}} \right) \cdot [I] + \dfrac{1}{\alpha \cdot \beta \cdot K_I \cdot K_{I(a)}} \cdot [I]^2 \right)} \tag{6}$$

When [I] = 0, v_i equals v_0, and equation (6) simplifies to:

$$\frac{v_0}{[S]_t} = \frac{k_{chem} \cdot [E]}{K_S + [E]} \tag{7}$$

$[S]_t \cdot k_{chem}$ is v_{max} under conditions [E]>>[S].

Dividing equation (7) by equation (6) and simplifying:

$$\frac{v_0}{v_i} = \frac{K_S + [E] \cdot \left(1 + \left(\dfrac{1}{\beta \cdot K_I} + \dfrac{1}{a \cdot K_{I(a)}} \right) \cdot [I] + \dfrac{1}{\alpha \cdot \beta \cdot K_I \cdot K_{I(a)}} \cdot [I]^2 \right)}{(K_S + [E]) \cdot \left(1 + \dfrac{1}{\alpha \cdot K_{I(a)}} \cdot [I] \right)} \tag{8}$$

Appendix 2: Materials & Equipment

Chemicals

Acrylamide M-Bis (50 % stock solution 24/1)	Gerbu
Agar Agar	Serva
Agarose	Roth
Ampicillin	Gerbu
Ammonium acetate	Fluka
Ammoniumperoxodisulfate	Roth
BlueSlick	Serva
Boric acid	Roth
Bromphenolblue (BPB)	Merck
Deoxynucleosidtriphosphates (dNTPs)	Boehringer
Disodiumhydrogenphosphate	Merck
Dithiothreitol (DTT)	Gerbu
Ethanol $\geq$ 99,8 %	Roth
Ethidiumbromide	Serva
Glycerol	Gerbu
Glycogen	Roche
Urea	Gerbu
Yeast extract	Gerbu
Isopropanol	Roth
Potassiumdihydrogenphosphate	Fluka
Sodiumacetate	Merck
Nucleosidtriphosphates (NTPs)	Boehringer
SELECT Peptone 140	Roth
Phenol	Roth
Bovine serum albumin (BSA)	Sigma
N,N,N',N'-Tetraethylmethylenediamin (TEMED)	Serva
Tris-(hydroxymethyl)aminomethane	Gerbu
Xylenecyanolblue (XCB)	Serva

All other chemicals (not listed above) were purchased from Sigma, Gerbu or Life Technologies and they posses a purity grade "pro analysis".

Radioisotopes

[γ-^{32}P]-ATP	Hartmann Analytic
	ICN Radiochemicals
[5`-^{32}P]-pCp	Hartmann Analytic
[α-^{32}P]-GTP	Hartmann Analytic
	ICN Radiochemicals

DNA size markers

1kb DNA ladder	Invitrogen
10 bp DNA ladder	Invitrogen
2 - Log DNA ladder	New England Biolabs

Enzymes

Alkaline Phosphatase	Roche
Nuclease P1	Biomol
Pfu-Polymerase	Stratagene
Pyrophosphatase	Roche
Restriction endonucleases	MBI Fermentas
	New England Biolabs
T4 DNA-ligase	Gibco BRL
	MBI Fermentas
T4-Polynucleotide-kinase	MBI Fermentas
	Gibco BRL
T4 RNA-ligase	New England Biolabs,
	MBI Fermentas
T7-RNA polymerase	MBI Fermentas

Syntetic DNA oligonucleotides (Primers)

The sequence of DNA oligonucleotides is given in the direction 5' → 3'. Restriction sites introduced with the primer are shown in bold. The overlapping region of two restriction sites is underlined.

Name	Application	Sequence (5' → 3')
Eco M1 5' Eco R I T7	PCR; construction of RNase P RNA - tRNA 5' -half tRNA sequence	CCG**GAATTC**TAATACGACTCACTATAGGAAGCTGACCAGACAGTCGCCGCTTCG
3' M1 Gly spacer	PCR; construction of RNase P RNA- tRNA 5' -half sequence	GGTCGTGCTCTACCGACTGAGCTACTCCCGCGAATACCTATGACCATGATTACGC
3' Gly spacer 2 compl.	Primer elongation reaction; construction of RNase P RNA-tRNA 5' -half sequence	GCGGGAGTAGCTCAGTCGGTAGAGCACGACCTTGTCACCGGATGT
3' Gly spacer 3	Primer elongation reaction; construction of RNase P RNA-tRNA 5' -half sequence	CGCGGATCCTTGTTTCGTCCTCACGGACTCATCAGACCGGAAAGCACATCCGGTGACAAG
t gly 3' -half 5' T7 EcoR I	PCR; cloning tRNA 3' -half sequence	CCG**GAATTC**TAATACGACTCACTATAGGACAAGGTCGGGGTCGCGGGTTCA
tgly 3' -half 3' Mfe I-Bahm H I	PCR; cloning tRNA 3' -half sequence	CGC**GGATCC̲AATTG**GAGCGGGAGACGGGACTTGAACCC
pUC 19-5'Hind III to Eco 147 I	Mutagenesis; pUC 19 Hind III to Eco 147 I	GACCTGCAGGCATGC**AGGCCT**GGCGTAATCATGGTC
pUC 19-3'Hind III to Eco 147 I	Mutagenesis; pUC 19 Hind III to Eco 147 I	GACCATGATTACGCC**AGGCCT**GCATGCCTGCAGGTC
Eco M1 5' Eco R I T7 short	PCR; construction of RNase P RNA–tRNA sequence	CCG**GAATTC**TAATACGACTCACTATAGGAA
3' ptRNA Mun I-Bam H I	PCR; construction of RNase P RNA–tRNA sequence	CGC**GGATCC̲AATTG**GAGCGGGAGACGGGACTTGAACCCGCGACC
3' ptRNA short	PCR; construction of RNase P RNA–tRNA sequence	CGCGGATCCAATTGGAGC
ptRNA loops	PCR; construction of RNase P RNA–tRNA sequence	GACTTGAACCCGCGACCCCGACCTTGGCAAGGTCGTGCTCTACCGACTG
ptRNA loops short	PCR; construction of RNase P RNA–tRNA sequence	GACTTGAACCCGCGACCC

Note: All DNA oligonucleotides were synthesised by Invitrogen GmbH, Karlsruhe.

Synthetic RNA oligonucleotides

The sequence of RNA oligonucleotides is given in the direction 5' → 3'. The modified bases are highlighted in red. The subscript indicates the type of modification: F for 2'–fluor, H for 2'- deoxy and LNA for locked nucleic acid modification. (rT) indicates a ribo-timine. All other nucleotides are unmodified.

Nr.	Sequence 5' to 3'	Application
1	CCCUUUCGCGGGAGUAGCUCAGUC	• RNA ligation – construction of ptRNA substrates with different ribose modifications (1 to 8) • alkaline hydrolysis (4 to 7) • hydrolysis by nuclease P1
2	CCCUUUC$_F$GCGGGAGUAGCUCAGUC	
3	CCCUUUC$_H$GCGGGAGUAGCUCAGUC	
4	CCCUU(rT)(rT)GCGGGAGUAGCUCAGUC	
5	CCCUU(T$_{LNA}$)(rT)GCGGGAGUAGCUCAGUC	
6	CCCUU(rT)(T$_{LNA}$)GCGGGAGUAGCUCAGUC	
7	CCCUU(rT)(rT)(G$_{LNA}$)CGGGAGUAG	
8	CCCUU(rT)(rT)(G$_H$)CGGGAGUAG	
9	CCCUUUC$_H$	size marker
10	UU(rT)(rT)GCGGGAG	NMR studies
11	UU(T$_{LNA}$)(rT)GCGGGAG	
12	UU(rT)(rT)(G$_{LNA}$)CGGGAG	
13	UU(T(T$_H$)GCGGGAG	
	UU(T(U$_F$)GCGGGAG	
	CUCCCGCUCCA	

Note: Oligonucleotides were purchased by :IBA, Göttingen (oligo 1 to 3); Alnylam, Kulmbach (oligos 8 to 13) or synthesised by Prof. Dr. Rolf Bald† and coworkers (oligos 4 to 7) from Freie Universität Berlin.

Plasmids DNA's

Plasmids constructed and/or used in this work are listed below. The recognition sites of restriction enzymes used for cloning or linearisation before transcription are indicated.

Plasmid name	Application	Restriction enzyme (recognition site)	Reference
pUC19	Cloning vector Template for mutagenesis; pUC19 Hind III to Eco 147 I	Eco R I (G↓AATTC) Bam H I (G↓GATCC) -	Life Technologies
pSBpt3'HH	PCR template; construction of tRNA 3' -half	-	Busch et al., 2000
pFL 117	PCR template; construction of P RNA - tRNA 5' -half conjugate	-	Prof. Dr. Liu, University of California, Berkeley
pXX	Template for T7 transcription; P RNA - tRNA 5' -half PCR template; construction of P RNA - tRNA conjugate	Bam H I (G↓GATCC) -	4.3.2
pXY and derivates	Cloning vector ; construction of P RNA tRNA conjugates with different linker length Template for T7 transcription; P RNA tRNA conjugates	Hind III (A↓AGCTT) Eco 47 III (AGC↓GCT) Mun I (C↓AATTG)	4.3.2
ptGly 3' -half	Template for T7 transcription; tRNA 3' -half	Mun I (C↓AATTG)	4.3.2
pdW98	Template for T7 transcription of *E. coli* P RNA wild type	Bsa A I (YAC↓GTR)	Busch et al., 2000
ptGly + 18	Template for T7 transcription; $tRNA_{18-79}$	Bam H I (G↓GATCC)	Person et al., 2003
pdW66 m1 wt	Template for T7 transcription; *B. subtilis* RNase P RNA wild type	Dra I (TTT↓AAA)	Warnecke et al., 1999

Equipment

Agarose gel chamber	Biorad, Mini Sub Cell
Gel documentation system	Cybertech, CS1 with Mitsubishi Video Copy Processor; Biostep, GelSystem MINI
Gel dryer	Biorad, Model 483 SLAB Dryer
Hand-monitor	Berthold, LB 1210 B
Heating blocks	Techne, Dri-Block DB-3D; Biometra, TB1
Imager cassettes	Fuji Film, Bas cassette 4043, Rego, 35,6x43,2cm
Magnetic stirrers	Heidolph, MR 2002
Microanalyses - filtersystem	Millipore
Power supply	Pharmacia, EPS 3500; Bio Rad, Power Supply160/1.6 (Power Pac 3000); Apelex, PS 9009T
PAA-gel chamber	Constructed by the workshop of the Clinic University of Lübeck
PCR cycler	Biometra, $T_{Gradient}$ Thermocycler
pH-Meter	WTW, pH Level 1
Phosphoimager	Raytest, Bio-Imaging Analyser BAS 1000 (Fujifilm); FLA 3000, (Fujifilm)
Pipettes	Gilson-Pipetman, P20, P200, P1000 Abimed 0.1÷2
Quartz cuvette	Hellma 104-QS, 105.202, 115B-QS, 105
Mixer	IKA, Vibrax-VXR; Eppendorf, Thermomixer 5436, Thermomixer comfort
Spectrophotometer	Hewlett Packard, Photometer 8453; Varian, Cary 50 Conc; Thermo Spectronic, Biomate 3
Software	PCBas/Aida Image Analyser v.3.45, Corel Graphics Suite; GraFit 3.0; Microsoft Office;
Scintillation counters	Perkin Elmer, Wallac WINSPECTRAL α/β 1414 Liquid Scintillation Counter; Packard, Tricarb 2000CA
Centrifuges	Heraeus, Biofuge pico, biofuge fresco; Sigma, Typ 112; Eppendorf, centrifuge 5810R, minispin plus Stratagene, PicoFuge

Appendix 3: List of abbreviations and unit

A_{260}	absorption at 260 nm	μmol	micromole
A	adenosine	μM	micromolar
Amp	ampicillin	NAIM	nucleotide analogue interference mapping
approx.	approximatively		
APS	ammonium peroxo-disulfate	NAIS	nucleotide analogue interference suppression
bp	base pair		
BPB	bromphenolblue	nm	nanometre
BSA	bovine serum albumin	nt	nucleotide
C	cytosine	NTP	Ribonucleosidtriphosphate
°C	degree Celsius	OD_{600}	optical density at 600 nm
C5	the protein subunit of *E. coli* RNase P	P	product
cpm	count per minute	p.a.	pro analysis
Da	Dalton	PAA	polyacrylamide
DMSO	dimethylsulfoxide	PAGE	polyacrylamide gel electrophoresis
DNA	deoxyribonucleic acid		
DNase	deoxyribonuclease	PCR	polymerase chain reaction
DTT	dithiothreitol	PEG	polyethyleneglycol
E	enzyme	PIPES	piperazine-1,4-bis(2-ethane sulphonic acid)
E	extinction		
ε	molar extinction coefficient		
EDTA	ethylenediamintetraacetic acid	pmol	picomole
e.g.	for example	P protein	protein subunit of RNase P
Fig.	figure	P RNA	RNA subunit of RNase P
g	gram	RNA	ribonucleic acid
G	guanosine	RNase	ribonuclease
h	hour	rpm	rounds per minute
HEPES	N-2-hydroxyethylpiperazine-N'-2-ethane sulphonic acid	S	substrate
		SDS	Sodiumdodecylsulfat
K_d	equilibrium dissociation constant	T	Thymine
		TBE	Tris-Borat-EDTA (buffer)
k_{obs}	observed rate constant	TEMED	N,N,N',N'-Tetraethyl-methylenediamine
l	liter		
LB	Luria-Bertani	T_m	melting temperature
LNA	Locked Nucleic Acid	Tris	Tris(hydroxymethyl)-aminomethane
m	metre	(p)tRNA	(pre)transfer-RNA
M	mol/l, molar	U	Uridine
mA	milliampere	U	Unit(s), Unit of enzyme activity
MBq	MegaBequerel	v/v	volume per volume
MES	2-(N-morpholino)-ethane sulfonic acid	wt	wild type
mg	milligram	w/v	weight per volume
min	minute		
MW	molecular weight		

Appendix 4: Index of buffers, solutions, tables and figures

Index of Buffers and Solutions

Index of Tables

Index of Figures

<u>References</u>

Altman, S. 1995. RNase P in research and therapy. *Bio/Technology*, 13: 327-329.

Altman, S., & Kirsebom, L. 1999. Ribonuclease P. *Cold Spring Harbor Laboratory Press, Cold Spring Harbor, NY*.

Altman, S., Kirsebom, L., & Talbot, S. 1993. Recent studies of ribonuclease P. *FASEB J*, 7(1): 7-14.

Altona, C., & Sundaralingam, M. 1972. Conformational analysis of the sugar ring in nucleosides and nucleotides. A new description using the concept of pseudorotation. *J Am Chem Soc*, 94: 8205-8212.

Altona, C., & Sundaralingam, M. 1973. Conformational analysis of the sugar ring in nucleosides and nucleotides. Improved methods for the interpretation of proton magnetic resonance coupling constants. *J Am Chem Soc*, 95: 2333-2344.

Bartel, D. P., & Szostak, J. W. 1993. Isolation of new ribozymes from a large pool of random sequences. *Science*, 261: 1411-1418.

Beaudry, A. A., & Joyce, G. F. 1992. Directed evolution of an RNA enzyme. *Science*, 257: 635-641.

Beebe, J. A., & Fierke, C. A. 1994. A kinetic mechanism for cleavage of precursor tRNA[Asp] Catalysed by the RNA Component of *Bacillus subtilis* Ribonuclease P. *Biochemistry*, 33: 10294-10304.

Birnboim, H. C. 1983. A rapid alkaline extraction method for the isolation of plasmid DNA. *Methods Enzymol*, 100: 243-255.

Birnboim, H. C., & Doly, J. 1979. A rapid alkaline extraction procedure for screening recombinant plasmid DNA. *Nucleic Acids Res*, 7(6): 1513-1523.

Brannvall, M., Pettersson, F. B. M., & Kirsebom, L. A. 2002. The residue immediately upstream of the RNase P cleavage site is a positive determinant. *Biochimie*, 84: 693-703.

Brannvall, M., & Kirsebom, L. A. 2005. Complexity in orchestration of chemical groups near different cleavage sites in RNase P RNA mediated cleavage. *J Mol Biol*, 351: 251-257.

Brannvall, M., & Kirsebom, L. A. 1999. Manganese ions induce miscleavage in the *Escherichia coli* RNase P RNA-catalysed reaction. *J Mol Biol*, 292: 53-63.

Brannvall, M., & Kirsebom, L. A. 2001. Metal ion cooperativity in ribozyme cleavage of RNA. *Proc Natl Acad Sci U S A*, 98: 12943-12947.

Brannvall, M., Mattsson, J. G., Svard, S. G., & Kirsebom, L. A. 1998. RNase P RNA structure and cleavage reflect the primary structure of tRNA genes. *J Mol Biol*, 283(4): 771-783.

Brannvall, M., Mikkelsen, N. E., & Kirsebom, L. A. 2001. Monitoring the structure of *Escherichia coli* RNase P RNA in the presence of various divalent metal ions. *Nucleic Acids Res*, 29: 1426-1432.

Brown, J. W., Nolan, J. M., Haas, E. S., Rubio, M. A., Major, F., & Pace, N. R. 1996. Comparative analysis of ribonuclease P RNA using gene sequences from natural microbial populations reveals tertiary structural elements. *Proc Natl Acad Sci U S A*, 93(7): 3001-3006.

Brown, J. W., & Pace, N. R. 1992. Ribonuclease P RNA and protein subunits from bacteria. *Nucleic Acids Res*, 20(7): 1451-1456.

Burgin, A. B., & Pace, N. R. 1990. Mapping the active site of ribonuclease P RNA using a substrate containing a photoaffinity agent. *EMBO J*, 9(12): 4111-4118.

Busch, S., Kirsebom, L. A., Notbohm, H., & Hartmann, R. K. 2000. Differential role of the intermolecular base-pairs G292-C(75) and G293-C(74) in the reaction catalysed by *Escherichia coli* RNase P RNA. *J Mol Biol*, 299: 941-951.

Cameron, V., & Uhlenbeck, O. C. 1997. 3'-Phosphatase activity in T4 polynucleotide kinase. *Biochemistry*, 16(23): 5120-5126.

Carola, C., & Eckstein, F. 1999. Nucleic acid enzymes. *Curr Opin Chem Biol*, 3: 274-283.

Carrara, G., Calandra, P., Fruscoloni, P., & Tocchini-Valentini, G. P. 1995. Two helices plus a linker: a small model substrate for eukaryotic RNase P. *Proc Natl Acad Sci U S A*, 92(7): 2627-2631.

Cassano, A. G., Anderson, V. E., & Harris, M. E. 2002. Evidence for direct attack by hydroxide in phosphodiester hydrolysis. *J Am Chem Soc*, 124: 10964-10965.

Cate, J. H., Gooding, A. R., Podell, E., Zhou, K., Golden, B. L., Kundrot, C. E., Cech, T. R., & Doudna, J. A. 1996. Crystal structure of a group I ribozyme domain: principles of RNA packing. *Science*, 273: 1678-1685.

References

Chen, J., Nolan, J. M., Harris, M. E., & Pace, N. 1998. Comparative photo-cross-linking analysis of the tertiary structures of *Escherichia coli* and *Bacillus subtilis* RNase P RNAs. *EMBO J*, 17(5): 1515-1525.

Chen, J., & Pace, N. 1997. Identification of the universally conserved core of ribonuclease P RNA. *RNA*, 3(6): 557-560.

Chen, Y., Li, X., & Gegenheimer, P. 1997. Ribonuclease P catalysis requires Mg^{2+} coordinated to the *pro*-RP oxygen of the scissile bond. *Biochemistry*, 36: 2425-2438.

Christian, E. L., & Harris, M. E. 1999. The track of the pre-tRNA 5' leader in the ribonuclease P ribozyme-substrate complex. *Biochemistry*, 38(39): 12629-12638.

Christian, E. L., Kaye, N. M., & Harris, M. E. 2000. Helix P4 is a divalent metal ion binding site in the conserved core of the ribonuclease P ribozyme. *RNA*, 6: 511-519.

Christian, E. L., Kaye, N. M., & Harris, M. E. 2002. Evidence for a polynuclear metal ion binding site in the catalytic domain of ribonuclease P RNA. *EMBO J*, 21(9): 2253-2262.

Christian, E. L., McPheeters, D. S., & Harris, M. E. 1998. Identification of individual nucleotides in the bacterial ribonuclease P ribozyme adjacent to the pre-tRNA cleavage site by short-range photo-cross-linking. *Biochemistry*, 37(50): 17618-17628.

Collins, C. A., & Guthrie, C. 2000. The question remains: is the spliceosome a ribozyme. *Nat Struct Biol*, 10: 850-854.

Cotton, F. A., & Wilkinson, G. 1988. *Advanced Inorganic Chemistry, 5th edn. John Wiley & Sons, NY, Chichester, Brisbane, Toronto, Singapore*.

Crary, S. M., Kurz, J. C., & Fierke, C. A. 2002. Specific phosphorothioate substitutions probe the active site of *Bacillus subtilis* ribonuclease P. *RNA*, 8(7): 933–947.

Crary, S. M., Niranjanakumari, S., & Fierke, C. A. 1998. The protein component of *Bacillus subtilis* ribonuclease P increases catalytic efficiency by enhancing interactions with the 5' leader sequence of pre-tRNAAsp. *Biochemistry*, 37(26): 9409-9416.

Cuzic, S., & Hartmann, R. K. 2005. Nucleotide analogue interference mapping: Application to the RNase P system. *Handbook of RNA Biochemistry, eds. R.K. Hartmann, A. Bindereif, A. Schön, E. Westhof, Wiley-VCH Verlag GmbH & Co. KGaA, Weinheim*.

Cuzic, S., & Hartmann, R. K. 2005 (b). Studies on *Escherichia coli* RNase P RNA with Zn^{2+} as the catalytic cofactor. *Nucleic Acids Res*, 33: 2464-2474.

Eckstein, F., & Lilley, D. M. J. 1996. *Catalytic RNA. Nucleic Acids and Molecular Biology*, Vol. 10, Springer, Berlin.

England, T. E., & Uhlenbeck, O. C. 1978. 3'-terminal labelling of RNA with T4 RNA ligase. *Nature*, 275(5680): 560-561.

Fedorova, O., Boudvillain, M., Kawaoka, J., & Pyle, A. M. 2005. Nucleotide analogue interference mapping and suppression: Specific applications in studies of RNA tertiary structure, dynamic helicase mechanism and RNA-Protein interactions. *Handbook of RNA Biochemistry, eds. R.K. Hartmann, A. Bindereif, A. Schön, E. Westhof, Wiley-VCH Verlag GmbH & Co. KGaA, Weinheim*.

Forster, A. C., & Altman, S. 1990. External guide sequences for an RNA enzyme. *Science*, 249: 783-786.

Frank, D. N., Adamidi, C., Ehringer, M. A., Pitulle, C., & Pace, N. R. 2000. Phylogenetic-comparative analysis of the eukaryal ribonuclease P RNA. *RNA*, 6(12): 1895-1904.

Frank, D. N., & Pace, N. R. 1998. Ribonuclease P: unit and diversity in tRNA processing ribozyme. *Annu Rev Biochem*, 67: 153-180.

Gesteland, R. F., & Atkins, J. F. 1993. *The RNA world. Cold Spring Harbor Laboratory Press*, Cold Spring Harbor, NY.

Gish, G., & Eckstein, F. 1988. DNA and RNA sequence determination based on phosphorothioate chemistry. *Science*, 240: 1520-1522.

Griffiths, A. D., Potter, B. V., & Eperon, I. C. 1987. Stereospecificity of nucleases towards phosphorothioate-substituted RNA: stereochemistry of transcription by T7 RNA polymerase. *Nucleic Acids Res*, 15: 4145-4162.

Guerrier-Takada, C., Gardiner, K., Marsh, T., Pace, N., & Altman, S. 1983. The RNA moiety of ribonuclease P is the catalytic subunit of the enzyme. *Cell*, 35: 849-857.

Guerrier-Takada, C., Haydock, K., Allen, L., & Altman, S. 1986. Metal ion requirements and other aspects of the reaction catalysed by M1 RNA, the RNA subunit of ribonuclease P from *Escherichia coli. Biochemistry*, 25(7): 1509-1515.

Guerrier-Takada, C., McClain, W. H., & Altman, S. 1984. Cleavage of tRNA precursors by the RNA subunit of *E. coli* ribonuclease P (M1 RNA) is influenced by 3'-proximal CCA in the substrates. *Cell*, 38(1): 219-224.

Guerrier-Takada, C., van Belkum, A., Pleij, C. W., & Altman, S. 1988. Novel reactions of RNase P with a tRNA-like structure in turnip yellow mosaic virus RNA. *Cell*, 53(2): 267-272.

Haas, E. S., Banta, A. B., Harris, J. K., Pace, N. R., & Brown, J. W. 1996. Structure and evolution of ribonuclease P RNA in Gram-positive bacteria. *Nucleic Acids Res*, 24(23): 4775-4782.

Haas, E. S., & Brown, J. W. 1998. Evolutionary variation in bacterial RNase P RNAs. *Nucleic Acids Res*, 26(18): 4093-4099.

Hall, T. A., & Brown, J. W. 2002. Archaeal RNase P has multiple protein subunits homologous to eukaryotic nuclear RNase P proteins. *RNA*, 8: 296–306.

Hampel, A., & Tritz, R. 1989. RNA catalytic properties of the minimum (-) sTRSV sequence. *Biochemistry*, 28: 4929-4933.

Hansen, A., Pfeiffer, T., Zuleeg, T., Limmer, S., Ciesiolka, J., Feltens, R., & Hartmann, R. K. 2001. Exploring the minimal substrate requirements for trans-cleavage by RNase P holoenzymes from *Escherichia coli* and *Bacillus subtilis*. *Mol Microbiol*, 41(1): 131-143.

Hardt, W. D., Erdmann, V. A., & Hartmann, R. K. 1996. Rp-deoxy-phosphorothioate modification interference experiments identify 2'-OH groups in RNase P RNA that are crucial to tRNA binding. *RNA*, 2(12): 1189-1198.

Hardt, W. D., Schlegl, J., Erdmann, V. A., & Hartmann, R. K. 1993. Role of the D arm and the anticodon arm in tRNA recognition by eubacterial and eukaryotic RNase P enzymes. *Biochemistry*, 32: 13046-13053.

Hardt, W. D., Warnecke, J. M., Erdmann, V. A., & Hartmann, R. K. 1995. Rp-phosphorothioate modifications in RNase P RNA that interfere with tRNA binding. *EMBO J*, 14(12): 2935-2944.

Harris, J. K., Haas, E. S., Williams, D., Frank, D. N., & Brown, J. W. 2001. New insight into RNase P RNA structure from comparative analysis of the archaeal RNA. *RNA*, 7(2): 220-232.

References

Harris, M. E., Nolan, J. M., Malhotra, A., Brown, J. W., & Pace, N. R. 1994. Use of photoaffinity crosslinking and molecular modelling to analyse the global architecture of ribonuclease P RNA. *EMBO J*, 13: 3953-3963.

Harris, M. E., & Pace, N. R. 1995. Analysis of the tertiary structure of bacterial RNase P RNA. *Mol Biol Rep*, 22(2-3): 115-123.

Hartmann, R. K., Heinrich, J., Schlegl, J., & Schuster, H. 1995. Precursor of C4 antisense RNA of bacteriophages P1 and P7 is a substrate for RNase P of *Escherichia coli. Proc Natl Acad Sci U S A*, 92(13): 5822-5826.

Haseloff, J., & Gerlach, W. L. 1988. Simple RNA enzymes with new and highly specific endoribonuclease activity. *Nature*, 334: 585-591.

Heide, C., Pfeiffer, T., Nolan, J. M., & Hartmann, R. K. 1999. Guanosine 2-NH2 groups of *Escherichia coli* RNase P RNA involved in intramolecular tertiary contacts and direct interactions with tRNA. *RNA*, 5(1): 102-116.

Herschlag, D., Eckstein, F., & Cech, T. R. 1993. The importance of being ribose at the cleavage site in the *Tetrahymena* ribozyme reaction. *Biochemistry*, 32: 8299-8311.

Holm, P. S., & Krupp, G. 1992. The acceptor stem in pre-tRNAs determines the cleavage specificity of RNase P. *Nucleic acids Res* 20(3): 421-423.

Jarrous, N., & Altman, S. 2001. Human ribonuclease P. *Methods Enzymol*, 342: 93-100.

Jovine, L., Djordjevic, S., & Rhodes, D. 2000. The crystal structure of yeast phenylalanine tRNA at 2.0 Å resolution: cleavage by Mg^{2+} in 15-year old crystals. *J Mol Biol*, 301: 401-414.

Juneau, K., Podell, E., Harrington, D. J., & Cech, T. 2001. Structural basis of the enhanced stability of a mutant ribozyme domain and a detailed view of RNA-solvent interactions. *Structure*, 9: 221-231.

Kahle, D., Wehmeyer, U., & Krupp, G. 1990. Substrate recognition by RNase P and by the catalytic M1 RNA: identification of possible contact points in pre-tRNAs. *EMBO J*, 9(6): 1929-1923.

Kaye, N. M., Christian, E. L., & Harris, M. E. 2002. NAIM and site-specific functional group modification analysis of RNase P RNA: magnesium dependent structure within the conserved P1-P4 multihelix junction contributes to catalysis. *Biochemistry*, 41: 4533-4545.

Kazakov, S., & Altman, S. 1991. Site-specific cleavage by metal ion cofactors and inhibitors of M1 RNA, the catalytic subunit of RNase P from *Escherichia coli*. *Proc Natl Acad Sci U S A*, 88: 9193-9197.

Kazantsev, A. V., Krivenko, A. A., Harrington, D. J., Carter, R. J., Holbrook, S. R., Adams, P. D., & Pace, N. 2003. High-resolution structure of RNase P protein from *Thermotoga maritima*. *Proc Natl Acad Sci U S A*, 100: 7497-7502.

Kazantsev, A. V., Krivenko, A. A., Harrington, D. J., Holbrook, S. R., Adams, P. D., & Pace, N. R. 2005. Crystal structure of a bacterial ribonuclease P RNA. *Proc Natl Acad Sci U S A*, 102(38): 13392-13397.

Kazantsev, A. V., & Pace, N. R. 1998. Identification by modification-interference of purine N-7 and ribose 2'-OH groups critical for catalysis by bacterial ribonuclease P. *RNA*, 4(8): 937-947.

Kirby, A. J., & Younas, M. 1970. The reactivity of phosphate esters. Reaction of diesters with nucleophiles. *J Chem Soc*, B: 1165-1172.

Kirsebom, L. A., & Svard, S. G. 1992. The kinetics and specificity of cleavage by RNase P is mainly dependent on the structure of the amino acid acceptor stem. *Nucleic Acids Res*, 20(3): 425-432.

Kirsebom, L. A., & Svard, S. G. 1994. Base pairing between *Escherichia coli* RNase P RNA and its substrate. *EMBO J*, 13(20): 4870-4876.

Kirsebom, L. A., & Vioque, A. 1995. RNase P from bacteria. Substrate recognition and function of the protein subunit. *Mol Biol Rep*, 22(2-3): 99-109.

Knap, A. K., Wesolowski, D., & Altman, S. 1990. Protection from chemical modification of nucleotides in complexes of M1 RNA, the catalytic subunit of RNase P from *E. coli*, and tRNA precursors. *Biochimie*, 72: 779-790.

Koizumi, M., Soukup, G. A., Kerr, J. N., & Breaker, R. R. 1999. Allosteric selection of ribozymes that respond to the second messengers cGMP and cAMP. *Nat Struct Biol*, 6(11): 1062-1071.

Komatsu, Y., Nobouka, K., Karino-Abe, N., Matsuda, A., & Ohtsuka, E. 2002. *In vitro* selection of hairpin ribozymes activated with short nucleotides. *Biochemistry*, 41(29): 9090-9098.

Komine, Y., Kitabatake, M., Yokogawa, T., Nishikawa, K., & Inokuchi, H. 1994. A tRNA-like structure is present in 10Sa RNA, a small stable RNA from *Escherichia coli*. *Proc Natl Acad Sci U S A*, 91(20): 9223-9227.

Koonin, E. V., Wolf, Y. I., & Aravind, L. 2001. Prediction of the archaeal exosome and its connections with the proteasome and the translation and transcription machineries by a comparative-genomic approach. *Genome Res*, 11: 240– 252.

Koshkin, A. A., Nielsen, P., Meldgaard, M., Rajwanshi, W. K., Singh, S. K., & Wengel, J. 1998. LNA (locked nucleic acid): an RNA mimic forming exceedingly stable LNA:LNA duplexes. *J Am Chem Soc*, 120: 13252-13253.

Kruger, K., Grabowski, P., Zaug, A., Sands, J., Gottschling, D., & Cech, T. 1982. Self-splicing RNA: autoexcision and autocyclisation of the ribosomal RNA intervening sequence of *Tetrahymena*. *Cell*, 31: 147–157.

Krupp, G., Kahle, D., Vogt, T., & Char, S. 1991. Sequence changes in both flanking sequences of a pre-tRNA influence the cleavage specificity of RNase P. *J Mol Biol*, 217(4): 637-648.

Kufel, J., & Kirsebom, L. A. 1996. Residues in *Escherichia coli* RNase P RNA important for cleavage site selection and divalent metal ion binding. *J Mol Biol*, 263(5): 685-698.

Kuimelis, R. G., & McLaughlin, L. W. 1998. Mechanism of ribozyme-mediated RNA cleavage. *Chem Rev*, 98: 1027-1044.

Kurz, J. C., & Fierke, C. A. 2002. The affinity of magnesium binding sites in the *Bacillus subtilis* RNase P x pre-tRNA complex is enhanced by the protein subunit. *Biochemistry*, 41: 9545-9558.

Lee, J. Y., Rohlman, C. E., Molony, L. A., & Engelke, D. R. 1991. Characterization of RPR1, an essential gene encoding the RNA component of *Saccharomyces cerevisiae* nuclear RNase P. *Mol Cell Biol*, 11(2): 721-730.

Loria, A., Niranjanakumari, S., Fierke, C. A., & Pan, T. 1998. Recognition of a pre-tRNA substrate by the *Bacillus subtilis* RNase P holoenzyme. *Biochemistry*, 37(44): 15466-15473.

Loria, A., & Pan, T. 1996. Domain structure of the ribozyme from eubacterial ribonuclease P. *RNA*, 2(6): 551-563.

Loria, A., & Pan, T. 1997. Recognition of the T stem-loop of a pre-tRNA substrate by the ribozyme from *Bacillus subtilis* ribonuclease P. *Biochemistry*, 36: 6317-6325.

Loria, A., & Pan, T. 1998. Recognition of the 5' leader and the acceptor stem of a pre-tRNA substrate by the ribozyme from *Bacillus subtilis* RNase P. *Biochemistry*, 37(6): 10126-10133.

Loria, A., & Pan, T. 1999. The cleavage step of ribonuclease P catalysis is determined by ribozyme-substrate interactions both distal and proximal to the cleavage site. *Biochemistry*, 38(27): 8612-8620.

Mans, R. M., Guerrier-Takada, C., Altman, S., & Pleij, C. W. 1990. Interaction of RNase P from *Escherichia coli* with pseudoknotted structures in viral RNAs. *Nucleic Acids Res*, 18(12): 3479-3487.

Massire, C., Jaeger, L., & Westhof, E. 1997. Phylogenetic evidence for a new tertiary interaction in bacterial RNase P RNAs. *RNA*, 3(6): 553-556.

Massire, C., Jaeger, L., & Westhof, E. 1998. Derivation of the three-dimensional architecture of bacterial ribonuclease P RNAs from comparative sequence analysis. *J Mol Biol*, 279(4): 773-793.

McClain, W. H., Guerrier-Takada, C., & Altman, S. 1987. Model substrates for an RNA enzyme. *Science*, 238: 527-530.

Milligan, J. F., & Uhlenbeck, O. C. 1989. Synthesis of small RNAs using T7 RNA polymerase. *Methods Enzymol*, 180: 51-62.

Morales, M. J., Dang, Y. L., Lou, Y. C., Sulo, P., & Martin, N. C. 1992. A 105-kDa protein is required for yeast mitochondrial RNase P activity. *Proc Natl Acad Sci U S A*, 89(20): 9875-9879.

Morales, M. J., Wise, C. A., Hollingsworth, M. J., & Martin, N. C. 1989. Characterization of yeast mitochondrial RNase P: an intact RNA subunit is not essential for activity *in vitro*. *Nucleic Acids Res*, 17(17): 6865-6881.

Morse, D. P., & Schmidt, F. J. 1992. Sequences encoding the protein and RNA components of ribonuclease P from *Streptomyces bikiniensis* var. zorbonensis. *Gene*, 117(1): 61-66.

Mueller, U., Schübel, H., Sprinzl, M., & Heinemann, U. 1999. Crystal structure of acceptor stem of tRNA[Ala] from *Escherichia coli* shows unique GU wobble base pair at 1.16 Å resolution. *RNA*, 5: 670-677.

References

Muth, G. W., Ortoleva-Donnelly, L., & Strobel, S. A. 2000. A single adenosine with a neutral pKa in the ribosomal peptidyl transferase centre. *Science*, 289: 947-950.

Nielsen, C. B., Singh, S. K., Wengel, J., & Jacobsen, J. P. 1999. The solution structure of a locked nucleic acid (LNA) hybridised to DNA. *J Biomol Struc Dyn*, 17: 175-191.

Nielsen, K. E., Singh, S. K., Wengel, J., & Jacobsen, J. P. 2000. Solution structure of an LNA hybridised to DNA: NMR study of the d(CT(L)GCT(L)T(L)CT(L)GC):d(GCAGAAGCAG) duplex containing four locked nucleotides. *Bioconj Chem*: 228-238.

Nissen, P., Hansen, J., Ban, N., Moore, B., & Steitz, T. A. 2000. The structural basis of ribosome activity in peptide bond synthesis. *Science*, 5481: 920–930.

Nolan, J. M., Burke, D. H., & Pace, N. R. 1993. Circularly permuted tRNAs as specific photoaffinity probes of ribonuclease P RNA structure. *Science*, 261(5122): 762-765.

Obika, S., Nanbu, D., Hari, Y., Mori, K., In, Y., Ishida, T., & Imanishi, T. 1997. Synthesis of 2' -O-,4' -C-methyleneuridine and cytidine. Novel bicyclic nucleosides having a fixed C3' -endo puckering. *Tetrahedron Lett*, 38: 8735.

Oh, B. K., & Pace, N. R. 1994. Interaction of the 3' -end of tRNA with ribonuclease P RNA. *Nucleic Acids Res*, 22(20): 4087-4094.

Ortoleva-Donnelly, L., Kronman, M., & Strobel, S. A. 1998. Identifying RNA minor groove tertiary contacts by nucleotide analogue interference mapping with N2-methylguanosine. *Biochemistry*, 37(12933-12942).

Pan, T. 1995. Higher order folding and domain analysis of the ribozyme from *Bacillus subtilis* ribonuclease P. *Biochemistry*, 34(3): 902-909.

Pan, T., Loria, A., & Zhong, K. 1995. Probing of tertiary interactions in RNA: 2'-hydroxyl-base contacts between the RNase P RNA and pre-tRNA. *Proc Natl Acad Sci U S A*, 92: 12510-12514.

Pascual, A., & Vioque, A. 1996. Cloning, purification and characterization of the protein subunit of ribonuclease P from the cyanobacterium *Synechocystis* sp. PCC 6803. *Eur J Biochem*, 241(1).

Pearson, R. G. 1963. Hard and soft acids and bases. *J Am Chem Soc*, 85: 3533-3539.

References

Perreault, J. P., Labuda, D., Usman, N., Yang, J. H., & Cedergren, R. 1990. Mixed deoxyribo- and ribo-oligonucleotides with catalytic activity. *Nature*, 344: 565-567.

Persson, T., Cuzic, S., & Hartmann, R. K. 2003. Catalysis by RNase P RNA: unique features and unprecedented active site plasticity. *J Biol Chem*, 278: 43394-43401.

Petersen, M., Bondensgaard, K., Wengel, J., & Jacobsen, J. P. 2002. Locked nucleic acid (LNA): NMR solution structure of LNA:RNA hybrids. *J Am Chem Soc*, 124: 5974-5982.

Petersen, M., Nielsen, C. B., Nielsen, K. E., Jensen, G. A., Bondensgaard, K., Singh, S. K., Rajwanshi, W. K., Koshkin, A. A., Dahl, B. M., Wengel, J., & Jacobsen, J. P. 2000. The conformations of locked nucleic acids (LNA). *J Mol Recognit*, 13: 44-53.

Pley, H. W., Flaherty, K. M., & McKay, D. B. 1994. Model for an RNA tertiary interaction from the structure of an intermolecular complex between a GAAA tetraloop and an RNA helix. *Nature*, 372: 111-113.

Rasmussen, T. A., & Nolan, J. M. 2002. G350 of *Escherichia coli* RNase P RNA contributes to Mg2+ binding near the active site of the enzyme. *Gene*, 294: 177-185.

Rox, C., Feltens, R., Pfeiffer, T., & Hartmann, R. K. 2002. Potential contact sites between the protein and RNA subunit in the *Bacillus subtilis* RNase P holoenzyme. *J Mol Biol*, 315: 551-560.

Rubin, J. R., Wang, J., & Sundaralingam, M. 1983. *X-ray* diffraction study of the zinc(II) binding sites in yeast phenylalanine transfer RNA. Preferential binding of zinc to guanines in purine-purine sequences. *Biochim Biophys Acta*, 756: 111-118.

Saiki, R. K., Scharf, S., Faloona, F., Mullis, K. B., Horn, G. T., Erlich, H. A., & Arnheim, N. 1985. Enzymatic amplification of beta-globin genomic sequences and restriction site analysis for diagnosis of sickle cell anemia. *Science*, 230(4732): 1350-1354.

Salavati, R., Panigrahi, A. K., & Stuart, K. D. 2001. Mitochondrial ribonuclease P activity of *Trypanosoma brucei*. *Mol Biochem Parasitol*, 115(1): 109-117.

Schedl, P., & Primakoff, P. 1973. Mutants of *Escherichia coli* thermosensitive for the synthesis of transfer RNA. *Proc Natl Acad Sci U S A*, 70(7): 2091-2095.

Schlegl, J., Hardt, W. D., Erdmann, V. A., & Hartmann, R. K. 1994. Contribution of structural elements to *Thermus thermophilus* ribonuclease P RNA function. *EMBO J*, 13: 4863-4869.

Siew, D., Zahler, N. H., Cassano, A. G., Strobel, S. A., & Harris, M. E. 1999. Identification of adenosine functional groups involved in substrate binding by the ribonuclease P ribozyme. *Biochemistry*, 38(6): 1873-1883.

Sigel, H., & Song, B. 1996. Solution structures of nucleotide-metal ion complexes. Isomeric equilibria. *Metal ions in biological systems*, 32(ed. A. Sigel, H. Sigel, Marcel Dekker, Inc., New York).

Singh, S. K., Nielsen, P., Koshkin, A. A., & Wengel, J. 1998. LNA (locked nucleic acid): synthesis and high-affinity acid recognition. *Chem Commun (4)*: 455-456.

Smith, D., Burgin, A. B., Haas, E. S., & Pace, N. R. 1992. Influence of metal ions on the ribonuclease P reaction. Distinguishing substrate binding from catalysis. *J Biol Chem*, 267: 2492-2436.

Smith, D., & Pace, N. R. 1993. Multiple magnesium ions in the ribonuclease P reaction mechanism. *Biochemistry*, 32: 5273-5281.

Spitzfaden, C., Nicholson, N., Jones, J. J., Guth, S., Lehr, R., Prescott, C. D., Hegg, L. A., & Eggleston, D. S. 2000. The structure of ribonuclease P protein from *Staphylococcus aureus* reveals a unique binding site for single-stranded RNA. *J Mol Biol*, 295: 105-115.

Stams, T., Niranjanakumari, S., Fierke, C. A., & Christianson, D. A. 1998. Ribonuclease P protein structure: Evolutionary origins in the translational apparatus. *Science*, 280: 752-755.

Steitz, T. A., & Moore, P. B. 2003. RNA, the first macromolecular catalyst: the ribosome is a ribozyme. *Trends Biochem Sci*, 28(8): 411-418.

Steitz, T. A., & Steitz, J. A. 1993. A general two-metal-ion mechanism for catalytic RNA. *Proc Natl Acad Sci U S A*, 90(14): 6498-6502.

Strobel, S. A. 1999. A chemogenetic approach to RNA function/structure analysis. *Curr Opin Struct Biol*, 9: 346-352.

Svard, S. G., & Kirsebom, L. A. 1992. Several regions of a tRNA precursor determine the *Escherichia coli* RNase P cleavage site. *Nucleic Acids Res*, 227(4): 1019-1031.

Symons, R. H. 1992. Small catalytic RNAs. *Annu Rev Biochem*, 61: 641-661.

Tatusov, R. L., Natale, D. A., Garkavtsev, I. V., Shankavaram, U. T., Rao, B. S., Kiryutin, B., Galperin, M. Y., Fedorova, N. D., & Koonin, E. V. 2001. The COG database: New developments in phylogenetic classification of proteins from complete genomes. *Nucleic Acids Res*, 29(22– 28).

Thomas, B. C., Gao, L., Stomp, D., Li, X., & Gegenheimer, P. A. 1995. Spinach chloroplast RNase P: a putative protein enzyme. *Nucleic Acids Symp Ser*, 33: 95-98.

Thurlow, D. L., Shilowski, D., & Marsh, T. L. 1991. Nucleotides in precursor tRNAs that are required intact for catalysis by RNase P RNAs. *Nuceic Acids Res*, 19(4): 885-891.

Torres-Larios, A., Swinger, K. K., Krasilnikov, A. S., Pan, T., & Mondragon, A. 2005. Crystal structure of the RNA component of bacterial ribonuclease P. *Nature*, 437(7058): 584-587.

Tsai, H., Masquida, B., Biswas, R., Westhof, E., & Gopalan, V. 2003. Molecular modelling of the three-dimensional structure of the bacterial RNase P holoenzyme. *J Mol Biol*, 325(4): 661-675.

Uhlenbeck, O. C. 1987. A small catalytic oligoribonucleotide. *Nature*, 328: 596-600.

Valadkhan, S., & Manley, J. L. 2001. Splicing-related catalysis by protein-free snRNAs. *Nature*, 413: 701 - 707.

van Eenennaam, H., Jarrous, N., van Venrooij, W. J., & Pruijn, G. J. 2000. Architecture and function of the human endonucleases RNase P and RNase MRP. *IUBMB Life*, 49(4): 265-272.

van Eenennaam, H., Lugtenberg, D., Vogelzangs, J. H., van Venrooij, W. J., & Pruijn, G. J. 2001. hPop5, a protein subunit of the human RNase MRP and RNase P endoribonucleases. *J Biol Chem*, 276(34): 31635-31641.

Walter, N. G., & Burke, J. M. 1998. The hairpin ribozyme: structure, assembly and catalysis. *Curr Opin Chem Biol*, 2: 24-30.

Wang, M. Y., Chien, L. F., & Pan, R. L. 1988. Radiation inactivation analysis of chloroplast CF0-CF1 ATPase. *J Biol Chem*, 263(18): 8838-8843.

Warnecke, J. M., Furste, J. P., Hardt, W. D., Erdmann, V. A., & Hartmann, R. K. 1996. Ribonuclease P (RNase P) RNA is converted to a Cd(2+)-ribozyme by a single Rp-phosphorothioate modification in the precursor tRNA at the RNase P cleavage site. *Proc Natl Acad Sci U S A*, 93: 8924-8928.

Warnecke, J. M., Held, R., Busch, S., & Hartmann, R. K. 1999. Role of metal ions in the hydrolysis reaction catalysed by RNase P RNA from *Bacillus subtilis*. *J Mol Biol*, 290(2): 433-445.

Wise, C. A., & Martin, N. C. 1991. Dramatic size variation of yeast mitochondrial RNAs suggests that RNase P RNAs can be quite small. *J Biol Chem*, 266(29): 19154-19157.

Xiao, S., Houser-Scott, F., & Engelke, D. R. 2001. Eukaryotic ribonuclease P: increased complexity to cope with the nuclear pre-tRNA pathway. *J Cell Physiol*, 187(1): 11-20.

Zahler, N. H., Christian, E. L., & Harris, M. E. 2003. Recognition of the 5' leader of pre-tRNA substrates by the active site of ribonuclease P. *RNA*, 9: 734-745.

Zahler, N. H., Lei, S., Christian, E. L., & Harris, M. E. 2005. The pre-tRNA nucleotide base and 2'-hydroxyl at N(-1) contribute to fidelity in tRNA processing by RNase P. *J Mol Biol*, 345: 969-985.

Zuleeg, T., Hansen, A., Pfeiffer, T., Schubel, H., Kreutzer, R., Hartmann, R. K., & Limmer, S. 2001. Correlation between processing efficiency for ribonuclease P minimal substrates and conformation of the nucleotide -1 at the cleavage position. *Biochemistry*, 40: 3363-3369.

<u>Acknowledgments</u>

Here I would like to thank …

… **Prof. Dr. Roland K. Hartmann** for excellent supervising of my work, for his encouragement, guidance and support during my entire PhD study. I would like to express my gratitude to him for being always open and available for discussion;

… **Prof. Dr. Albrecht Bindereif**, the second referee of my work, **Prof Dr. Maike Petersen** and **PD Dr. Klaus Reuter** for participation in the examination commission;

… **Dr. Jens Wöhnert** for performing the structural analyses of 2' –ribose modified model substrates;

… **Dominik Helmecke** and **Sybille Siedler** who helped me in performing my experiments. For preparing buffers and stock solutions and for performing experimental work with high accuracy;

… **Dr. Ralph Feltens** for helping me with various topics of research and for very useful discussions. For many good advises, moral support and proofreading of my dissertation;

… **Dr. Dagmar Willkomm** for proofreading of my dissertation;

… **Dr. Rolf Bald** and the company **"Alnylam"** for the synthesis of RNA-oligonucleotides used in this work;

… **All colleagues** from Lübeck and Marburg for their patience and for creating such a friendly atmosphere. For providing discussions, ideas and suggestions during our group seminar, essential to the planning and execution of this research;

… Finally but not least **all my family** and especially **Carmen** and **Dorinel Verdes** who encouraged me to choose the road of scientific exploration and for providing moral and financial support during the time I was applying for PhD positions. I might not have begun this PhD work without their advice.

Curriculum vitae

Name:	Simona Daniela Cuzic - Feltens
Date of birth:	26.01.1973
Place of birth:	Corlateni-Botosani, Romania

Education:

1979 – 1983	Primary School Carasa, Corlateni-Botosani
1983 – 1985	Secondary School Carasa, Corlateni-Botosani
1985 – 1987	continuing Secondary School Dorohoi-Botosani
1987 – 1991	"Mihai Eminescu" High School Botosani
July 1991	Final high school exam
1991 – 1996	Biochemical Engineering-Study "Gh. Asachi" University of Iasi Faculty of Chemistry Department of Organic Chemistry
July 1996	Dipl. Ing. Biochemical Engineering
1996 – 1997	Natural Products Biologically Active-Master "Gh. Asachi" University of Iasi Faculty of Chemistry Department of Organic Chemistry
July 1997	Master degree

Work experience

August 1997	S.C. Köber SRL Piatra Neamt
September 1998	S.C. Compania Conex S.A. Iasi
May 2001	PhD work
	Group of Prof. Dr. R. K. Hartmann
	Institute of Biochemistry
	University Lübeck
September 2001	continuing PhD work
	Group of Prof. Dr. R. K. Hartmann
	Institute of Pharmaceutical Chemistry
	University Marburg

List of Publications

Persson, T., **Cuzic, S**., & Hartmann, R. K. 2003. Catalysis by RNase P RNA: unique features and unprecedented active site plasticity. *J Biol Chem.*, 278: 43394-43401.

Cuzic, S., & Hartmann, R. K. 2005. Studies on *Escherichia coli* RNase P RNA with Zn^{2+} as the catalytic cofactor. *Nucl Acids Res.*, 33: 2464-2474.

Cuzic, S., & Hartmann, R. K. 2005. Nucleotide Analogue Interference Mapping: Application to the RNase P System. Handbook of RNA Biochemistry, eds. R. K. Hartmann, A. Bindereif, A. Schön, E. Westhof, Wiley-VCH Verlag GmbH & Co. KGaA, Weinheim, 1: 294-318.

Erklärung

Ich versichere, daß ich meine Dissertation

„*Investigation of the catalytic mechanism of RNase P: the role of divalent metal ions and functional groups important for catalysis*"

selbständig ohne unerlaubte Hilfe angefertigt und mich dabei keiner anderen als der von mir ausdrücklich bezeichneten Quellen bedient habe.

Die Dissertation wurde in der jetzigen oder einer ähnlichen Form noch bei keiner anderen Hochschule eingereicht und hat noch keinen sonstigen Prüfungszwecken gedient.

Marburg, den..........................

....
(Unterschrift mit Vor- und Zuname)